Advanced Fluorescence Spectroscopy for Quantitative Liquid-Phase Analysis in Green Solvent Spray Processes

Hannah M. Ulrich

Acknowledgments

This thesis and the associated research were conducted during my time at the LTT (FAU) in Erlangen and later at the Institute of Thermodynamics at the UniBw München. Along this journey, I had the privilege of meeting and collaborating with many exceptional colleagues whom I want to thank for their support.

First and foremost, I extend my profound gratitude to my supervisor, Prof. Dr.-Ing. habil. Lars Zigan, for encouraging me to seize this opportunity and for his support and trust in my research ideas. I am also thankful to Prof. Dr. Sebastian Kaiser for serving as a reviewer for this thesis and to Univ.-Prof. Dr.-Ing. Roger Förstner for acting as the examination chair. Additionally, I was fortunate to collaborate with Dr. Edouard Berrocal and his team in Lund. I sincerely thank them for their outstanding cooperation and continuous sharing of expertise.

My PhD journey would not have been the same without the incredible colleagues I had the pleasure of working with at both institutes. My sincere thanks go to Dr. Ulrich Retzer, who transitioned from being my supervisor during my Master's thesis to my office and bouldering partner. Your invaluable input and support made my transition into PhD life so much smoother. I am especially grateful to have embarked on this journey alongside Phillip Bräuer and Bastian Lehnert. Your inspiring and motivating discussions, whether during long days in the office and lab or evenings at the bar, were immensely valuable. I also want to thank Niko Schmidt for always having an open ear and for joining Uli and me for much-needed bouldering or yoga sessions. A big thanks go to Dr. Matthias Kögl and Markus Labus, who also moved to Munich and supported me in the final years of this work. I am grateful to the entire "Mundt group" at UniBw for their warm welcome to the new institute and for the Sprittwochs. Finally, my gratitude extends to my current office mate, Niklas Syguda, for our countless conversations about institute life and the everyday challenges we faced.

I also deeply appreciate the students who contributed to my research over the years. Without your help, this thesis would not have been possible. In Erlangen, Sophie Sigl, Michael Möhnle, and Silvan Keim did outstanding work in the lab. In Munich, Nathalie Lankl and Richard Weiß provided excellent assistance with setups and measurements.

Lastly, my deepest gratitude goes to my family and Fabi. You endured all my moods and challenges over the years, and your unwavering support has been truly invaluable.

Abstract

In order to design more responsible production processes, "green," environmentally friendly solvents are being considered as alternatives to more complex substances. Achieving greater sustainability across various industrial applications requires deeper knowledge to support the development and optimization of these processes. Specifically, transient two-phase systems, such as sprays, present complex, dynamic phenomena that demand more comprehensive research to understand the mechanisms of atomization, evaporation and mixing. Optical diagnostics enable more detailed analyses of these processes and offer a precise, spatially and temporally resolved quantification of relevant parameters, such as temperature, droplet size and mixture composition. This work presents the advancement and application of fluorescence-based measurement techniques for the quantitative characterization of the liquid phase in sprays and droplets. Especially, first-time applications of micrometric droplet LIF thermometry imaging are presented. The optimization of the two-color technique and additionally reviewed fluorescence approaches aim for a comprehensive characterization of the liquid phase in sprays through planar fluorescence diagnostics.

The fluorescent tracers fluorescein disodium and sulforhodamine 101 are admixed to ethanol, water and binary mixtures of each. The temperature-dependent photophysical behavior of the dyes is used for ratiometric two-color laser induced fluorescence thermometry. For a minimization of measurement uncertainties caused by dye influences, extensive investigations of the emission behavior are required. Corresponding calibration measurements are conducted in a temperature-controlled, monodisperse ethanol droplet chain. The enhanced technique is further applied to study heat transfer and evaporation along the heated droplet chain. A microscopic imaging system is used to record the spatially resolved droplet temperatures. Additional investigations in differently tempered atomizing ethanol jets allow for a review of the method's applicability in polydisperse droplet systems. These studies are conducted with a spectrometer detection setup, providing spectrally resolved information to estimate the influences of stimulated fluorescence emission and reabsorption effects on the recorded spectra.

Furthermore, two-photon excitation is utilized to image technical sprays of a commercial injector by laser-induced fluorescence. The microscopic visualization enables the sizing of individual liquid structures even in dense spray regions. As a result, the acquired information provides insight into different breakup mechanisms and the influence of the solvent's liquid properties on the spray structure.

Kurzfassung

Um in der Industrie eine nachhaltige Produktion umzusetzen, wird unter anderem die Substitution von oftmals schädlichen, komplexen Substanzen durch umweltfreundliche, sogenannte „grüne Lösungsmittel" vorgeschlagen. Der Wandel hin zu einer höheren Nachhaltigkeit in industriellen Verfahren erfordert Grundlagenwissen für eine Entwicklung und Optimierung solcher Prozesse. Insbesondere instationäre Zweiphasensysteme, wie Sprays, stellen durch komplexe, dynamische Mechanismen wie Zerstäubung, Verdampfung und Mischung eine große Herausforderung dar und erfordern umfassendere Forschungen für ein verbessertes Verständnis. Optische Messtechniken ermöglichen detaillierte Untersuchungen dieser Prozesse und bieten die Möglichkeit einer präzisen, räumlich und zeitlich aufgelösten Quantifizierung relevanter Parameter wie Temperatur, Tropfengröße und Gemischzusammensetzung.

Die vorliegende Arbeit behandelt die Weiterentwicklung und Anwendungen fluoreszenzbasierter Messtechnik zur quantitativen Charakterisierung der Flüssigphase in Sprays und Tropfen. Diese Arbeit präsentiert die erstmalige Anwendung einer bildgebenden LIF-Thermometrie-Methode für mikrometrische Tropfen. Durch die optimierte Zwei-Farben Technik und zusätzlich untersuchte Fluoreszenzkonzepte wird eine umfassende Charakterisierung der Flüssigphase in Sprays anhand der planaren Fluoreszenzmesstechnik angestrebt. Dafür werden die beiden Fluoreszenzfarbstoffe Uranin (Fluorescein Natriumsalz) und Sulforhodamin 101 den Lösungsmitteln Ethanol, Wasser und binären Mischungen beider Stoffe beigemischt. Die verhältnisbasierte Methode der laserinduzierten Zwei-Farben Fluoreszenz nutzt das temperaturabhängige, photophysikalische Verhalten der Farbstoffe. Umfassende Studien des Emissionsverhaltens sind erforderlich, um Messfehler durch Farbstoffeinflüsse zu minimieren. Entsprechende Kalibriermessungen werden in einer temperierten, monodispersen Ethanol-Tropfenkette durchgeführt. Die optimierte Messmethode wird erstmals angewandt, um die Verdampfung und den Wärmeübergang entlang einer temperierten, mikrometrischen Tropfenkette zu untersuchen. Hierzu wird ein mikroskopisches Kamerasystem für die Detektion räumlich aufgelöster Tropfentemperaturen genutzt. Zusätzliche Untersuchungen der Zerstäubung von unterschiedlich temperierten Ethanoleinspritzstrahlen ermöglichen die Anwendung der entwickelten Methodik im Rahmen von polydispersen Tropfensystemen. Letztere werden anhand eines Spektrometer-Aufbaus betrachtet, wodurch die Fluoreszenzsignale spektral aufgelöst werden. Dadurch können Einflüsse von stimulierten Fluoreszenz- und Reabsorptionseffekten auf das Fluoreszenzspektrum abgeschätzt werden.

Darüber hinaus werden technische Sprays eines kommerziellen Injektors durch laser-induzierte Zwei-Photonen Anregung bildgebend untersucht. Anhand der mikroskopischen Visualisierung wird eine Größenbestimmung einzelner Flüssigkeitsstrukturen auch in dichten Spraybereichen ermöglicht. Mithilfe der analysierten Größen werden Einblicke in die vorliegenden Zerfallsmechanismen und den Einfluss unterschiedlicher Fluideigenschaften auf das Sprayverhalten gegeben.

Table of Contents

0 Symbols and Abbreviations

Latin symbols

Symbol	Unit	Description
c	m·s^{-1}	Speed of light
d	m	Diameter
E_T	J	Transition energy
h	J·s	Planck's constant
I	W·m^{-2}	Fluorescence intensity
J	-	Rotational quantum number
l	m	Characteristic length
M	-	Spin multiplicity
n	-	Electronic quantum number
N	-	Number of molecules
N_A	mol^{-1}	Avogadro's constant
Oh	-	Ohnesorge number
r	m	Radial distance
Re_L	-	Liquid Reynolds number
s	%/K	Sensitivity
S	-	Total spin quantum number
S_0	-	Singlet ground state
S_1	-	First excited singlet state
T	K	Temperature
T_1	-	First excited triplet state
v	-	Vibrational quantum number

Greek Symbols

Symbol	Unit	Description
η	N·s/m^2	Dynamic viscosity
λ	m	Wavelength
υ	m·s^{-1}	Velocity
π	-	Bonding orbital
π^*	-	Antibonding orbital
ρ	kg/m^3	Density
σ	N/m	Surface tension
σ	-	Bonding orbital
σ^*	-	Antibonding orbital
τ	s	Lifetime

Abbreviations

2c-LIF	Two-color laser-induced fluorescence
2p-LIF	Two-photon laser-induced fluorescence
BI	Ballistic imaging
CCD	Charge coupled device
CERS	Cavity-enhanced Raman spectroscopy
DISI	Direct-injection spark-ignition
FSP	Flame spray pyrolysis
GRR	Global Raman refractometry
HOMO	Highest occupied molecular orbital
ISC	Intersystem crossing
IR	Infrared
LAS	Laser absorption spectroscopy
LIEF	Laser-induced exciplex fluorescence
LIF	Laser-induced fluorescence
LUMO	Lowest unoccupied molecular orbital
MDR	Morphology dependent resonances
Mie	Mie scattering
Nd:YAG	Neodymium-doped yttrium aluminium garnet
OBN	Oil blue N
OC	Optical connectivity
PDA	Phase Doppler anemometry
PM597	Pyrromethene 597
PMT	Photomultiplier tube
RhB	Rhodamine B
sCMOS	Scientific complementary metal-oxide-semiconductor
SD	Spray drying
SI	Spark ignition
SLIPI	Structured laser illumination planar imaging
SMD	Sauter mean diameter
SRh	Sulforhodamine 101
TCSPC	Time-correlated single-photon counting
UV-vis	Ultraviolet/visible
VR	Vibrational relaxation
vSOI	Visible start of injection

1 Introduction

"Responsible consumption and production" is one of 17 goals on the United Nations' 2030 Agenda for Sustainable Development [1]. A specific emphasis is placed on green chemistry, aiming for a minimization of health and safety risks and impacts on the environment. This objective is primarily directed at the industry, which offers a substantial opportunity regarding ecological process transitions, specifically in the areas of chemicals and waste [2]. Sustainability in related industries affects many topics, which are summarized in Figure 1. Accordingly, the principles of green and sustainable chemistry relate to the whole product lifecycle, ranging from green feedstock, ecologically benign production and potential reuse up to safe consumer products [3]. Many of the presented dimensions include the use of a solvent as a fluid for heat transfer or to carry, stabilize or dilute a specific other species. As a consequence, an important aspect in the transformation of technical processes is the use of sustainable solvents [4].
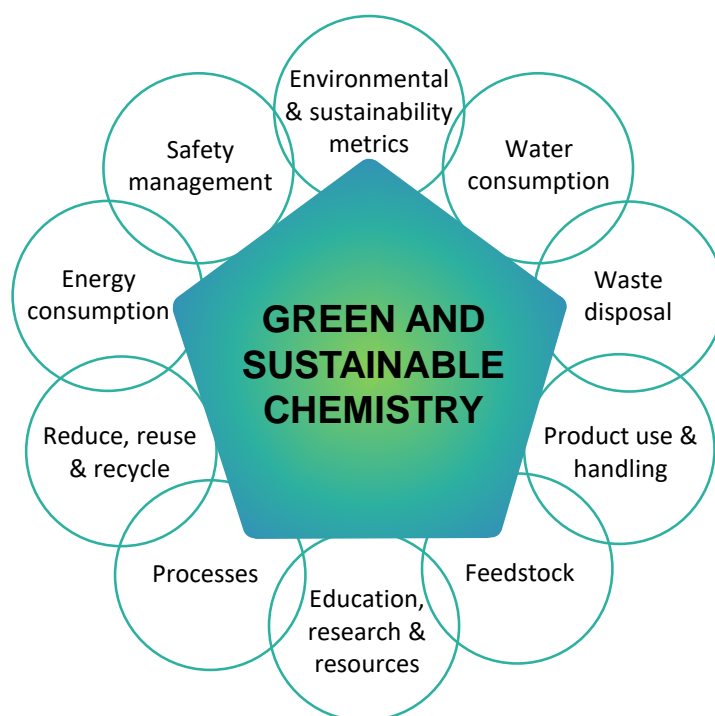

Figure 1: Sustainability and the related topics in industries with participating chemicals, adapted from Hill et al. [3].

Water and simple alcohols like ethanol are considered as so-called green solvents and substitutes for complex organic solvents, such as dioxane or toluene, with adverse impacts on human and environmental health [5, 6]. Both water and ethanol have gained relevance due to advantages like reduction of health and safety concerns during manufacturing as well as in the final product. Additionally, they offer the potential of recovery, reusability or even biodegradation, while also impacting cost efficiency [7].

Various industrial sectors utilize ethanol, water or a mixture of each as solvents and show the diversity of their appearance in industrial spray applications [8–10]. Specifically, in sprays, the transition from conventional to green solvents will affect atomization and mixing quality due to varied fluid properties, thereby altering subsequent processes like e.g. particle formation. Optimizing these processes is the key motivation of this thesis, which focuses on the development of optical, *laser-induced fluorescence* (LIF) techniques to study specific ethanol and water spray characteristics, such as temperature, structure size, and mixture composition. The relevance of such injection processes is presented in the subsequent paragraphs, providing a selection of research based on ethanol/water sprays for various widespread industrial applications.

Due to the rising awareness of environmental pollution and oil reserve deficiency, the addition of biofuels like ethanol are common practice in *spark ignition* (SI) engines. While anhydrous ethanol is commonly used, the separation of water involves a significant amount of energy [11, 12]. Therefore, substantial research is being conducted to study the impact of hydrous ('wet') ethanol on spray formation, the subsequent combustion efficiency and emission characteristics [13, 14]. Different mixtures of gasoline and anhydrous and hydrous ethanol were investigated under various conditions. Results reveal positive influences of hydrous ethanol, such as significant reductions of emissions at low loads [15] or an enhanced thermal efficiency and thus performance [14]. With further investigations of the spray and combustion behavior, hydrous ethanol is suggested as a promising biofuel alternative [11, 13].

Another successful use case of atomized ethanol and water is as a coolant. Spray cooling is implemented in high energy processes in order to enhance the lifetime of electrical components. A high performance of the coolant is achieved by its vaporization, using enhanced heat transfer due to the phase change of the liquid [16]. In order to lower the saturation temperature to optimize the cooling performance and meet ideal operation conditions of electronical devices, ethanol is admixed with aqueous sprays [17]. The liquid-phase composition is an essential parameter for the performance of the evaporative cooling [18, 17], while spray characteristics like *Sauter mean diameter* (SMD or d_{32}), droplet temperature and volumetric liquid flow are also crucial to determine the optimum heat transfer of the spray [19, 20].

Further processes like *flame spray pyrolysis* (FSP) or *spray drying* (SD) make use of the atomization and evaporation of a precursor solution, in order to synthesize particles. With the intention of advancing the procedures to operate more sustainably and

cost-efficiently, water and ethanol are gaining consideration as solvents. The adjustment of the solvent mixture ratio offers attractive effects which allow a deliberate influence on particle characteristics [21–23]. Spray drying processes in the food and pharmaceutical industries have shown the influence of varied ethanol/water contents on parameters like particle size, shape and density, as well as the amorphous content [24, 25]. By controlling the aerosol and particle performance, the addition of ethanol could be implemented without a compromise in protein or enzymatic activities [26]. Along with controlling particle characteristics, the combination of ethanol and water as 'wet fuel' is used in FSP applications, especially for the production of temperature-sensitive materials. Ethanol serves as fuel with a high local combustion temperature close to the nozzle to create a stable flame. Due to the water content, the droplet temperatures can be reduced to ensure ideal synthesis conditions and functionality of the produced particles [27].

Industrial processes, like the above mentioned, are constantly developed further to ensure enhanced product quality and reduce energy, costs and resources. Concluding from the review of spray applications, the temperature is a key quantity in sprays, determining atomization, droplet heat-up and evaporation. Liquid and vapor temperatures are closely tied to solvent properties, such as evaporation enthalpy, their boiling point or transport coefficients (e.g. heat and mass diffusion). Both, mixing and reaction rates can be controlled by the temperature and directly impact the efficiency and pollutant emissions in combustion processes. In heat exchangers, using sprays of liquid coolants, both rates affect the heat dissipation and cooling efficiency. Aiming for a better understanding and improvement of such complex spray applications, spatio-temporal in-situ parameter investigations on e.g. the temperature and concentration fields are required. Such studies pose a challenge for commonly used measurement techniques, such as thermocouples for thermometry or chemical sensors for composition determinations. However, optical diagnostic techniques offer the ability to conduct these measurements with a high degree of accuracy, precision and resolution. Numerical investigations additionally provide support in understanding complex spray fundamentals and mathematical models can be consulted to determine ideal process parameters, like e.g. liquid and ambient temperature in FSP [28]. Nevertheless, there remains a necessity to experimentally investigate and validate the parameters influencing the atomization and evaporation behavior.

While a large share of research engages with the vaporized or gas phase of sprays [29, 30], this work focuses on investigations of the liquid phase, especially in ethanol

sprays. The main aim is the development of a thermometry method, based on laser-induced fluorescence of organic dyes. Corresponding measurements were taken to gather fundamental knowledge on *two-color* (2c) LIF droplet thermometry. Experimental studies of single micrometric droplets of a tempered droplet chain are presented, which can be used as calibration or validation data in future research. Studies in additional solvents raise the question of the applicability of 2c-LIF for solvent composition investigations. Thus, LIF calibrations in binary ethanol/water droplets are realized and the results offer a prospect on future work following up on this thesis.

Using the droplet generator, complex spray processes such as droplet formation, collision, or coalescence, along with the respective disturbing optical effects, can be isolated. This allows precise observation of influences on the diagnostic method, helping to further reduce measurement inaccuracies.

Additional challenges affecting the signal strength include polydisperse structure size distributions, reabsorption effects (particularly in dense spray regions) and *morphology dependent resonances* (MDR) within spherical droplets. A possibility to accomplish measurements in dense spray regions may be the use of *two-photon* (2p) excitation for LIF. This approach is another key subject of the work with attention paid to structure sizes and how they are influenced by different fluid properties of the solvent.

This thesis comments on the fundamental photophysical processes and consolidates the relevant literature on LIF droplet thermometry and liquid-phase spray characterization. Novel data sets are presented in a collection of all peer-reviewed, published results providing key information into the application of the different LIF approaches on ethanol/water droplets and sprays.

2 State of the Art

The following section presents the current state of the art on fluorescent dye-based measurement techniques in sprays and droplets, focussing on 2c-LIF thermometry. A brief overview on the theoretical background of occurring photophysical processes, linked to the applied metrology, is given. Subsequently, the procedure of the dye selection with respect of lasing challenges in droplets is described. Finally, optical spray characterization is directly thematised and active fields of research on the used measurement approaches are addressed.

2.1 Absorption and Emission Processes

LIF is based on the absorption and ensuing emission of photons. Molecules or atoms, respectively, are shifted to higher energetic levels by the absorption of photon energy from a light source. Simply one definite energy value can be assumed for a spatially bound system at a time. Consequently, a particular molecule can only absorb specific wavelengths. At the same time the molecule gets excited, which is explained in more detail below. The relaxation back to the ground state can arise in a photochemical or photophysical way [31]. If the deactivation occurs photophysically, i.e. by emission of electromagnetic radiation, the process is called luminescence. Fluorescence as one sort of luminescence is emphasized in this work.

The absorption process of a molecule has a strong dependence on its molecular structure and more specifically the bonding theory, visualising the electron occupation in the shells around the nuclei of the involved atoms. In this work, two organic dyes, *fluorescein disodium/uranin* (FL) and *sulforhodamine 101* (SRh) are used to study the liquid behavior of a solvent by taking advantage of their photophysical properties. The dyes are both xanthene derivates and belong to fluoresceins and rhodamines, respectively [32]. When considering the fundamentals of bonding theory, the individual participating atoms form molecular orbitals for reasons of stability. In organic molecules, the molecular orbitals are depicted by linear combinations of s- and p- atom orbitals of different symmetry. This includes electrons in bonding σ and π orbitals and antibonding σ^* and π^* orbitals. Nonbonding n orbitals are occupied by electrons that do not participate in the covalent bonding. The *highest occupied molecular orbital* (HOMO) mainly belongs to the bonding orbitals, while the *lowest unoccupied molecular orbital* (LUMO) usually is an antibonding one. Therefore, organic dyes are predominantly undergoing $\pi \rightarrow \pi^*$ transitions in an absorption event. Depending on the

functional groups of the molecule $n{\rightarrow}\pi^*$ transitions are another possibility. The characterization of every electronic level is described by the total spin S and the spin multiplicity M of the occupying electrons. If all electrons are paired with antiparallel spin, the spin multiplicity is $M=1$ and the state is therefore called singlet state. In general, organic molecules in the ground state are in such a singlet state S_0, while the subscript describes the degree of excitation. If the electrons are aligned parallelly, the spin multiplicity is $M=3$ and the state is called triplet state accordingly. Compared to a singlet state of the same degree of excitation, the triplet state is located energetically lower, which will be attended to subsequently.

Figure 2 schematically outlines the interaction of light and matter in case of an absorption event with following emission of a fluorescence photon. In the case of organic dyes, the respective light source is a laser beam operating at *ultraviolet-visible* (UV-vis) excitation wavelength. One of the most commonly used lasers for applications in this range of the electromagnetic spectrum is the Nd:YAG laser. Typically, it emits *infrared* (IR) light at 1064 nm, but it can operate at the frequencies of its harmonics: 266 nm, 355 nm or – as used for the excitation of the dyes in this work – 532 nm, visualized by the green color of the absorption between two energy levels in Figure 2.
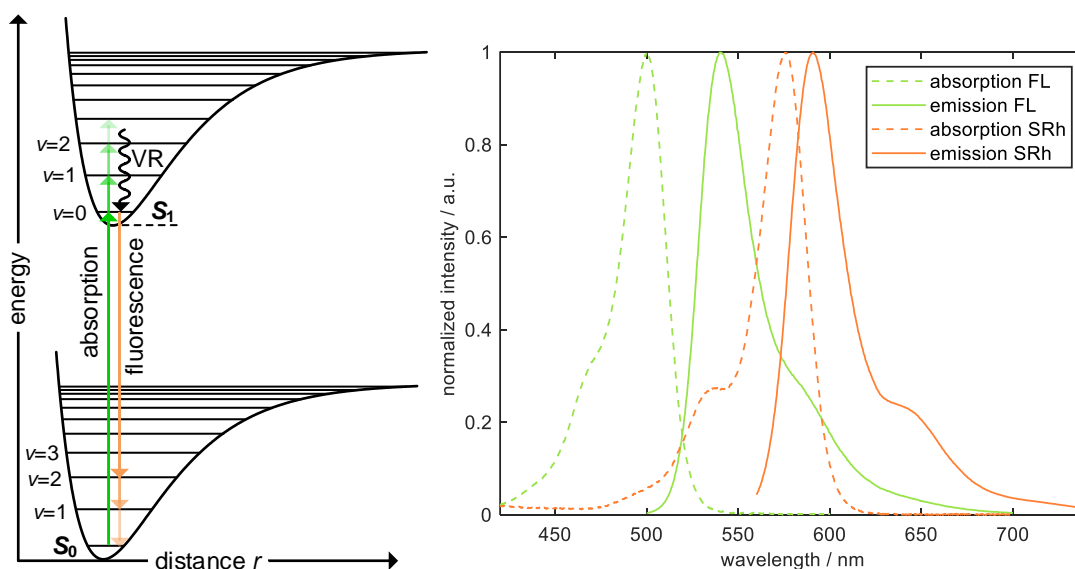

Figure 2: Franck-Condon diagram depicting the energy levels of absorption and emission mechanisms, relevant for laser induced fluorescence applications (adopted from [33]). Vibrational energy levels are visible in both electronic ground state S_0 and first exited state S_1. Exemplary absorption and emission spectra of both single dyes dissolved in ethanol, as used in this work. All spectra originate from the PhotochemCAD™ database and are normalized to their maximum [34, 35].

A molecule can occupy exactly one energy level at a time, which is characterized by its quantum numbers according to the molecules rotational J, vibrational v and electronic energy n. For dissolved molecules the rotations are limited by the solvent and additionally, the resolution of rotational states is hardly possible for large molecules

[36]. Thus, only electronic and vibrational levels are discussed further.

The left figure shows a potential curve for the electronic ground state S_0, concluding several vibrational energy levels v depicted as straight horizontal lines. Through interaction with light, photons with specific wavelengths can be absorbed by the molecule, which is then excited to its first electronic level $E = 1$. If the electrons still have parallel spins after the excitation, the spin multiplicity is unaltered and the molecule is in an excited singlet state S_1. The excited states have a short lifetime and therefore aim for an immediate relaxation back to the ground level. In S_1 the molecule can undergo *vibrational relaxation* (VR) due to collisions with other molecules. This can lower the energy to the vibrational ground state of the excited electron level, from where spontaneous photon emission – fluorescence – can occur. While the according transitions are sketched as arrows in Figure 2, they represent photons with a specific wavelength or energy, respectively. For a molecule to absorb a photon and transition from one to the other energy level, the photon energy has to match the energy difference of both levels exactly. Therefore, a spectrum presents the transition possibility over the according wavelength. Due to the molecules specific structure, each species has a unique absorption and also emission spectrum – the so-called molecular fingerprint.

The relation between the transition energy E_T and the light quantum's frequency is expressed by Bohr and Einstein via $E_T = N_A \cdot h \cdot c / \lambda$ and states the proportionality of a photon's energy to the wavelength [32, 31]. $N_A = 6.022 \cdot 10^{23}$ mol^{-1} is Avogadro's constant, $h = 6.626 \cdot 10^{-34}$ J·s is Planck's constant, $c = 299,792,458$ m·s^{-1} the speed of light in vacuum and λ the photon's wavelength. While transitioning between two electronic levels with absorption of UV-vis photons, the electron can be lifted to a random vibrational level in the excited electronical state, depending on the particular amount of energy. Consequently, instead of single lines at specific wavelengths a broadband absorption spectrum is detected, reflecting on the spacing between vibrational levels in the S_1 state. This can be observed with the green absorption arrows in Figure 2 on the left. Due to VR, the emission of the photon originates from the $v=0$ state in S_1 and thus, the fluorescence spectrum reflects the vibrational spacing in the electronic ground state S_0. The vibrational level spacing is often similar in S_0 and S_1, which results in absorption and fluorescence spectra that appear with mirrored symmetry as shown in Figure 2 (right) by the respective spectra of FL and SRh. Compared to the absorption, the fluorescence spectrum undergoes a Stokes shift, which means it is shifted towards longer wavelengths [32]. Reason for this bathochromic shift is the energy reduction

due to VR in S_1, which results in a lower transition energy during photon emission.
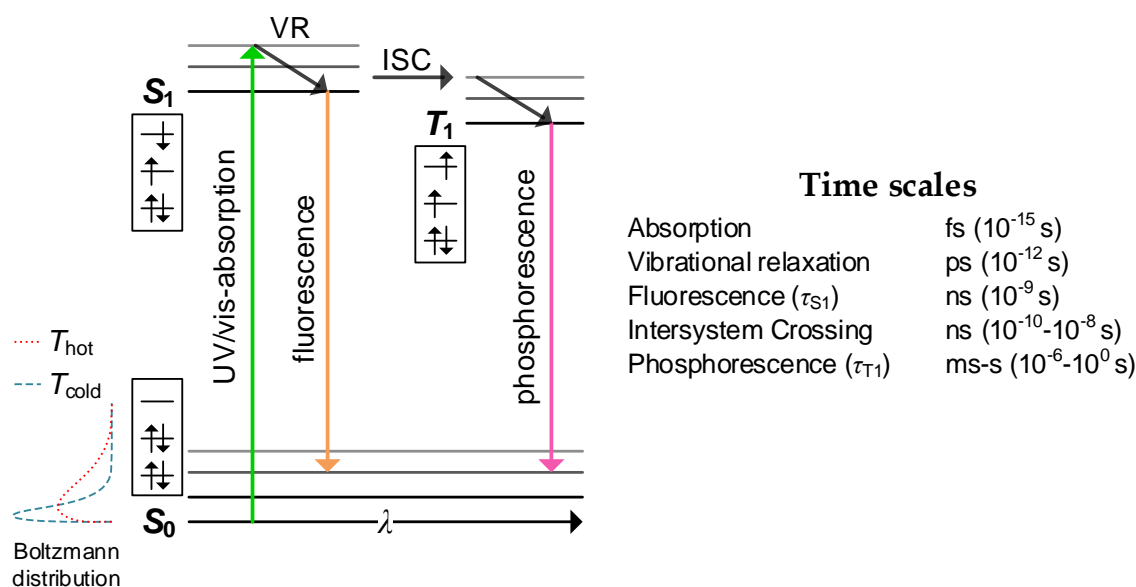

Figure 3: Transition possibilities between singlet and triplet states of a molecule. The electron configuration of the regarding states is depicted in the boxes. The Boltzmann distribution schematically shows the probability function of the energetic occupation of the vibrational levels in S_0 in a hot and a cold case. Typical time scales for transitioning processes are listed, according to [37, 32].

The energy diagram in Figure 3 further describes the excitation and radiative deactivation processes. In addition, electron occupations for S_0, S_1 and T_1 are shown exemplary and characteristic time scales for the photophysical processes are presented. The additionally included luminescence process, which originates from the excited triplet state T_1, is phosphorescence.

Contrary to fluorescence, phosphorescence is a very slow process with a longer lifetime τ, as it is a spin forbidden transition between T_1 and S_0. According to quantum mechanical selection rules, transitions between electronical levels are only allowed without a change of spin multiplicity. As the electron configurations in Figure 3 show, the singlet states are occupied with antiparallel electrons, while the electrons in the half-occupied orbitals of the triplet state are aligned parallelly. Therefore, fluorescence as a spin permitted process can happen spontaneously in a short time scale of only few nanoseconds. For phosphorescence to occur, the spin of the elevated electron needs to be reversed, which happens during emission-less *intersystem crossing* (ISC). After transitioning to an excited triplet state during ISC, VR may follow and deactivation to the electronic ground state can occur by emission of a photon. Due to the previous $S_1 \rightarrow T_1$ transition and the relaxation in T_1, the energy emitted via radiation during phosphorescence is lower and consequently the wavelength is larger as during absorption and fluorescence. This work utilizes the spectral information of absorption but primarily focuses on the subsequent spontaneous emission during fluorescence.

2.1.1 Temperature Dependence

Since both absorption and fluorescence of certain molecules can exhibit temperature-sensitive behavior, this effect can be utilized, for example, in measurements in context of the spray applications mentioned previously. In a surrounding with alternating temperatures, several processes can influence the radiation behavior. Increased kinetic energy of the molecules may intensify the molecular motion and collision rate and therefore affect the energetic state. Chemical processes such as the thermal degradation of a dye or solvent could also influence the absorption and fluorescence intensity. As for the investigated setup frameworks in this work, the temperature dependence of the dyes photophysical characteristics are the decisive factor, which is taken advantage of. Depending on the temperature, a spectral shift – mostly bathochromic or hyperchromic – is observed for some dyes. This shift is attributed to the so-called Boltzmann distribution, which describes the allocation of the molecules of one species over different molecular energy levels at a certain temperature. Thus, the distribution shows the number of molecules N, occupying certain energy levels [33]. Exemplary population distributions for a hot and a cold temperature are shown on the left side of Figure 3. A temperature increase leads to an amplified amount of occupied vibrational levels, resulting in a broader occupation distribution. This can also be observed for the excited S_1 state, causing an extension of transition possibilities. As a result of the overlapping spectral bands, the fluorescence spectra can broaden [32]. As the varying population distribution also entails a spectral shift of the absorption spectrum, an elevated absorption cross section at a specific wavelength can be the consequence. The decisive factor is the spectral position of the exciting light source relative to the absorption spectrum. In case of an intensified absorption at the specific laser wavelength, the increase of excited molecules leads to a subsequently higher fluorescence intensity (i.e. a hyperchromic shift). While this describes the most frequently observed behaviors in temperature sensitive dyes, the spectral temperature influence depends on molecular structure and how the structure is affected by a temperature change.

2.1.2 Solvent Dependence

The photophysical properties of some dye molecules can be influenced by the solvent they are diluted in. As the name suggests, the solvatochromic shift or effect refers to spectral shifts resulting from changes in the solvent environment (the so-called solvation shell) around the dye [32, 31]. Factors, such as polarity, viscosity and hydrogen bonding can alter the photon emission of the dyes. Depending on the characteristics of both the dye and the solvent, different interactions can cause a stabilization of the

energy states. During the transition between ground state and excited state, electron reallocation and often a change of the dipole moment occur [31]. Thus, interactions in the mixture can be affected and lead to a solvent relaxation. This relaxation process affects the solvation shell around a dye molecule, lowering the energy of the excited state. In highly polar solvents this results in a decrease of the excited state's energy, causing the subsequently emitted photon to have a lower energy and longer wavelength, leading to a bathochromic (red) shift in the spectrum [32].

In addition to solvent polarity, the viscosity can strongly influence the emission spectrum. High solvent viscosity can reduce rotational and vibrational relaxation processes, mitigating non-radiative decay processes and potentially resulting in hyperchromic (higher intensity) or hypsochromic (blue) shifted fluorescence emission. Moreover, high viscosity can slow down the reorganization of solvent molecules in the solvation shell. Thus, the effect of solvent relaxation is reduced, if it occurs slowly compared to the fluorescence life time [32].

Another solvent-related factor affecting the emission spectrum of a dye is solvent absorption. In contrast to the previously mentioned effects, solvent absorption does not impact the emission process itself but can prevent the detection of emitted photons. This occurs when the solvent molecules absorb light in the emitted wavelength region, decreasing the number of photons that exit the liquid and thus reducing the detected fluorescence intensity.

2.2 Dye Selection

Fluorescent dyes are used in broad spread applications, allowing the visualization of liquid properties and flows. Due to their complex and unique photophysical behavior, the dye selection requires precise spectral investigations. Therefore, influences on the analysed processes can be excluded and a correct interpretation of the detected signal is aimed for. Inspired by fluorescence microscopy in biological and medical research, various dyes have been applied for spectroscopy measurements in two-phase flows. The requirements for the spectral properties of the dyes are determined based on the measurement task and therefore, dependent on the experimental parameters. For example, in order to visualize a flow via 1c-LIF, the focus of the technique is the experimental setup and not any specific dye characteristics. In this work, 1c-LIF spray imaging is conducted via multi-photon excitation by an upfront extensively researched femtosecond laser system and detection with telecentric imaging, whereas no particular dye concept is necessary.

However, in applications of 2c-LIF, the requirements for the fluorophore can be summed up into three key criteria: solubility in the respective solvent, a minimum

effect on the solvent's inherent liquid properties, and the capability of multiphoton absorption and thus excitation at the laser wavelength. Since these factors do not require extensive preliminary studies or calibration, the following section focuses on the dye selection for 2c-LIF thermometry in droplets.

In 2c-LIF, two spectral bands are selected within the emission spectrum of the dye and an intensity signal ratio of the signals is formed, which has a specific temperature sensitivity. To achieve a high temperature dependence of the ratio, one spectral band is selected to be minimally affected by temperature, while the other is chosen to exhibit a high degree of temperature sensitivity. Considering a dye-based 2c-LIF approach, several factors are decisive for the final dye selection and need to be addressed. Important aspects can be subdivided into three main topics: photophysical properties of the dye itself and the interaction between dye and solvent, the emitted fluorescence signal in the respective type of two-phase flow and the subsequent color band/optical filter selection for the detection system.

Early on, single fluorophores were used for visualization purposes in flows [38, 39]. However, the concept of ratiometric emission detection originates from cell biology research, implementing the LIF approach for pH [40] and species measurements [40, 41]. Fluorescein [42] and *rhodamine B* (RhB) [43, 44] were the first prevailed dyes used as tracers to determine flow scalars by 2c-LIF in water and also ethanol [45]. An alternative of the technique was the use of a dye combination, e.g. RhB and Rh101, to reach a higher ratiometric sensitivity (on the desired flow scalar) [44, 46]. With further development of the measurement approach, some research focused on the characterization of different fluorophores to provide additional possibilities in the dye selection. Coppeta and Rogers presented nine different water-soluble dyes and proposed suitable dye combinations to investigate temperature and pH in flows [42]. Nonetheless, the majority of research on 2c-LIF thermometry was primarily conducted using argon ion lasers (488 nm or 514.5 nm) for excitation and the fluorophore RhB as tracer [47–49]. Rhodamine is widely used, due to its solubility in water and beneficial spectral properties for temperature determination. Sutton et al. published a review with an overview on dyes used in LIF thermometry approaches. Findings include fluorescein 27 being proposed as an alternative to RhB, offering an enhanced temperature sensitivity of the signal ratio [50]. Since then, a variety of fluorescent dyes, such as *pyrromethene 597* (PM597) [51, 52] and coumarin 152 [53] emerged in 2c-LIF research apart from rhodamine and fluorescein derivates, due to their improved solubility in oils and fuels. Mishra et al. and Prenting et al. each analysed several fluorophore/ethanol mixtures

in the UV-vis range, presenting an overview of dye characterizations with regard to their spectral properties and resulting temperature sensitivities [54, 55]. A comparable study was conducted by Chaze et al. for dyes in aqueous solution [56]. The absorption and emission spectra shown in these publications offer the possibility of an initial assessment on whether a dye is suitable for a given application.

2.2.1 Consideration of Photophysical Properties

Due to the previously addressed high temperature sensitivity, fluorescein derivates are taken into consideration. The *sodium salt of fluorescein* (FL) – uranin – provides good solubility and stability in ethanol and water and is categorized as environmentally friendly and non-hazardous. Working in the visible wavelength region with a commonly used Nd:YAG laser, the typical excitation wavelength is 532 nm. The absorption spectrum peak of FL is positioned at shorter wavelengths, see also Figure 2, which means the energy of 532 nm photons is too low (or the wavelength too high) to reach a high absorption rate. Therefore, a large LIF signal requires a relatively high laser fluence or dye concentration in the solvent. As a result of the Stokes shift between absorption and emission spectra, the laser wavelength is positioned in the central section of the fluorescence spectrum. Nonetheless, the dye offers some unique advantages, such as a marginal overlap between absorption and emission spectra, as can be seen in Figure 2. Therefore, self-absorption of the emitted fluorescence by other dye molecules in the probe rarely occurs and thus has a minor effect on temperature sensitivity. Otherwise, in case of a small Stokes shift between the two spectra, the shape of the fluorescence spectrum could be affected because of a possibly reduced fluorescence intensity in the overlapping wavelength region. This is particularly problematic in applications with varying dye concentrations, such as evaporating droplets.

For 2c-LIF, two spectral color bands, as contrary temperature dependent as possible, are determined and the ratio of both signals is formed. Approaching the measurements with a spectrometric detection method, an arbitrary filter width can be selected for the color channels to aim for a maximum temperature sensitivity of the intensity ratio. However, an imaging approach uses commercial optical filters, which define the width and position of the respective color bands. Furthermore, the data, recorded by the detection devices set up behind the optical filters can only be analysed, when the color band is wide enough to transmit sufficient signal. In the case of FL, the fluorescence spectrum, disrupted by the laser wavelength, offers only little possibility for two color bands. Therefore, a two-dye 2c-LIF technique, as introduced by Coppeta and Rogers,

is pursued. Several rhodamine derivates were presented, which are contrarily temperature dependent to fluorescein [42]. Sutton et al. suggest rhodamine derivates RhB and *kiton red* (KR) as additional dye for the use of fluorescein 27 [50]. As a result of FL pairings with RhB, KR and SRh, Chaze et al. propose a mixture of FL and SRh for further thermometry research. This combination showed minimum influence of laser irradiance on the temperature sensitivity [56].

In literature, the temperature sensitivity of the signal ratio is studied in detail as this commonly determines the dye selection for thermometry. Since this quantity is strongly dependent on surrounding factors such as the solvent, the detection device or the filter selection, a direct comparison of literature data seems inconclusive and will not be discussed in this work.

The molecular structures of both selected dyes are depicted in Figure 4. Both are based on the structure of the organic molecule xanthene. In contrast to common fluorescein, uranin is the strongly fluorescent disodium (FL) derivate of fluorescein [32].
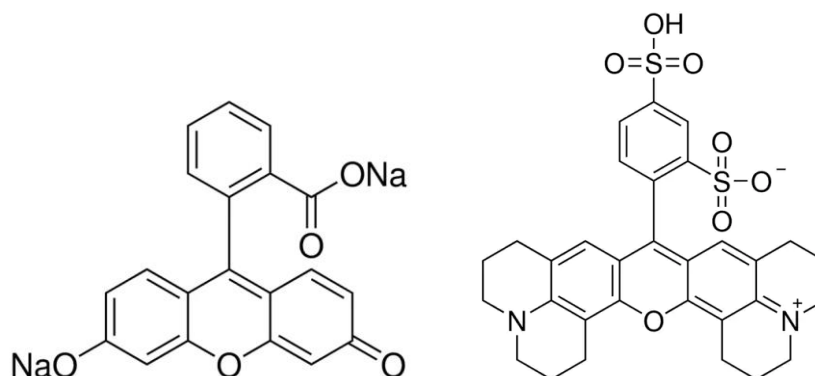

Figure 4: Structure formulas of both fluorescent dyes, fluorescein disodium (left) and sulforhodamine 101 (right).

Sulforhodamine 101 (SRh) is a derivate of the rhodamines, which also include the widespread dyes RhB and KR (sulforhodamine B). Contrary to both, the nitrogen atoms in SRh are bound in julolidyl rings, which stabilizes the molecule and leads to a reduction of non-radiative deexcitation [32]. Therefore, the fluorescence spectrum of SRh is barely temperature dependent, as confirmed by published spectra of Coppeta and Rogers and Chaze et al. [42, 56]. Due to the heteronitrogen atoms in the aromatic dye structure, polar solvents act as hydrogen-bond donating solvents and a red-shift of the SRh fluorescence is observed compared to non-polar solvents.

2.2.2 Fluorescence Emission in Droplets and Sprays

Breaking down the complex spray process, preliminary investigations are conducted

in single droplets of a monodisperse droplet chain. Thus, optical interactions with liquid structures are simplified and easier accessible, so the measurement technique can be optimized. Sprays as atomized liquids disintegrate into structures in various sizes and shapes and eventually form droplets. During the emission process fluorescence photons of different wavelengths are emitted inside the droplet. Depending on the angle they encounter the droplet boundary, single photons may exit the droplet or – with the right contact angle – total reflection inside the droplet occurs, see Figure 5. This happens because of significant differences in refractive indices of the liquid and the surrounding gas and the spherical droplet therefore acts as an optical cavity. The light waves circulate within the droplet in a ring-like pattern, along the droplet's surface. When the light waves return to their originating point in phase, constructive interference occurs, resulting in an intensity increase at specific wavelengths. These MDR appear as bright, ring-shaped structures within the droplet. Furthermore, when the droplet is illuminated unidirectionally, two bright, point-like regions become visible on opposite sides of the droplet. These high-intensity points on the droplet's surface arise from the superposition of the resonating light waves and can be observed in the single shot image in Figure 5. Numerical investigations by Frackowiak and Tropea showed similar bright regions in small micrometric droplets (below 50 µm) with fluorophores excited at a low absorption cross section [57]. This effect was reported in several LIF investigations under conditions, such as droplet size, fluence etc., comparable to this work [58, 52].
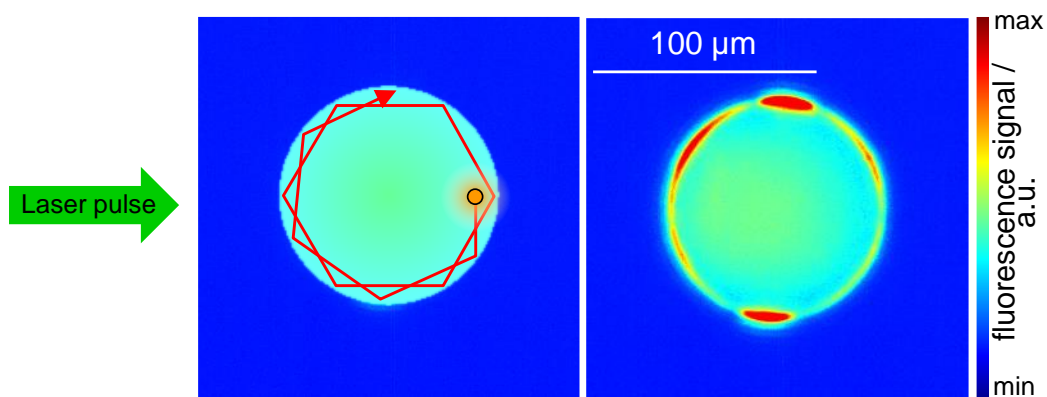

Figure 5: Schematic drawing of light traveling along the inside droplet rim (left). Single shot of a droplet with visible high fluorescence intensity points and lasing effects (right).

In regions of high MDR intensity the photon density within the droplet is maximized. Internally reflected photons encountering a dye molecule in these regions near the droplet rim can lead to stimulated photon emission in addition to spontaneous fluorescence. Contrary to this, the inner droplet region is unaffected by MDR and only

spontaneous emission occurs. However, the stimulated emission arises due to fluorescence resonance and is referred to as „MDR lasing" or simply „lasing" in the literature. Lasing is observed if the gain by the number of photons emitted through stimulated emission exceeds the inherent photon loss, which results from self-absorption and LIF signal exiting the droplet [52, 59]. Consequently, stimulated emission requires a high excitation intensity to offset these losses. The superposition of spontaneous and stimulated fluorescence produces characteristic peaks in the fluorescence spectrum. Furthermore, droplets in motion are rarely completely spherical and thus, the lasing is not a single line but occurs as a peak in the spectrum. However, apart from the droplet size, the lasing wavelength is affected by the physical properties of the dye/solvent mixture and the laser intensity [52].

As the temperature in 2c-LIF is determined with the intensity signal ratio in two spectral color channels, the high MDR signals at a specific wavelength disturb the ratio. Thus, the resulting temperature values are falsified and the measurement approach has to be adapted, to avoid detection of MDR in the first place. Perrin et al. proposed the addition of a further dye, *oil blue N* (OBN) as possibility for PM597 thermometry [51]. OBN acts as absorber in the wavelength region of the MDR signals, while it does not fluoresce itself. Palmer et al. conducted additional investigations on *enhanced energy transfer* (EET) and applied the technique to hollow-cone ethanol sprays [60]. However, the absorber also reduces the emission and alters the form of the fluorescence spectrum. Additionally, the effect of concentration changes through droplet evaporation and resulting influence of self- or reabsorption is not discussed in the study.

Additional possibilities to circumvent MDR detection without forfeiting temperature sensitivity, due to reduced emission signal, are considered. Controlled color switching is a form of EET and thus, is using another dye to absorb the emission in the lasing wavelength range. In this case the absorber dye is another fluorophore and therefore the reabsorption results in another photon emission at a longer wavelength [61]. FL shows lasing in a temperature sensitive spectral region, where the emission spectrum overlaps with the absorption spectrum of SRh, when using the combination of FL/SRh. Thus, SRh acts as absorber molecule in a mixture of both dyes and the lasing signal is shifted towards longer wavelengths. While the "switched" MDR signal could affect signals detected from the SRh spectrum, the MDR position is considered in the filter selection and hence, its detection is circumvented.

2.2.3 Filter Selection

With regard to the previously mentioned effects of spectral properties and the prevention of lasing detection, the color bands for the 2c-LIF approach are determined. While two optimal wavelength regions for a maximum temperature sensitivity of the intensity ratio are identified, the priority is the accuracy of the technique in case of changes in the measurement environment, like e.g. variations of droplet sizes. Additional focus lies on the commerical availability of the respective optical filters, each transmitting the wavelengths of one color band. In order to enhance the accuracy of the approach, several spectral conflicts need to be considered [42, 56]. As previously mentioned, FL shows very little self-absorption. In the two-dye approach, reabsorption by the other species can occur. While this effect should generally be avoided, it is intentionally used in the FL-SRh combination to prevent MDR lasing in the FL spectrum. Normalizing the ratio to a reference, a reduction of the accuracy can be prevented. Nevertheless, investigations of the ratio dependence on droplet size need to be conducted.

A further conflict relates to the overlap of respective single dye emission spectra. For the chosen fluorophores FL and SRh this applies in a wavelength region between 560 nm and 620 nm. However, the respective influence on the temperature dependent behavior of the other dye is minimal. To ensure accuracy of the approach, the concentration ratio of the dyes needs to be kept constant during all related measurements.

Resulting from the mentioned criteria and the calculated fluorescence temperature sensitivity coefficient s, two commercial bandpass filters are selected. The sensitivity can be calculated with two fluorescence signals I, each at a specific temperature T [56]:

$$s(\lambda) = \frac{\ln(I(T_2(\lambda))/I(T_1(\lambda)))}{(T_2 - T_1)} \tag{1}$$

Visualizing the influence of temperature on all individual spectral positions, it is depicted over the wavelength with a grey curve in Figure 6. Moreover, the spectra of the dye combination at 293 K and 343 K are presented. Shaded areas show the bandpass ranges of the selected color channels and respective filters. Consequently, wavelength bands between 539 nm and 568 nm, as well as 600 nm and 630 nm are transmitted onto the detecting cameras in the experimental setup and also used in the spectra processing. Additionally, the absorption spectrum of the dye couple in ethanol is shown in the graph to visualize the position of the reabsorption regime of the dyes.
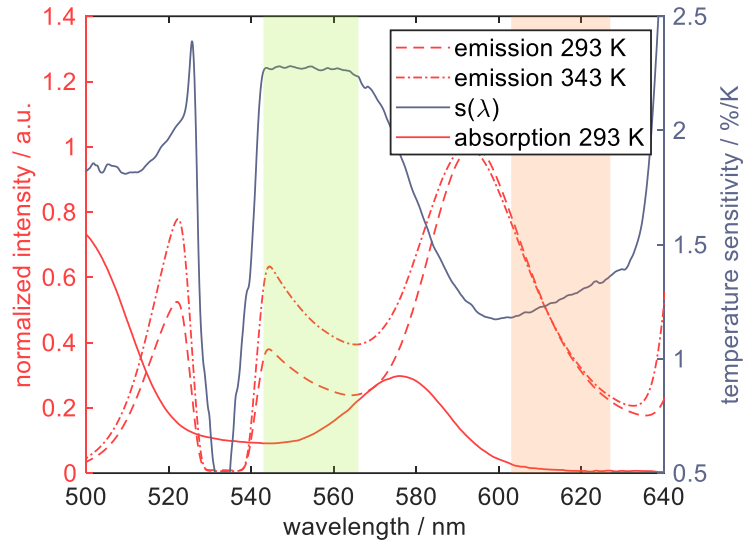
Figure 6: Normalized emission spectra of the dye couple FL and SRh in ethanol at 293 K and 343 K, depicted by the red dashed lines. The grey curve shows the calculated sensitivity, calculated from the emission signals. To demonstrate the filter selection, the absorption spectrum at 293 K is presented additionally with the solid red curve.

2.3   Spray Processes and Characterization

Sprays are one of the most complex two-phase flows, representing the interaction between liquid and gas phase with the atomization of the liquid and the subsequent droplet evaporation [62, 63]. The disintegration of a jet into ligaments and droplets is determined by various factors, such as the nozzle geometrics, liquid and gas velocity, liquid properties and many more [64]. To further characterize the spray, various variables can be experimentally determined. With the focus on the liquid phase, the breakup and evaporation processes are defined by measurable quantities like spray-associated liquid penetration and cone angle or droplet size, velocity or temperature distributions. For a more in-depth discussion on experimental approaches for sprays, please refer to Fansler and Parrish [63].

The breakup process can be divided into primary breakup, which covers the disintegration of the liquid core and the secondary decay of the ligaments and liquid structures into small droplets. Depending on the characteristics of gas, liquid and the nozzle, the primary breakup can be categorized in the four mechanisms Rayleigh breakup, 1st and 2nd wind induced breakup and atomization [65]. The classification is implemented according to a diagram, suggested by Ohnesorge [66] and adapted by Reitz [65], which depicts dimensionless quantities Reynolds number Re over Ohnesorge number Oh, see Figure 7. The liquid (L) Reynolds number represents the ratio of inertial to viscous forces. It is calculated using density ρ, dynamic viscosity η, velocity (in

this scenario the nozzle exit velocity) v and the characteristic length l, which in this case is the nozzle diameter.

$$Re_{\mathrm{L}} = \rho \cdot v \cdot l / \eta \tag{2}$$

In contrast, the Ohnesorge number describes the ratio of viscous forces to inertial and surface forces. It equally considers the dynamic viscosity η, density ρ, and the characteristic length l and additionally the surface tension σ.

$$Oh = \eta \cdot (l \cdot \rho \cdot \sigma)^{-0.5} \tag{3}$$

It should be noted that all fluid properties relate to the liquid. Covered applications of this thesis and their categorization into regimes of the Ohnesorge diagram are depicted in Figure 7. The schematics on the right side give an optical impression on the breakup behaviors. Calculations of the respective cases are further addressed in the respective publications in chapter 3. The operating points of the *direct-injection spark-ignition* (DISI) injector in P[1] lie within the atomization regime [67], whereas the droplet generator in P[2] and P[3] is operated in the wind induced region [68, 69].
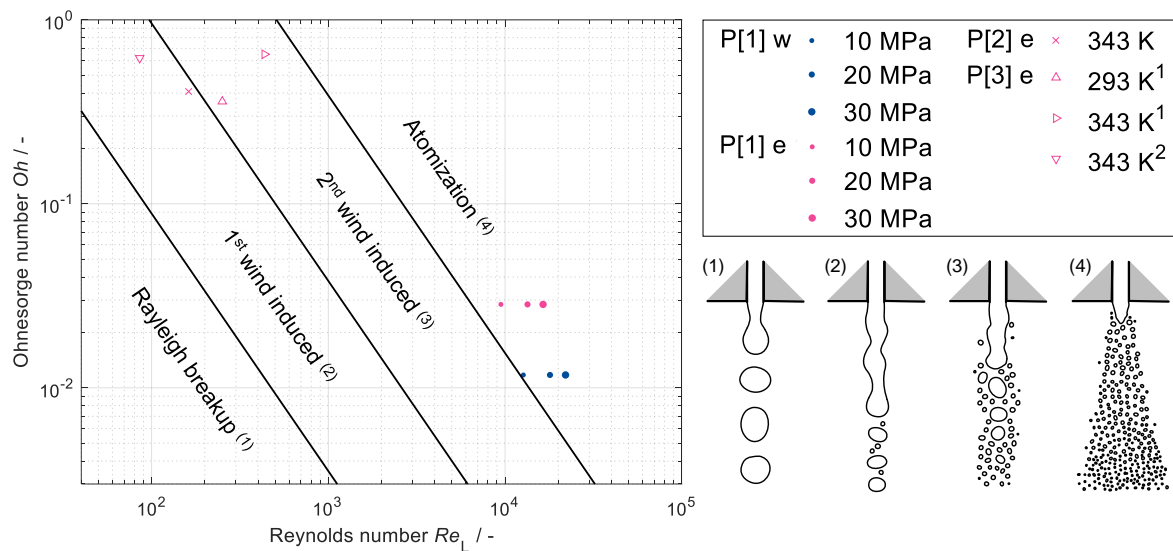

Figure 7: Ohnesorge diagram with respective breakup regions [70, 71] and marked settings of the applications, investigated within the publications in this work (left). Schematic drawings of liquid breakup in the different regimes of the diagram are depicted according to Schneider [71], from left to right (bottom right).

At high velocities, thus high *Re* or alternatively high *Oh*, atomization of the injected liquid occurs (atomization regime in Figure 7). The most current and comprehensive model describing the breakup in this regime is proposed by Fath [72], as schematically outlined in Figure 8. Dominating breakup mechanisms include cavitation due to vapour bubbles formed inside the nozzle and the interaction of the liquid jet with the

surrounding gas phase. Due to the shear forces at the interface, Kelvin-Helmholtz instabilities occur, leading to droplet displacement in the aerodynamic breakup regime. The resulting surface waves originate from initial disturbances at the liquid surface caused by turbulent fluctuations during turbulence-induced breakup.
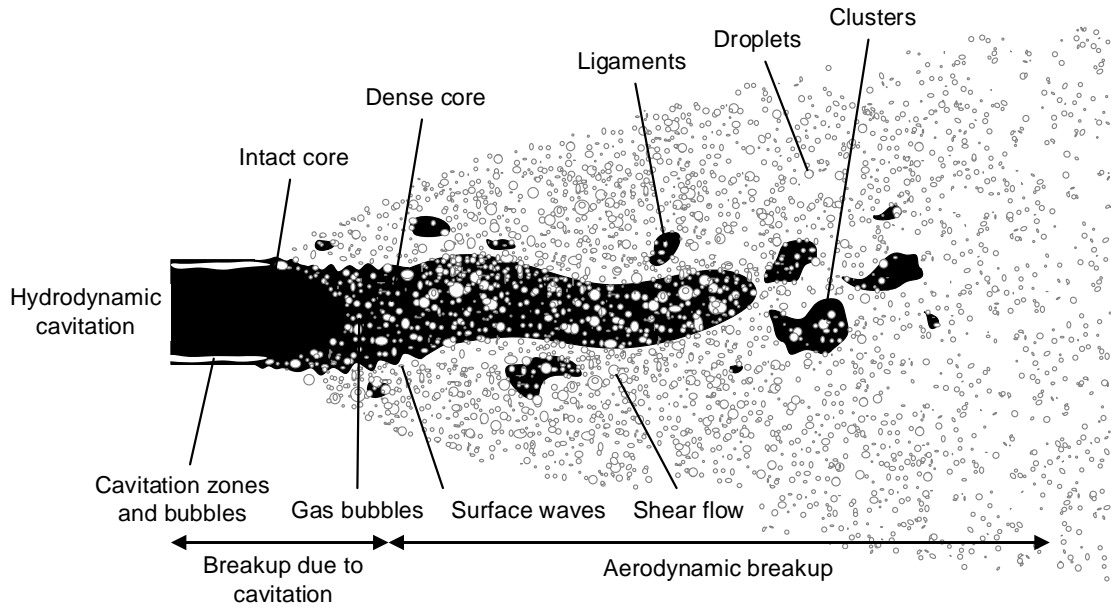

Figure 8: Spray breakup based on a two-phase flow according to Fath [72] and reprinted from Ulrich et al. 2022 [67] with permission of AIP Publishing.

Exiting the nozzle as an intact liquid core, the cavitation bubbles lead to interferences in the liquid surface, which detach ligaments in the dense core. Subsequently, secondary droplet decay results in small droplets taking on a spherical shape due to surface tension. Therefore, partial research of this thesis is conducted in single droplets.

The evaporation of single droplets is determined by simultaneous heat and mass transfer between droplet boundary and gaseous environment. While convection and conduction are predominant heat transfer mechanisms, diffusion and convection of vapor regulate the mass transfer process. Many parameters, for example droplet size, liquid and gas temperature, relative velocity of the droplets, and transport properties directly influence the droplet heating and evaporation rate [70]. Nevertheless, the evaporation process can be estimated by models, such as the infinite-diffusion model. It assumes rapid mixing and a constant temperature distribution within a spherical droplet. Therefore, no radial, but only temporal dependence of temperature is considered inside the droplet. However, in case of binary droplets, a radial dependence on the species concentration inside the droplet as a function of drop size is expected under certain injection conditions [73].

Optical, non-intrusive measurement techniques may offer access to the different spray

regions. These techniques include line of sight imaging, such as shadowgraphy, which is often used for spray visualization and investigation of sizes like the spray penetration depth or cone angle [74, 75]. Multiple diagnostic overviews describe the range of possible technologies for spray investigation [76–78]. However, high liquid structure densities in the nozzle near-field (dense core) challenge common approaches for spray characterization due to e.g. laser beam steering, multiple scattering of the signal or attenuation of laser and signal. To get further insight into the evaporation process, three liquid-phase variables of interest are droplet size, temperature and – for multi-component mixtures – composition distribution. A brief state of the art on optical measurement techniques for the determination of all three sizes in droplets and sprays is given in the following sections.

2.3.1 Spray Structure and Droplet Sizing

Droplet sizing in sprays is commonly conducted to characterize the atomization quality of a nozzle. Specifically, droplet sizing in dilute spray regions is an appropriate technique to assess the degree of evaporation in a spray. Measurement approaches range from intrusive mechanical and electrical techniques to various optical methods [70]. Optical diagnostics offer the advantage of non-intrusive investigation possibilities, depending on the respective application. Therefore, various factors, such as optical accessibility or the required precision and resolution of the result influence the selection of the measurement technique [78].

Point measurement techniques scan single locations, which can be combined to attain an overview of droplet size distributions in the spray. These single-point approaches include rainbow refractometry, which uses the behavior of light encountering a droplet and creating a rainbow pattern due to wavelength dependent refraction. Accordingly, the angle of the detected rainbow pattern is influenced by e.g. the droplet size, temperature and droplet composition [79, 80]. Another frequently applied method for drop sizing is the utilization of the Doppler shift in scattered light at a droplet in *phase Doppler anemometry* (PDA) [81, 82]. The interference structure changes proportional to the droplet's diameter, allowing for point-wise measurements within the spray structure [83].

Direct (high-speed) imaging approaches can visualize the integral spray and offers insights into shape and behavior of liquid structures. Shadowgraphy can be utilized to image the formation of liquid structures in sprays by making use of light extinction and the contrast to a backlight. An exemplary image is provided in Figure 9 (left). Dark

spray zones correspond to very dense spray regions while light-grey zones are characterized by low droplet concentrations. Due to its easy experimental setup, shadowgraphy is commonly used to determine visually measurable macroscopic and microscopic spray quantities, such as spray penetration, cone angle or structure sizes [84, 85]. Overlaps of liquid structures and single droplets may challenge such line-of-sight techniques and thus, clear visualisation is hindered in dense spray regions [86].
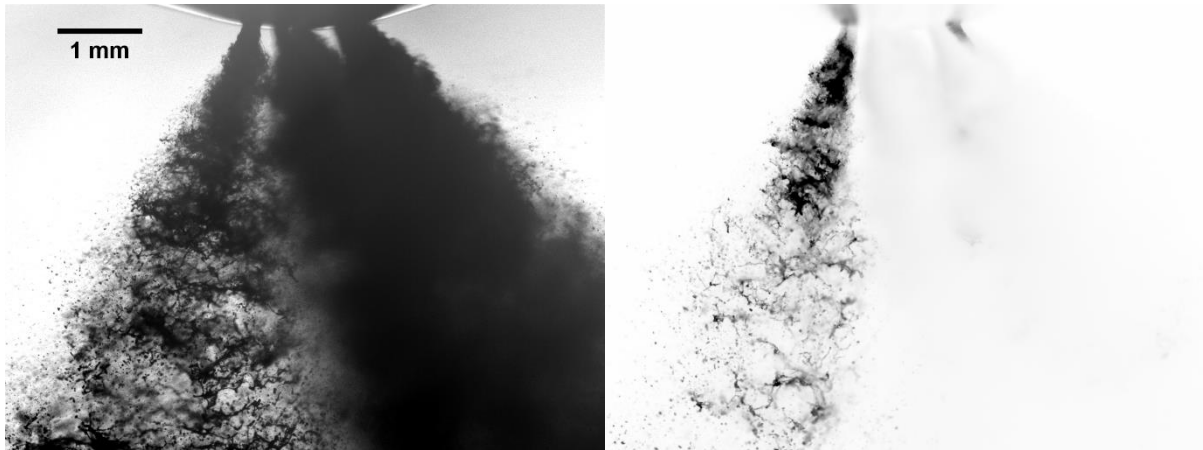

Figure 9: Comparison of a shadowgraphy image (left) and display of inverted 2p fluorescence signal (right) at 20 MPa injection pressure and at 220 μs after *visual start of injection* (vSOI). Both images are part of the publication and reprinted from Ulrich et al. 2022 [67] with permission of AIP Publishing.

Besides qualitative information on macroscopic spray quantities, planar approaches may allow the determination of the SMD over a two-dimensional section of the spray by applying a laser light sheet. Several intensity ratio techniques for planar drop sizing can be found in literature and range from Raman/*Mie-scattering* ("Mie") [87] to *laser-induced exciplex fluorescence* (LIEF)/Mie [88] and LIF/Mie [89] approaches. Each proposal is based on a d^2 (surface) dependence of the Mie signal (in case of a perpendicular polarization of the laser beam) and a d^3 (volumetric) dependence of the respective additional signal, which in ratio provide SMD information.

Nevertheless, the dense spray region in the nozzle near-field challenges all of the above-mentioned techniques due to the high droplet concentration. Single-point and line-of-sight techniques can not differentiate overlapping liquid formations in the depth of the field. Additional planar imaging methods are affected in terms of limited accuracy as well as laser and signal attenuation, due to multiple light scattering. Accordingly, detected photons originating from the dense spray region undergo multiple encounters with off-axis liquid structures, which results in a masking of the investigated spray core [90, 91]. This topic in particular is frequently addressed and various techniques have emerged to measure droplet sizes in dense spray applications, each

with its own advantages and limitations. Review papers by Coghe and Cossali [92] followed by Linne [86] present experimental proposals for imaging the nozzle near-field, not affected by multiple light scattering.

Two established transillumination (line-of-sight) methods are X-ray radiography and *ballistic imaging* (BI) [63]. X-rays radiography is based on the linear absorption of monochromatic X-rays by turbid media [93]. Furthermore, the index of refraction differs in contrast to an application with visible light, changing the physical behavior when interacting with liquid from a spray [86]. Due to this, effects like refraction and scattering can be neglected, especially in case of low photon energies of X-rays with a long wavelength [92]. BI, in comparison to X-ray radiography, is performed with ultra-short-pulsed light in the visible or near-IR wavelength range and offers an improved imaging quality [94]. The technique is based on "ballistic" photons, traveling through the spray without experiencing any scattering. Optical filters or temporal gates in the detection setup enable differentiation of ballistic (unscattered) photons, partially scattered "snake" photons and "diffuse" or "corrupted", multiple scattered photons [92] (see Figure 10 for further explanation). Consequently, ballistic and snake photons represent intact spray structures in a shadowgram [86].

With the demand for sharp, unblurred images of high-velocity spray-cores, a solution for the signal attenuation due to multiple scattering in planar techniques like LIF or Mie scattering is required [94]. *Structured laser illumination planar imaging* (SLIPI) detects several images with phase-shifted structured patterns to allow filtering of multiple scattered photons in the image post-processing [63]. The structural pattern is generated in the laser beam by the use of optical gratings and was first proposed for spray visualization by Berrocal et al. [95] and Kristensson et al. [96].

Another approach for planar imaging in dense sprays is based on multiphoton LIF and was first described by Berrocal et al. [90]. Originating in biological microscopy [97], *two-photon LIF* (2p-LIF) uses increased excitation wavelengths at high laser fluence to transfer electrons to an excited electronical level. Specifically, the combined energy of two photons, which simultaneously encounter with a fluorescing molecule, is required for the electron elevation. The process of 2p-LIF is depicted in Figure 10 in comparison to common one-photon LIF. Multiple Mie scattering of laser photons is unaffected by multiple photon absorption and occurs in both 1p and 2p techniques. Regardless, excitation wavelengths are typically not detected or processed in LIF imaging. However, the scattered laser photons distribute randomly in the spray and the probability of a

temporally and spatially concurrent interaction with a dye molecule is unlikely. Therefore, out of focus excitation and fluorescence does not occur and the detected fluorescence image represents only spray structures in the illuminated plane.
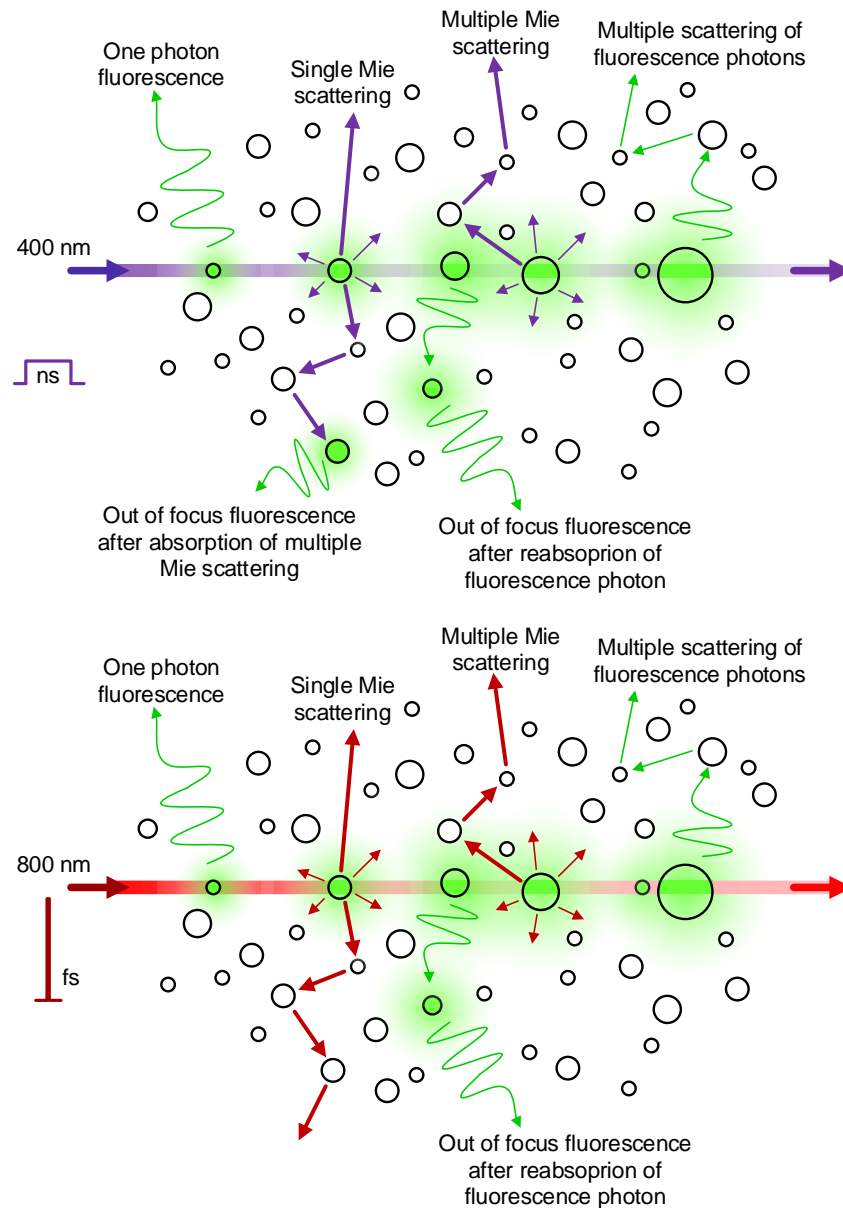

Figure 10: Schematic representation of one-photon LIF and two-photon LIF according to Berrocal et al. [90] and reprinted from Ulrich et al. 2022 [67] with permission of AIP Publishing.

Berrocal et al. proposed the application for breakup studies and applied the technique by imaging a DISI spray [90]. A femtosecond laser system is used for excitation of fluorescein in water at 800 nm wavelength. Resulting images show single ligaments, droplets and the liquid core. Specifically, the comparison with shadowgraphy and 1p-LIF images emphasizes the advantage of limited distortion in the detected 2p-LIF signal. A measurement example shows the comparison of a shadowgraphical (left) and an inverted 2p-LIF image (right) at the same injection conditions in Figure 9. 2p-LIF allows high-contrast spray imaging and precise sizing of liquid structures in dense

regions close to the nozzle. Thus, it contributes to an improved identification of liquid structures and a comprehensive analysis of the atomization in comparison to conventional fluorescence techniques. Visible by the absence of blurred (out-of-focus and high liquid structure overlap) spray regions, this advantage of the planar compared to other (line-of-sight) techniques, such as shadowgraphy, BI or X-ray radiography, is demonstrated.

Guénot et al. continued the investigations by first time combination of X-ray radiation and 2p-LIF. A similar setup to the previous study was used to image a commercial fuel port injector with water and fluorescein [91]. As a part of this thesis, Ulrich et al. conducted further investigations with the setup to visualize water and ethanol sprays of a DISI injector [67]. Focus of the study is the influence of the different liquid properties on the structure sizes in the spray. The publication is included in this thesis and for further information it is referred to section 3.1. Similar imaging was conducted just recently by Vegad et al. with the aim of characterizing the early stage atomization of a swirl atomizer [98]. Therefore, 2p-LIF images are processed in regard to the surface curvature distributions of liquid structures and verified by PDA measurements. For illumination, PM567 is used as fluorophore diluted in n-heptane as fuel substitute.

A combination of 2p-LIF and *optical connectivity* (OC) is described by Wang et al., providing more extensive information on the spray [99]. The new approach is introduced for the study of liquid jet surfaces with nanosecond excitation at 1064 nm. Investigations are conducted with a water/RhB mixture, injected by a specifically manufactured nozzle, coupling the laser into the liquid jet. Originating through the nozzle, laser excitation in spray direction is used in OC, which disables the application for commercial injectors. However, due to the illumination direction the majority of laser photons is trapped inside the intact spray core and leads to emission by the dye molecules. Consequently, the atomized liquid structures and droplets around the liquid core show only minimal fluorescence signal. As a result, 2p-LIF imaging and especially the combination with other imaging techniques, such as X-ray radiation or OC, delivers valuable information on spray processes.

2.3.2 Determination of Mixture Composition

Multicomponent sprays and droplets pose a challenge in fundamental research regarding the increased complexity of the evaporation process. Therefore, many numerical approaches of droplet vaporisation are based on the assumption of uniform species

distribution in the liquid phase [100, 101]. In reality, different quantities (such as volatility) of individual species in multicomponent mixtures indicate the effect of preferential evaporation. Therefore, component distributions in the liquid phase reveal crucial details on differential vaporisation. Regarding measurements for composition determination, only little research is conducted in spray or droplet systems. Especially for ethanol/water systems, most investigations refer to sessile, mm-sized droplets of binary composition evaporating from different surface materials [102–104]. The investigations focus on image processing and measure droplet volume, radius and contact angle, which show a dependence on the component ratio.

Another technique, applied for measuring the mixture vaporisation of ethanol/water droplets on a substrate is time resolved IR-spectroscopy [105]. However, no spatial composition distribution can be determined with simple configurations, due to the line-of-sight arrangement of light source and detector. For this purpose, a more complex setup would be required to realize a detection from several perspectives. Furthermore, temperature dependencies of the absorption bands must be considered.
Hopkins et al. proposed a method, combining spectral LIF and *cavity enhanced Raman scattering* (CERS) to determine droplet size, temperature and composition near the surface [106]. While the investigation demonstrates the temporally resolved behavior of the droplets, the setup uses different light sources and a simultaneous implementation to visualize the size distributions in spray applications seems very complex.
Additional approaches, such as rainbow refractometry, are suggested for component investigations in droplets of different species. Ni et al. for instance, studied the dependence of the refractive index on composition and used experimental results for the validation of simulations [107].

Successful imaging of the mixing dynamics of two liquids in microfluidic droplets was published by Zeng et al. [108]. The fluorescence lifetime differentiation between the two fluorophores Alexa 430 and Lucifer yellow (each dissolved in one liquid) allows the reconstruction of the mixing process in the droplet. Nevertheless, for preferential evaporation in sprays instead of droplets, the majority of published research is conducted in the vapor phase. For instance, quantitative investigations of vapor mass distributions on binary component fuel sprays are presented with a UV-vis *laser absorption spectroscopy* (LAS) technique [109, 110].

Furthermore, fluorescence imaging approaches are designed to separate spatial distributions of vaporized multicomponent fuel species [111–113]. Gas-phase tracer LIF is

based on the 2c-LIF technique, using two cameras, which each detect the fluorescence of one tracer. Both tracers are selected, to match the evaporation behavior of one of the contrary volatile fuel components.

First proposals for a similar approach, of using 2c-LIF for measurements in the liquid spray phase were published by Koegl et al. [114, 115]. Spectral studies on n-decane/butanol mixtures using Nile red as solvent-dependent fluorophore are presented. Conducted in a cuvette, the measurements focus on the characterization of the spectral shift of Nile red in different mixture compositions. Two color channels are selected and the signal ratio is calculated to form a calibration curve [114]. Similar investigations are performed for a fuel/water emulsion with the dye Eosin-Y. In order to improve the miscibility of water in fuel, the emulsion is blended with ethanol. Images of the coefficient of variation are depicted for various mixtures, detected in a flow cell [115].

The combination of ethanol and water as investigated biofuel (hydrous ethanol) and admixed to fuel represents one of the motivations of this work. However, this thesis emphasizes 2c-LIF thermometry, which is the decisive factor for the dye selection. Therefore, the selected dye combination of FL and SRh in ethanol and water droplets is additionally analysed to examine the possibility of composition determination in liquids.

2.3.3 Thermometry

LIF thermometry in two-phase flows, such as spray or droplet systems, is the core topic of this thesis. Therefore, the majority of research related to liquid-phase dye-LIF is already mentioned in chapter 2.2 regarding the utilized dyes. However, other optical, non-intrusive techniques for determination of temperature distributions in liquid flows are briefly reviewed in the following paragraph. Several studies on 2c-LIF are recapitulated, with an emphasis on the respective setup and application. For detailed descriptions on the methods and their developments, reference is made to review articles, such as Lemoine and Castanet [116].

Regarding the methodology, the techniques can be categorized in relation to the interaction of laser photons with the liquid. As mentioned above, photoluminescence is a process, based on the absorption of excitation photons by a species, admixed tracer or particle in the liquid and includes both, fluorescence and phosphorescence. Both processes can be used for thermometry in respect of the emitted signal (ratiometric 2c-

method) or the lifetime of the signal. The phosphorescence techniques exploit the photophysical behavior of phosphor particles, which are added to the examined flow. Applications in liquid and gas flows are widespread and phosphorescence is an established method, which is described in detail in comprehensive review articles, such as Abram et al. [117]. As to measurements in the liquid phase of sprays and droplets, phosphorescence techniques are challenged by the instantaneous systems in regard to signal intensity, as well as spatial and temporal resolution. Investigations of droplet temperatures have been performed in mm-sized water or methanol droplets, respectively [118, 119]. However, Omrane et al. reported a non-uniform particle distribution inside the droplet [118] and discussed, if the luminescence of phosphors could also be detected in the gas-phase after evaporation of the liquid [120]. Thus, the size of the phosphors could lead to imaging difficulties in the µm-sized structures, as they are investigated in the present thesis. However, phosphorescence thermometry is successfully applied to jets and sprays, although low signal levels pose a challenge [121]. Consequently, increased exposure times of the detection devices lead to a temporal averaging of the instantaneous spray process [122].

Other thermometry techniques make use of elastic or inelastic scattering of photons. Elastic scattering processes exclude a change in the wavelength, but entail only the photon trajectory. Rainbow scattering for instance, exploits the sensitivity of the refractive index on parameters like temperature or composition (see also section 2.3.1). While standard rainbow refractometry is only applicable to spherical droplets, *global rainbow refractometry* (GRR) was proposed by van Beeck et al. [123]. The method is based on the detection of an average rainbow, consisting of the signal of at least 1000 droplets. Therefore, investigations of non-spherical liquid structures can be obtained by GRR, although they result in a mean temperature with slightly reduced accuracy [124].

In inelastic scattering processes, the photon experiences a change of impulse and an energy reduction. Raman spectroscopy is based on the respective, temperature-dependent spectral shift, which primarily can be observed for hydrogen bonds in liquids. Respectively, various studies on water sprays and droplets are based on the detection of the OH stretching band shift [125, 126]. Furthermore, a detection of spontaneous Raman scattering was applied to ethanol sprays, generated by a DISI injector by Mueller et al. [127]. To obtain spectra according to a specific spray region, the detected signal is averaged over multiple laser pulses to achieve a sufficiently high intensity. When measuring in such evaporating systems, typically the spectra contain signal of liquid and gas phase. Moreover, due to a polarization dependence, the technique is

limited to spray regions without occurrence of multiple scattering.

Fluorescence-based thermometry concepts offer the possibility of planar temperature distribution imaging in liquid structures. Although the addition of fluorophores is essential, the dyes can be completely dissolved in respective solvents without compromising the flow. Nevertheless, current LIF methods are endowed with limitations, which require continued research to finally aim for an unobstructed application. For a detailed state of the art review, Lemoine and Castanet presented a work, combining thermometry and composition measurements in sprays [116]. Additionally, a more recent summarization on LIF-based temperature determination was published by Eghtesad [128]. The development of LIF thermometry measurements in ethanol and water droplet systems is briefly outlined in the following section.

As stated before, temporally- and spectrally-resolved luminescence processes can be used for temperature measurements. Fluorescence lifetime approaches are based on the temperature-dependent exponential decay of emitted photons after excitation. Although the method is commonly applied in other fields of research, such as microbiology, studies on spray or droplet measurements are rare [129, 130]. Only recently, Stiti et al. proposed *time-correlated single-photon counting* (TCSPC) as a technique for time-resolved detection of mean water spray temperatures [131].
However, various research groups investigated the spectrally-resolved fluorescence in ethanol and water two-phase systems. The application of LIF to study evaporation processes with thermometry was introduced by Lemoine et al. in RhB-doped, turbulent water jets, detected by a single *photomultiplier tube* (PMT) [43, 49]. Subsequently, 2c-LIF was presented as an optimization of the technique for independence on factors such as probe volume and laser intensity [48]. The ratiometric concept puts two detected spectral signals into relation, as applied to ethanol droplets and a detection system using two PMT [47]. As a result, many investigations established this thermometry concept for different flow systems and various liquids [132, 51, 133]. To gather further insights into the emission spectrum, Hopkins et al. analysed binary ethanol/water droplet temperatures by splitting the detected signal with a diffraction grating [106]. A similar detection concept showed a spectrograph, which was coupled to a *charged coupled device* (CCD) camera to detect temperatures in ethanol droplets with focus on EET using an additional absorber dye [52].

While the described techniques offer a point-wise detection, 2c-LIF with imaging by a camera system was, to the authors best knowledge, first proposed by Düwel et al.

[134]. Two intensified CCD cameras allowed spatially resolved two-color thermometry in an ethanol spray flame. According to the respective applications, the imaging approach was further adjusted in terms of selected dyes, filters and the excitation source. Prenting et al. published averaged temperature visualizations of an ethanol SpraySyn burner flame [55]. Thermometry on a turbulent water jet was shown by Chaze et al. with the same dye concept, used in this thesis [56]. In a subsequent work, the temperature of impinging water droplets could be imaged [135].

However, the presented two-phase flows challenge the technique in the matter of multiple scattering in dense spray regions, reabsorption effects of dye molecules, MDR effects at the droplet rim or low signal intensities in μm-sized droplets. As reviewed in chapter 2.3.1, some methods are proposed to overcome scattering effects in the near-nozzle field and first attempts are made to combine those techniques with LIF thermometry. Mishra et al. investigated the application of SLIPI in combination with 2c-LIF measurements in a water spray [136]. Just recently, Stiti et al. published first measurements of tempered water in a cuvette by 2p-2c-LIF with two *scientific complementary metal–oxide–semiconductor* (sCMOS) cameras [137].

In conclusion, many approaches emerged in recent years, which were successfully applied to respective two-phase flows. Nevertheless, most concepts focus on the optically dilute spray regions and their respective challenges, while neglecting other effects and sources of error that occur in the complete system. This highlights the necessity of further development in LIF thermometry, but concurrently shows the potential of the technique.

3   Results and Publications

Investigations of sprays and droplets with the previously described LIF techniques present the core of this thesis. While the analysis of the solvents ethanol and water was prioritized in all measurements, the centre of the work is the development and optimization of the applied diagnostic methods. Therefore, according studies were conducted in cooperation with different institutes (Lund University, FAU Erlangen-Nürnberg, UniBw München) and researchers with the results published in several scientific journal contributions. The present thesis "Advanced Fluorescence Spectroscopy for Quantitative Liquid-Phase Analysis in Green Solvent Spray Processes" is based on the three peer-reviewed publications, which are attached in the Appendix as listed below:

P[1]   Ulrich H., Lehnert B., Guénot D., Svendsen K., Lundh O., Wensing M., Berrocal E., Zigan L.
Effects of liquid properties on atomization and spray characteristics studied by planar two-photon fluorescence
Physics of Fluids, Volume 34, 2022.

P[2]   Ulrich H., Sigl S., Möhnle M., Berrocal E., Zigan L.
Droplet thermometry based on an optimized two dye two-color laser-induced fluorescence concept
Frontiers in Physics, Volume 11, 2023.

P[3]   Ulrich H., Weiß R., Zigan L.
Two-dye two-color laser-induced fluorescence spectroscopy on droplets of green solvent water/ethanol mixtures for thermometry and mixture composition
Experiments in Fluids, Volume 65, 2024.

Further journal publications and conference proceedings with related topics, which emerged during the period of the present thesis, are listed in the Extended List of Publications below the Appendix.

3.1   Structure Sizing in Ethanol and Water Jets

Publication 1

Femtosecond laser excitation is explored in order to visualize a DISI spray doped with fluorescein by detecting the fluorescence signal without the influence of multiple scattered excitation photons. For this purpose, a specially designed laser system [138] is operated to produce 38 fs pulses at 800 nm to create a laser light sheet. Thus, the illuminated plane of 100 μm thickness and with 10 mJ pulse energy is led through one of the six spray plumes. As described in chapter 2.3.1, the longer excitation wavelength requires two simultaneously present photons to attain electron transition to an excited state. Therefore, absorption of scattered laser light by dye molecules in droplets outside the focal plane is practically unattainable. However, out-of-focus fluorescence can occur due to reabsorption and scattering of emitted photons. Figure 11 shows a comparison of 2p-LIF images in ethanol and water at the same injection conditions. The possibility of identifying and sizing single liquid structures is provided by the planar imaging technique with reduced multiple light scattering in 2p-LIF.
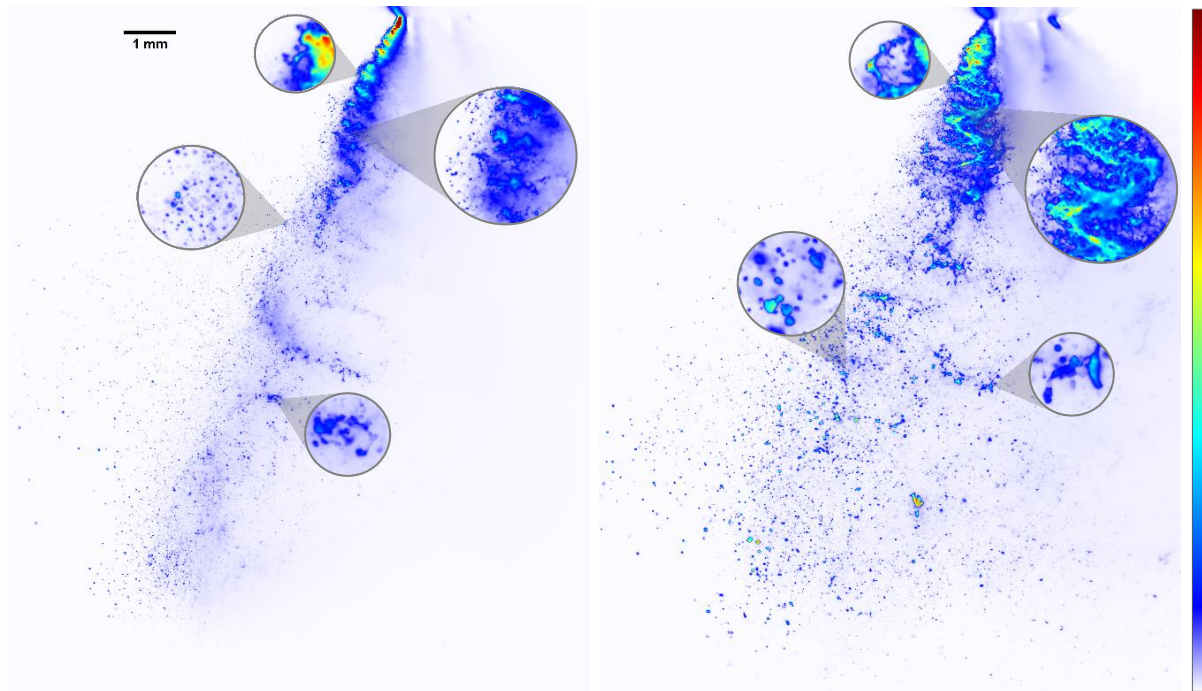

Figure 11: Comparison of liquid structures in ethanol (left) and water (right) sprays, injected with 20 MPa into ambient air and detected 520 μs after vSOI. Adapted and reprinted from Ulrich et al. 2022 [67] with permission from AIP Publishing.

In this publication P[1], quantification of liquid structure sizes with focus on the influence of liquid properties on spray formation is conducted. For the first time, according investigations are realised in dense near-nozzle regions of spray at technically relevant conditions. Both, sprays of ethanol and water injected at different fuel pressures

are imaged by a telecentric camera system covering the approximately 20 mm large illuminated spray section. Due to the formation of mostly non-spherical droplets in the nozzle near field, structure sizes are quantified by evaluation of the Feret's diameter. This quantity is defined by the maximum two-dimensional distance of a liquid body. Additionally, the cone angle in the nozzle-near spray is studied. Both variables are analysed in regard to distance from the nozzle, but also as a function of injection pressure.

3.2 Thermometry Approach for Ethanol Droplets and Sprays

Publication 2

Based on the obtained structure size information, further knowledge on temperature distributions in sprays is beneficial to acquire more detailed understanding on the evaporation and mixing process. Therefore, 2c-LIF is considered as technique for temperature studies in the liquid phase of sprays. For calibration purposes and due to manifold optical effects occurring at gas-liquid interfaces, single droplets are investigated as section of the complex spray system. Due to increased distances between individual droplets in a droplet chain, multiple scattering plays a minor role. Consequently, fluorescence excitation by single-photon absorption is sufficient in such configurations with individual droplets.

For a considerate dye selection an extensive literature review on fluorescent dyes including their photophysical behavior is conducted initially. Accordingly, the basic fluorophore concept is adapted from Chaze et al., using a two-dye combination proposed for water [56]. In the present work, this technique is optimized, using the FL and SRh dye-combination in ethanol. Compared to one-dye concepts, advantages of the two-dye approach include an enhanced temperature sensitivity, signal independence on evaporation-related concentration changes and EET by MDR absorption of the second dye.

Focus of the publication P[2] is the advancement and application of an imaging method to realize first time droplet temperature measurements in small micrometric ethanol droplets on a single shot basis. Additionally, the integration of a fibre-coupled spectrometer as point-wise, spectral detection system allows further insights into spectral fluorescence shifts and the nature of lasing effects. The circumvention of MDR detection in the fluorescence images enables significantly improved accuracy of the 2c-LIF thermometry technique. Figure 12 shows a schematic drawing of the setup around the

temperature-controlled, monodisperse droplet chain. Laser pulses at 532 nm are generated by a pulsed Nd:YAG laser with a fluence of 2.7 mJ/cm^2 to achieve fluorescence in the 100 µm-sized droplets studied.
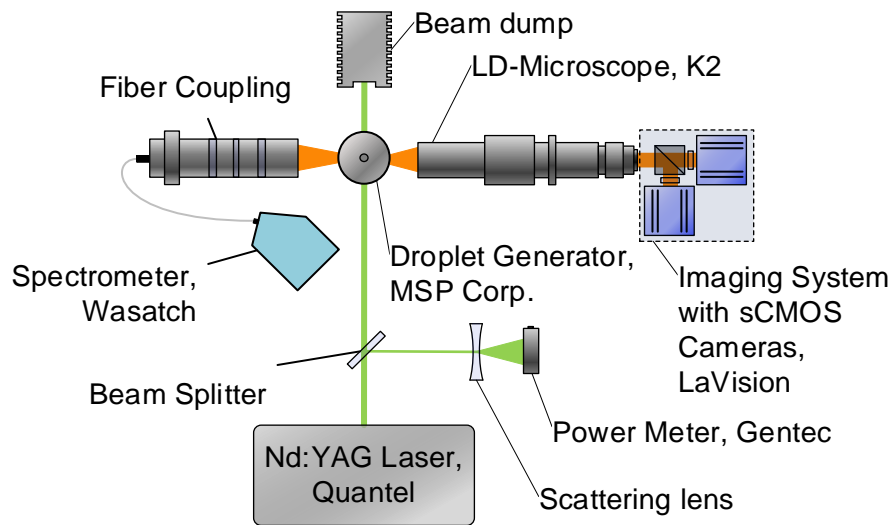

Figure 12: Schematic assembly around the droplet generator, including laser, microscopic imaging and spectral detection system. Optical setup reprinted from Ulrich et al. 2023 [68] with permission of Frontiers Media.

While calibration measurements are taken at a fixed position below the nozzle of the droplet generator, a further heat transfer and evaporation study alongside the droplet chain is conducted. In case of 100 µm sized droplets, the solvent exits the nozzle as a liquid core. This dripping of the liquid jet can be expected to fall within the wind induced breakup region of the Ohnesorge diagram (Figure 7) and can be observed in exemplary single shot images of different positions downstream the nozzle exit in Figure 13.
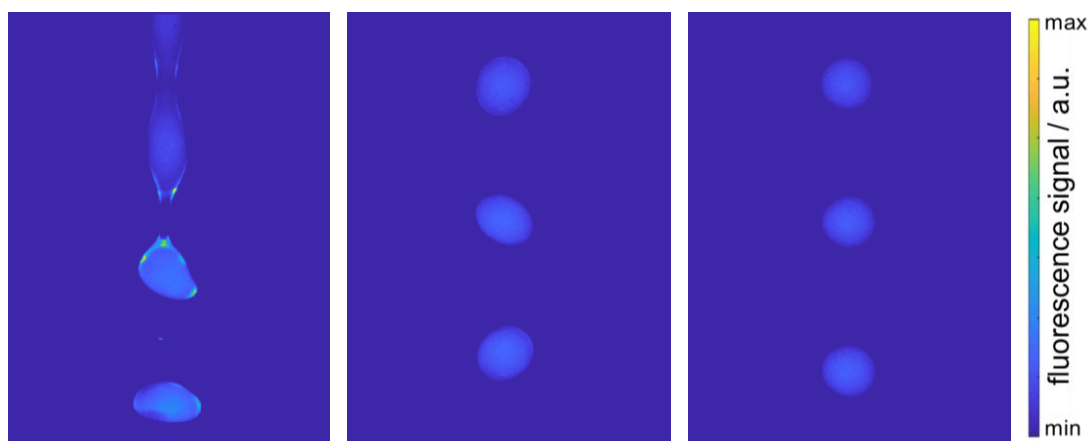

Figure 13: Exemplary single shot images of the liquid jet breakup during monodisperse (100 µm) droplet chain formation at distances of 0.5 mm (left), 2 mm (center) and 5 mm (right) to the nozzle exit.

The publication presents the method development, including the selection of dyes, concentrations, settings and optical components such as filters. Calibration measure-

ments are conducted in monodisperse droplets and results of the two detection systems are compared. Finally, the imaging system is used to assess the temperature progression alongside the droplets chain. Therefore, the two spectrally separated intensity images are mapped to form a pixel by pixel ratio imaging. Furthermore, the temperature reduction in the droplet by convective heat transfer are compared to results of a lumped capacitance model.

3.3 Limitations and Possibilities of 2c–LIF Method

Publication 3

Comparing the imaging with the spectral detection method, the previous publication P[2] demonstrated only minimal deviation in the temperature-dependent signal ratio. Therefore, the spectroscopic detection system is used as primary means of investigation in this publication P[3], while the previous studies focused on the imaging technique. This is based on the spectral, point-wise measurement approach being more cost-effective and providing enhanced accessibility to technical spray processes.

Building upon the foundation of the preceding method development, the measurement technique is examined from a more comprehensive perspective. In this context, the concept is tested for a temperature measurement application in water, as additional solvent. Evaluations of detection limits are conducted for the examined solvents within the operational droplet size range of the droplet generator. Specific focus is placed on low-fluorescence signal droplets with initial sizes between 30 µm and 50 µm.
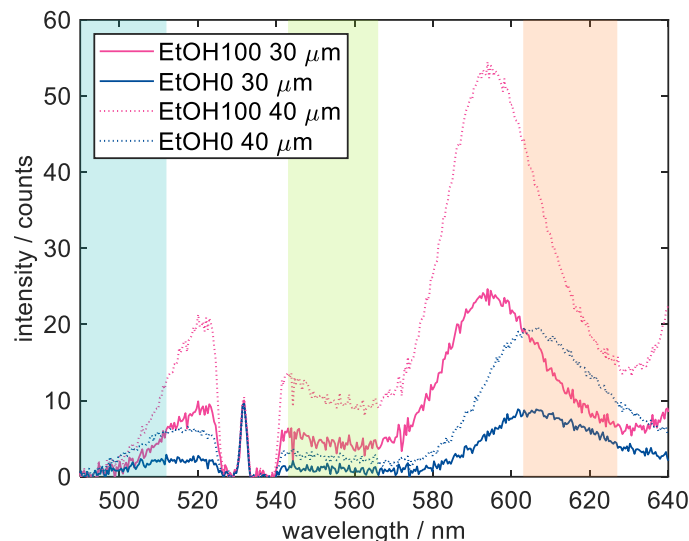

Figure 14: Base-line corrected emission spectra of ethanol (EtOH100) and water (EtOH0) in 30 µm sized, compared to spectra in 40 µm sized droplets. The spectral shift between the two liquids is visible, especially in the "orange" color channel.

Figure 14 demonstrates the investigated signal dependence on the droplet size with

exemplary emission spectra of 30 μm and 40 μm sized water and ethanol droplets. The challenge of LIF detection in processes of polydisperse structure sizes is indicated by the low signal intensity and correspondingly relative high noise in small micrometric droplets. Nevertheless, a comparison of calibration curves for differently sized droplets confirms similar behavior. Therefore, the approach is tested in a polydisperse droplet environment, measuring liquid-phase temperatures along the axis of an atomizing jet, produced by the droplet generator operated at high focussing air flow rates. Ethanol jets of different initial temperature and liquid flow velocity are studied at several positions downstream the nozzle. Resulting temperature progressions are discussed for three injection conditions. The influence of convective heat transfer is considered by calculations according to the lumped capacitance model [139].

In addition to ethanol and water, binary droplets are analysed regarding the applicability of the approach in mixtures of each. Apart from the lower intensity in droplets of high water fraction, a composition-dependent spectral shift is observed in the selected color bands (depicted in Figure 14). Consequently, the binary ethanol/water mixtures are analysed to evaluate the possibility of mixture fraction determination via 2c-LIF. A concept is proposed, which uses a third color channel (blue in Figure 14) to explicitly allocate intensity ratios to the mixture composition in binary ethanol/water droplets.

4 Conclusion and Prospect

In this work, LIF techniques were enhanced in order to access and analyse the liquid phase of transient two-phase systems. Applied to droplets and sprays, these methods allow the investigation of atomization, heat transfer and evaporation processes and measurements of relevant parameters, such as temperature, structure sizes and mixture composition. This leads to an improved understanding of the fundamental phase transition from liquid to gas phase, which can additionally enable process optimizations in industrial spray applications and support the development of models and numerical simulations. The presented studies focus on concepts for the green solvents ethanol and water, aiming for greater sustainability while providing the potential for reuse and improved health and safety measures.

This thesis presents the most common applications of ethanol/water sprays and emphasizes their necessity. The benefits of optical measurement techniques for spray analysis and the corresponding theoretical fundamentals of photophysical processes were demonstrated. A literature review of investigation approaches for liquid-phase parameters in droplet and spray systems was provided in the context of the current state of the art. This includes a description of spray processes such as breakup behavior and atomization, as well as the challenges these processes pose for measurement concepts. Regarding the fluorescence measurement techniques, special attention was given to two methods, namely 2c-LIF and 2p-LIF. The centre of the work addressed the optimization and application of these LIF methods within three peer-reviewed publications.

The application of 2c-LIF for thermometry in technically relevant sprays requires further optimization of the concept, particularly regarding the dyes, filter selection and temperature calibration. Therefore, fundamental investigations of the photophysical fluorophore behavior in the respective solvent and present liquid form support the enhancement of the ratiometric two-dye approach. For initial conception studies within this work, the system was limited to spherical droplets of ethanol as solvent. Temperature-dependent studies of the single dyes FL and SRh, as well as the dye combination mixed with ethanol were conducted for absorption and emission information. While the absorption behavior is primarily relevant at the excitation wavelength of 532 nm, a first impression on temperature dependent spectral shifts was provided. Accordingly, a high temperature sensitivity could be observed in the absorption spectrum of FL. In contrast, SRh showed a contrary temperature dependence with a slightly decreasing absorption peak in the spectrum.

The subsequently measured fluorescence spectra were recorded by a spectrometer setup from monodisperse, 100 μm sized droplets at temperatures between 293 K and 343 K. Normalized to the SRh peak, the spectra in the region of the FL peak revealed a relative signal increase of more than factor 1.5 for the 50 K temperature difference. Due to the possibility of spectrally monitoring the droplet signal, occurring lasing effects at the phase boundary of the droplet could be allocated to a specific wavelength region. Those MDR effects can majorly influence the fluorescence signal and therefore lead to a falsification of the measured temperature data. Nevertheless, the signal could be spectrally separated from the relevant dye fluorescence information and thus, a considerate selection of optical filters could circumvent the detection of the respective spectral region with the imaging setup. The resulting calibration curve was obtained by a linear fit to the temperature-dependent ratios of two spectrally distinct intensity signals – each covering a region of the spectrum corresponding to one dye. In case of the imaging system with two sCMOS cameras, a temperature sensitivity of 2.02%/K was achieved.

A first application of the 2c-LIF imaging approach was conducted, studying the evaporation of a heated droplet chain of 100 μm diameter in an ambient surrounding during the first 10 mm after nozzle exit. Between 2 mm and 9 mm the measured temperature revealed a nearly constant decrease. In this region, a temperature change of 17.7 K was observed due to evaporation and heat transfer with the surroundings. Using a model for uniformly mixed droplets with fast internal heat conduction, approximately 7.3 K of the temperature decrease could be attributed to heat transfer. However, this study only considered 100 μm sized ethanol droplets. To verify the applicability of the 2c-LIF approach in polydisperse droplet environments, which are relevant for industrial spray applications, further evaporation measurements were conducted in ethanol jets. Therefore, three differently adjusted jets disintegrating into droplets with diameters between 10 μm and 40 μm were investigated spectrally. While the heated jets revealed a high temperature decline of approximately 30 K over the course of 20 mm after exiting the nozzle, minor temperature changes could be resolved in a cold jet. In this case, the liquid was tempered to 293 K and injected into ambient air with a temperature of 296.2 K. At 10 mm distance to the nozzle, a temperature increase of 3.8 K was recorded, compared to the initially measured 292.3 K at the nozzle exit. In the subsequent 10 mm, a cooling down to 294.8 K was observed. However, the temperature changes could be partly attributed to measurement uncertainties, as the variations fall within the range of shot-to-shot variations.

The successfully applied 2c-LIF concept for ethanol was further considered for the use

in additional solvents, such as water and mixtures of both. Consequently, droplets of various ethanol/water mixtures were analysed and reveal a solvent-dependent spectral shift. Fundamental investigations were conducted to propose a 3c-LIF concept to determine mixture compositions in binary droplets.

Additionally, 2p-LIF is considered for planar measurements in dense spray regions. The excitation method was applied to ethanol and water sprays from a commercial fuel injector to image and size individual liquid structures. In addition to liquid-phase temperature, the structure and droplet sizes are critical parameters for evaporation and mixing processes in technical sprays. Focus of the injector measurements was the influence of the liquid properties on the spray formation. Therefore, the sprays were studied in the far field (5 mm to 10 mm) and a region close to the nozzle (up to 4 mm to the nozzle exit), where large spray structures between 80 μm and 130 μm were detected. In contrast, small droplets of up to 20 μm were resolved at 10 mm distance to the nozzle. Generally, ethanol exhibits a more pronounced aerodynamic breakup, as indicated by its higher Weber number compared to water. This was confirmed by the average structure size in ethanol sprays being 24% smaller than in water sprays.

To enable a more detailed insight into the fundamental processes of technical sprays, 2c-LIF thermometry measurements should be conducted with 2p-LIF excitation. This would allow temperature investigations in commercial sprays with the possibility of simultaneous structure sizing through microscopic imaging. With the aim of reducing multiple scattered and additional out-of-focus fluorescence photons (due to reabsorption), a time-gated measurement concept could offer further improvements in spray visualization.

Furthermore, additional studies are necessary to assess the 3c-LIF technique for mixture composition analysis. This work introduced a proof of concept for isothermal investigations. Nevertheless, the technique covers the simultaneous detection of two-color thermometry information. Extensive parameter studies at varied temperatures and mixture compositions could provide information for the development of an evaluation method to attain both variables at the same time. Possible techniques could be an iterative solution or a spectral approach, using a fitting algorithm for a clear allocation of spectral shifts.

References

[1]   United Nations, Department of Economic and Social Affairs
       The Sustainable Development Goals Report 2020
       United Nations Publications, Bloomfield (2020).

[2]   Zuin, V. G., Eilks, I., Elschami, M., Kümmerer, K.
       Education in green chemistry and in sustainable chemistry: perspectives towards sustainability
       Green Chemistry **23** (2021), 1594–1608.

[3]   Hill, J., Kumar, D. D., Verma, R. K.
       Challenges for chemical education: Engaging with green chemistry and environmental sustainability
       Journal of the American Institute of Chemists **86** (2013), 24–31.

[4]   González-Campos, J. B., Pérez-Nava, A., Valle-Sánchez, M., Delgado-Rangel, L. H.
       Deep eutectic solvents applications aligned to 2030 United Nations Agenda for Sustainable Development
       Chemical Engineering and Processing - Process Intensification **199** (2024), 109751.

[5]   Monroy, Y. M., Rodrigues, R. A., Sartoratto, A., Cabral, F. A.
       Influence of ethanol, water, and their mixtures as co-solvents of the supercritical carbon dioxide in the extraction of phenolics from purple corn cob (Zea mays L.)
       The Journal of Supercritical Fluids **118** (2016), 11–18.

[6]   Chemat, F., Abert Vian, M., Ravi, H. K., Khadhraoui, B., Hilali, S., Perino, S., Tixier, A.-S. F.
       Review of alternative solvents for green extraction of food and natural products: Panorama, principles, applications and prospects
       Molecules **24** (2019), 3007.

[7]   Capello, C., Fischer, U., Hungerbühler, K.
       What is a green solvent? A comprehensive framework for the environmental assessment of solvents
       Green Chemistry **9** (2007), 927–934.

[8]   Bhatt, N. H., Lily, Raj, R., Varshney, P., Pati, A. R., Chouhan, D., Kumar, A., Munshi, B., Mohapatra, S. S.
       Enhancement of heat transfer rate of high mass flux spray cooling by ethanol-water and ethanol-tween20-water solution at very high initial surface temperature
       International Journal of Heat and Mass Transfer **110** (2017), 330–347.

[9]   Taheri, V., Ebrahimi Rahnama, H., Morad, M. R.
       High flow rate electrospray cooling performance of water–ethanol mixtures
       Applied Thermal Engineering **239** (2024), 122200.

[10] Qi, D. H., Chen, H., Matthews, R. D., Bian, Y.
Combustion and emission characteristics of ethanol–biodiesel–water micro-emulsions used in a direct injection compression ignition engine
Fuel **89** (2010), 958–964.

[11] Martinez-Frias, J., Aceves, S. M., Flowers, D. L.
Improving ethanol life cycle energy efficiency by direct utilization of wet ethanol in HCCI engines
Journal of Energy Resources Technology **129** (2007), 332–337.

[12] Munsin, R., Laoonual, Y., Jugjai, S., Imai, Y.
An experimental study on performance and emissions of a small SI engine generator set fuelled by hydrous ethanol with high water contents up to 40%
Fuel **106** (2013), 586–592.

[13] Aleiferis, P. G., Shukla, J., Brewer, M., Cracknell, R. F.
Effect of water content in ethanol on spray formation at subcooled and flash-boiling conditions
International Journal of Heat and Mass Transfer **182** (2022), 121884.

[14] Deng, X., Chen, Z., Wang, X., Zhen, H., Xie, R.
Exhaust noise, performance and emission characteristics of spark ignition engine fuelled with pure gasoline and hydrous ethanol gasoline blends
Case Studies in Thermal Engineering **12** (2018), 55–63.

[15] Wang, X., Chen, Z., Ni, J., Liu, S., Zhou, H.
The effects of hydrous ethanol gasoline on combustion and emission characteristics of a port injection gasoline engine
Case Studies in Thermal Engineering **6** (2015), 147–154.

[16] Bostanci, H., He, B., Chow, L. C.
Spray cooling with ammonium hydroxide
International Journal of Heat and Mass Transfer **107** (2017), 45–52.

[17] Liu, H., Cai, C., Yin, H., Luo, J., Jia, M., Gao, J.
Experimental investigation on heat transfer of spray cooling with the mixture of ethanol and water
International Journal of Thermal Sciences **133** (2018), 62–68.

[18] Karpov, P. N., Nazarov, A. D., Serov, A. F., Terekhov, V. I.
Evaporative cooling by a pulsed jet spray of binary ethanol-water mixture
Technical Physics Letters **41** (2015), 668–671.

[19] Yin, H., Chen, H., Cai, C., Liu, H., Zhao, C.
Spray cooling heat transfer enhancement by ethanol additive: Effect of Sauter mean diameter and fluid volumetric flux

Heat and Mass Transfer **59** (2023), 1459–1475.

[20] Zhou, N., Chen, F., Cao, Y., Chen, M., Wang, Y.
Experimental investigation on the performance of a water spray cooling system
Applied Thermal Engineering **112** (2017), 1117–1128.

[21] Tok, A., Boey, F., Du, S. W., Wong, B. K.
Flame spray synthesis of ZrO2 nano-particles using liquid precursors
Materials Science and Engineering: B **130** (2006), 114–119.

[22] Harjunen, P., Lehto, V.-P., Välisaari, J., Lankinen, T., Paronen, P., Järvinen, K.
Effects of ethanol to water ratio in feed solution on the crystallinity of spray-dried lactose
Drug development and industrial pharmacy **28** (2002), 949–955.

[23] Gad, S., Tajber, L., Corrigan, O. I., Healy, A. M.
Preparation and characterisation of novel spray-dried nano-structured para-aminosalicylic acid particulates for pulmonary delivery: impact of ammonium carbonate on morphology, chemical composition and solid state
The Journal of pharmacy and pharmacology **64** (2012), 1264–1274.

[24] Ye, Q., Woo, M. W., Selomulya, C.
Modification of molecular conformation of spray-dried whey protein microparticles improving digestibility and release characteristics
Food chemistry **280** (2019), 255–261.

[25] Gilani, K., Najafabadi, A. R., Barghi, M., Rafiee-Tehrani, M.
The effect of water to ethanol feed ratio on physical properties and aerosolization behavior of spray dried cromolyn sodium particles
Journal of pharmaceutical sciences **94** (2005), 1048–1059.

[26] Ji, S., Thulstrup, P. W., Mu, H., Hansen, S. H., van de Weert, M., Rantanen, J., Yang, M.
Effect of ethanol as a co-solvent on the aerosol performance and stability of spray-dried lysozyme
International journal of pharmaceutics **513** (2016), 175–182.

[27] Madero, J. E., Li, J., Shen, K.-Y., Wojtak, J., Axelbaum, R. L.
An approach to low-temperature flame spray pyrolysis for the synthesis of temperature-sensitive materials: Application to Li1.2Mn0.54Ni0.13Co0.13O2
Applications in Energy and Combustion Science **5** (2021), 100020.

[28] Narasu, P., Gutheil, E.
Modeling and parameterization of the evaporation and thermal decomposition of an iron(III) nitrate nonahydrate/ethanol droplet for flame spray pyrolysis
Fluids **7** (2022), 146.

[29] Retzer, U., Ulrich, H., Will, S., Zigan, L.

Burst-mode 1-methylnaphthalene laser-induced fluorescence: extended calibration and measurement of temperature and fuel partial density in a rapid compression machine
Applied Physics B **128** (2022), 144.

[30] Storch, M., Lind, S., Will, S., Zigan, L.
Influence of ethanol admixture on the determination of equivalence ratios in DISI engines by laser-induced fluorescence
Applied optics **55** (2016), 8532–8540.

[31] Lambert, J. B., Gronert, S., Shurvell, H. F., Lightner, D. A.
Spektroskopie - Strukturaufklärung in der Organischen Chemie
Pearson, London (2012).

[32] Valeur, B., Berberan-Santos, M. N.
Molecular fluorescence - Principles and applications
Wiley-VCH, Weinheim (2012).

[33] Bräuer, A.
In situ spectroscopic techniques at high pressure
Elsevier, Amsterdam (2015).

[34] Taniguchi, M., Lindsey, J. S.
Database of absorption and fluorescence spectra of 300 common compounds for use in PhotochemCAD
Photochemistry and photobiology **94** (2018), 290–327.

[35] Taniguchi, M., Du, H., Lindsey, J. S.
PhotochemCAD 3: Diverse modules for photophysical calculations with multiple spectral databases
Photochemistry and photobiology **94** (2018), 277–289.

[36] Fresenius, W., Huber, J. F. K., Pungor, E., Rechnitz, G. A., Simon, W., Tölg, G., West, T. S., Perkampus, H.-H.
UV-VIS-Spektroskopie und ihre Anwendungen
Springer Berlin Heidelberg, Berlin (1986).

[37] Schulz, C., Sick, V.
Tracer-LIF diagnostics: quantitative measurement of fuel concentration, temperature and fuel/air ratio in practical combustion systems
Progress in Energy and Combustion Science **31** (2005), 75–121.

[38] Koochesfahani, M. M., Dimotakis, P. E.
Laser-induced fluorescence measurements of mixed fluid concentrationin a liquid plane shear layer
AIAA Journal **23** (1985), 1700–1707.

[39] Breidenthal, R.
      Structure in turbulent mixing layers and wakes using a chemical reaction
      Journal of Fluid Mechanics **109** (1981), 1–24.

[40] Bassnett, S., Reinisch, L., Beebe, D. C.
      Intracellular pH measurement using single excitation-dual emission fluorescence ra-
      tios
      The American journal of physiology **258** (1990), C171-C178.

[41] Morris, S. J.
      Real-time multi-wavelength fluorescence imaging of living cells
      BioTechniques **8** (1990), 296–308.

[42] Coppeta, J., Rogers, C.
      Dual emission laser induced fluorescence for direct planar scalar behavior measure-
      ments
      Experiments in Fluids **25** (1998), 1–15.

[43] Lemoine, F., Wolff, M., Lebouche, M.
      Simultaneous concentration and velocity measurements using combined laser-induced
      fluorescence and laser Doppler velocimetry: Application to turbulent transport
      Experiments in Fluids **20** (1996), 319–327.

[44] Sakakibara, J., Adrian, R. J.
      Whole field measurement of temperature in water using two-color laser induced fluo-
      rescence
      Experiments in Fluids **26** (1999), 7–15.

[45] Lavieille, P., Delconte, A., Blondel, D., Lebouch, M., Lemoine, F.
      Non-intrusive temperature measurements using three-color laser-induced fluores-
      cence
      Experiments in Fluids **36** (2004), 706–716.

[46] Kim, H. J., Kihm, K. D.
      Two-color (Rh-B & Rh-110) laser induced fluorescence (LIF) thermometry with sub-
      millimeter measurement resolution
      Journal of Heat Transfer **124** (2002), 596.

[47] Castanet, G., Lavieille, P., Lebouch, M., Lemoine, F.
      Measurement of the temperature distribution within monodisperse combusting drop-
      lets in linear streams using two-color laser-induced fluorescence
      Experiments in Fluids **35** (2003), 563–571.

[48] Lavieille, P., Lemoine, F., Lavergne, G., Lebouché, M.
      Evaporating and combusting droplet temperature measurements using two-color la-
      ser-induced fluorescence

Experiments in Fluids **31** (2001), 45–55.

[49] Lemoine, F., Antoine, Y., Wolff, M., Lebouche, M.
      Simultaneous temperature and 2D velocity measurements in a turbulent heated jet us-
      ing combined laser-induced fluorescence and LDA
      Experiments in Fluids **26** (1999), 315–323.

[50] Sutton, J. A., Fisher, B. T., Fleming, J. W.
      A laser-induced fluorescence measurement for aqueous fluid flows with improved
      temperature sensitivity
      Experiments in Fluids **45** (2008), 869–881.

[51] Perrin, L., Castanet, G., Lemoine, F.
      Characterization of the evaporation of interacting droplets using combined optical
      techniques
      Experiments in Fluids **56** (2015), 29.

[52] Palmer, J., Reddemann, M. A., Kirsch, V., Kneer, R.
      Temperature measurements of micro-droplets using pulsed 2-color laser-induced fluo-
      rescence with MDR-enhanced energy transfer
      Experiments in Fluids **57** (2016), 177.

[53] Prenting, M. M., Baik, S.-J., Dreier, T., Endres, T., Kempf, A., Schulz, C.
      Liquid-phase temperature in the SpraySyn flame measured by two-color laser-induced
      fluorescence thermometry and simulated by LES
      Proceedings of the Combustion Institute **39** (2023), 2621–2630.

[54] Mishra, Y. N., Yoganantham, A., Koegl, M., Zigan, L.
      Investigation of five organic dyes in ethanol and butanol for two-color laser-induced
      fluorescence ratio thermometry
      Optics **1** (2020), 1–17.

[55] Prenting, M. M., Bin Dzulfida, M. I., Dreier, T., Schulz, C.
      Characterization of tracers for two-color laser-induced fluorescence liquid-phase tem-
      perature imaging in sprays
      Experiments in Fluids **61** (2020), 77.

[56] Chaze, W., Caballina, O., Castanet, G., Lemoine, F.
      The saturation of the fluorescence and its consequences for laser-induced fluorescence
      thermometry in liquid flows
      Experiments in Fluids **57** (2016), 58.

[57] Frackowiak, B., Tropea, C.
      Fluorescence modeling of droplets intersecting a focused laser beam
      Optics letters **35** (2010), 1386–1388.

[58] Koegl, M., Dai, H., Qomi, M. P., Bauer, F., Eppinger, B., Zigan, L.

Morphology-dependent resonances in laser-induced fluorescence images of micrometric gasoline/ethanol droplets utilizing the dye nile red
Applied optics **60** (2021), 5000–5011.

[59] Chen, G., Mohiuddin Mazumder, M., Chang, R. K., Christian Swindal, J., Acker, W. P.
Laser diagnostics for droplet characterization: Application of morphology dependent resonances
Progress in Energy and Combustion Science **22** (1996), 163–188.

[60] Palmer, J., Reddemann, M., Kirsch, V., Kneer, R.
Development steps of 2-color laser-induced fluorescence with MDR-enhanced energy transfer for instantaneous planar temperature measurement of micro-droplets and sprays
28th European Conference on Liquid Atomization and Spray Systems, Valencia (2017).

[61] Zheng, L., Zhi, M., Chan, Y., Khan, S. A.
Multi-color lasing in chemically open droplet cavities
Scientific Reports **8** (2018), 14088.

[62] Lamanna, G., Tonini, S., Cossali, G. E., Weigand, B.
Droplet Interactions and Spray Processes
Springer, Cham (2020).

[63] Fansler, T. D., Parrish, S. E.
Spray measurement technology: a review
Measurement Science and Technology **26** (2015), 012002.

[64] Ashgriz, N.
Handbook of Atomization and Sprays: Theory and Applications
Springer, New York (2011).

[65] Reitz, R. D.
Atomization and Other Breakup Regimes of a Liquid Jet
Princeton University (PhD thesis) (1978).

[66] Ohnesorge, W. V.
Die Bildung von Tropfen an Düsen und die Auflösung flüssiger Strahlen
ZAMM - Journal of Applied Mathematics and Mechanics **16** (1936), 355–358.

[67] Ulrich, H., Lehnert, B., Guénot, D., Svendsen, K., Lundh, O., Wensing, M., Berrocal, E., Zigan, L.
Effects of liquid properties on atomization and spray characteristics studied by planar two-photon fluorescence
Physics of Fluids **34** (2022), 83305.

[68] Ulrich, H., Sigl, S., Möhnle, M., Berrocal, E., Zigan, L.

Droplet thermometry based on an optimized two dye two-color laser-induced fluorescence concept
Frontiers in Physics **11** (2023), 1235847.

[69] Ulrich, H., Weiß, R., Zigan, L.
Two-dye two-color laser-induced fluorescence spectroscopy on droplets of green solvent water/ethanol mixtures for thermometry and mixture composition
Experiments in Fluids **65** (2024).

[70] Lefebvre, A. H., McDonell, V. G.
Atomization and sprays
CRC Press, Boca Raton (2017).

[71] Schneider, B. M.
Experimentelle Untersuchungen zur Spraystruktur in transienten, verdampfenden und nicht verdampfenden Brennstoffstrahlen unter Hochdruck
Eidgenössische Technische Hochschule Zürich (PhD thesis) (2003).

[72] Fath, A.
Charakterisierung des Strahlaufbruch-Prozesses bei der instationären Druckzerstäubung
Friedrich-Alexander-Universität Erlangen-Nürnberg (PhD thesis) (1997).

[73] Stiesch, G.
Modeling engine spray and combustion processes
Springer, Berlin (2003).

[74] Reitz, R. D.
Mechanism of atomization of a liquid jet
Physics of Fluids **25** (1982), 1730.

[75] Crua, C., Heikal, M. R., Gold, M. R.
Microscopic imaging of the initial stage of diesel spray formation
Fuel **157** (2015), 140–150.

[76] Dumouchel, C.
On the experimental investigation on primary atomization of liquid streams
Experiments in Fluids **45** (2008), 371–422.

[77] Tropea, C.
Springer handbook of experimental fluid mechanics
Springer, Berlin (2007).

[78] Tropea, C.
Optical Particle Characterization in Flows
Annual Review of Fluid Mechanics **43** (2011), 399–426.

[79] Luo, M., Wu, Y., Haidn, O. J.
      Temperature and size measurements of cryogenic spray droplets with global rainbow refractometry
      Journal of Propulsion and Power **35** (2019), 359–368.

[80] Roth, N., Anders, K., Frohn, A.
      Simultaneous measurement of temperature and size of droplets in the micrometer range
      Journal of Laser Applications **2** (1990), 37–42.

[81] Albrecht, H.-E., Borys, M., Damaschke, N., Tropea, C.
      Laser Doppler and Phase Doppler Measurement Techniques
      Springer Berlin Heidelberg, Berlin (2003).

[82] Bachalo, W.D. and Houser, M.J.
      Phase/doppler spray analyzer for simultaneous measurements of drop size and velocity distributions
      Optical Engineering **23** (1984), 583–590.

[83] Koegl, M., Mishra, Y. N., Storch, M., Conrad, C., Berrocal, E., Will, S., Zigan, L.
      Analysis of ethanol and butanol direct-injection spark-ignition sprays using two-phase structured laser illumination planar imaging droplet sizing
      International Journal of Spray and Combustion Dynamics **11** (2019), 1-16.

[84] Biasiori-Poulanges, L., El-Rabii, H.
      High-magnification shadowgraphy for the study of drop breakup in a high-speed gas flow
      Optics letters **44** (2019), 5884–5887.

[85] Welss, R., Bornschlegel, S., Seeger, J., Deinhard, B., Wensing, M.
      Correlating gasoline spray propagation in Constant Volume Chamber and optically accessible engines
      9th International Conference on Modeling and Diagnostics in Advanced Engine Systems, Okayama (2017).

[86] Linne, M.
      Imaging in the optically dense regions of a spray: A review of developing techniques
      Progress in Energy and Combustion Science **39** (2013), 403–440.

[87] Malarski, A., Schürer, B., Schmitz, I., Zigan, L., Flügel, A., Leipertz, A.
      Laser sheet dropsizing based on two-dimensional Raman and Mie scattering
      Applied optics **48** (2009), 1853–1860.

[88] Zeng, W., Xu, M., Zhang, Y., Wang, Z.
      Laser sheet dropsizing of evaporating sprays using simultaneous LIEF/MIE techniques
      Proceedings of the Combustion Institute **34** (2013), 1677–1685.

[89]   Domann, R., Hardalupas, Y.
       Quantitative measurement of planar droplet Sauter mean diameter in sprays using planar droplet sizing
       Particle & Particle Systems Characterization **20** (2003), 209–218.

[90]   Berrocal, E., Conrad, C., Püls, J., Arnold, C. L., Wensing, M., Linne, M., Miranda, M.
       Two-photon fluorescence laser sheet imaging for high contrast visualization of atomizing sprays
       OSA Continuum **2** (2019), 983–993.

[91]   Guénot, D., Svendsen, K., Björklund Svensson, J., Ekerfelt, H., Persson, A., Lundh, O., Berrocal, E.
       Simultaneous laser-driven x-ray and two-photon fluorescence imaging of atomizing sprays
       Optica **7** (2020), 131–134.

[92]   Coghe, A., Cossali, G. E.
       Quantitative optical techniques for dense sprays investigation: A survey
       Optics and Lasers in Engineering **50** (2012), 46–56.

[93]   Powell, C. F., Yue, Y., Poola, R., Wang, J.
       Time-resolved measurements of supersonic fuel sprays using synchrotron X-rays
       Journal of synchrotron radiation **7** (2000), 356–360.

[94]   Basu, S., Agarwal, A. K., Mukhopadhyay, A., Patel, C.
       Droplets and Sprays - Applications for Combustion and Propulsion
       Springer, Singapore (2018).

[95]   Berrocal, E., Kristensson, E., Richter, M., Linne, M., Aldén, M.
       Application of structured illumination for multiple scattering suppression in planar laser imaging of dense sprays
       Optics express **16** (2008), 17870–17881.

[96]   Kristensson, E., Berrocal, E., Richter, M., Pettersson, S.-G., Aldén, M.
       High-speed structured planar laser illumination for contrast improvement of two-phase flow images
       Optics letters **33** (2008), 2752–2754.

[97]   Xu, C., Zipfel, W., Shear, J. B., Williams, R. M., Webb, W. W.
       Multiphoton fluorescence excitation: new spectral windows for biological nonlinear microscopy
       Proceedings of the National Academy of Sciences of the United States of America **93** (1996), 10763–10768.

[98]   Vegad, C. S., Idlahcen, S., Huang, L., Cabot, G., Renou, B., Duret, B., Reveillon, J., Demoulin, F.-X.

Planar two-photon fluorescence imaging of dense spray to estimate spray characteristics: application in pressure-swirl atomizers
Atomization and Sprays **34** (2024), 15–35.

[99] Wang, T., Liu, Y., Chen, C., Hardalupas, Y.
Combined two-photon optical connectivity and planar laser induced fluorescence for instantaneous characterisation of liquid interface during primary atomisation
Experimental Thermal and Fluid Science **147** (2023), 110935.

[100] Keller, P., Knorsch, T., Wensing, M., Hasse, C.
Experimental and numerical analysis of iso-octane/ethanol sprays under gasoline engine conditions
International Journal of Heat and Mass Transfer **84** (2015), 497–510.

[101] Davy, M., Williams, P., Han, D., Steeper, R.
Evaporation characteristics of the 3-pentanone–isooctane binary system
Experiments in Fluids **35** (2003), 92–99.

[102] Liu, C., Bonaccurso, E., Butt, H.-J.
Evaporation of sessile water/ethanol drops in a controlled environment
Physical Chemistry Chemical Physics **10** (2008), 7150–7157.

[103] Sefiane, K., Tadrist, L., Douglas, M.
Experimental study of evaporating water–ethanol mixture sessile drop: influence of concentration
International Journal of Heat and Mass Transfer **46** (2003), 4527–4534.

[104] Sefiane, K., David, S., Shanahan, M. E. R.
Wetting and evaporation of binary mixture drops
The Journal of Physical Chemistry B **112** (2008), 11317–11323.

[105] Innocenzi, P., Malfatti, L., Costacurta, S., Kidchob, T., Piccinini, M., Marcelli, A.
Evaporation of ethanol and ethanol-water mixtures studied by time-resolved infrared spectroscopy
The Journal of Physical Chemistry A **112** (2008), 6512–6516.

[106] Hopkins, R. J., Reid, J. P.
Evaporation of ethanol/water droplets: examining the temporal evolution of droplet size, composition and temperature
The Journal of Physical Chemistry A **109** (2005), 7923–7931.

[107] Ni, Z., Hespel, C., Han, K., Foucher, F.
Evaluations of the preferential evaporation of binary droplet by rainbow technique and simulation
Experimental Thermal and Fluid Science **136** (2022), 110649.

[108] Zeng, Y., Jiang, L., Zheng, W., Li, D., Yao, S., Qu, J. Y.

Quantitative imaging of mixing dynamics in microfluidic droplets using two-photon fluorescence lifetime imaging
Optics letters **36** (2011), 2236–2238.

[109] Qi, W., Zhou, Y., Zhang, Y.
Laser-based measurements and analyses on cycle-to-cycle variations of mixture formation in binary-component fuel sprays
Experiments in Fluids **61** (2020), 87.

[110] Chen, R., Nishida, K., Shi, B.
Quantitative investigation on the spray mixture formation for ethanol-gasoline blends via UV–Vis dual-wavelength laser absorption scattering (LAS) technique
Fuel **242** (2019), 425–437.

[111] Kranz, P., Kaiser, S. A.
LIF-based imaging of preferential evaporation of a multi-component gasoline surrogate in a direct-injection engine
Proceedings of the Combustion Institute **37** (2019), 1365–1372.

[112] Itani, L. M., Bruneaux, G., Di Lella, A., Schulz, C.
Two-tracer LIF imaging of preferential evaporation of multi-component gasoline fuel sprays under engine conditions
Proceedings of the Combustion Institute **35** (2015), 2915–2922.

[113] Bardi, M., Di Lella, A., Bruneaux, G.
A novel approach for quantitative measurements of preferential evaporation of fuel by means of two-tracer laser induced fluorescence
Fuel **239** (2019), 521–533.

[114] Koegl, M., Pahlevani, M., Zigan, L.
A novel approach for measurement of composition and temperature of n-decane/butanol blends using two-color laser-induced fluorescence of Nile red
Sensors **20** (2020), 5721.

[115] Koegl, M., Mull, C., Mishra, Y. N., Will, S., Zigan, L.
Characterization of fuel/water mixtures and emulsions with ethanol using laser-induced fluorescence
Applied optics **59** (2020), 1136–1144.

[116] Lemoine, F., Castanet, G.
Temperature and chemical composition of droplets by optical measurement techniques: a state-of-the-art review
Experiments in Fluids **54** (2013), 1–34.

[117] Abram, C., Fond, B., Beyrau, F.
Temperature measurement techniques for gas and liquid flows using thermographic

phosphor tracer particles
Progress in Energy and Combustion Science **64** (2018), 93–156.

[118] Omrane, A., Santesson, S., Alden, M., Nilsson, S.
Laser techniques in acoustically levitated micro droplets
Lab on a chip **4** (2004), 287–291.

[119] Särner, G., Richter, M., Aldén, M.
Two-dimensional thermometry using temperature-induced line shifts of ZnO:Zn and ZnO:Ga fluorescence
Optics letters **33** (2008), 1327–1329.

[120] Omrane, A., Särner, G., Aldén, M.
2D-temperature imaging of single droplets and sprays using thermographic phosphors
Applied Physics B **79** (2004), 431–434.

[121] Lawrence, M., Zhao, H., Ganippa, L.
Gas phase thermometry of hot turbulent jets using laser induced phosphorescence
Optics express **21** (2013), 12260–12281.

[122] Brübach, J., Patt, A., Dreizler, A.
Spray thermometry using thermographic phosphors
Applied Physics B **83** (2006), 499–502.

[123] van Beeck, J. P., Giannoulis, D., Zimmer, L., Riethmuller, M. L.
Global rainbow thermometry for droplet-temperature measurement
Optics letters **24** (1999), 1696–1698.

[124] Saengkaew, S., Godard, G., Blaisot, J. B., Gréhan, G.
Experimental analysis of global rainbow technique: sensitivity of temperature and size distribution measurements to non-spherical droplets
Experiments in Fluids **47** (2009), 839–848.

[125] Hankel, R. F., Günther, A., Wirth, K.-E., Leipertz, A., Braeuer, A.
Liquid phase temperature determination in dense water sprays using linear Raman scattering
Optics express **22** (2014), 7962–7971.

[126] Heinisch, C., Wills, J. B., Reid, J. P., Tschudi, T., Tropea, C.
Temperature measurement of single evaporating water droplets in a nitrogen flow using spontaneous Raman scattering
Physical Chemistry Chemical Physics **11** (2009), 9720–9728.

[127] Müller, T., Grünefeld, G., Beushausen, V.
High-precision measurement of the temperature of methanol and ethanol droplets using spontaneous Raman scattering
Applied Physics B **70** (2000), 155–158.

[128] Eghtesad, A., Bijarchi, M. A., Shafii, M. B., Afshin, H.
A state-of-the-art review on laser-induced fluorescence (LIF) method with application in temperature measurement
International Journal of Thermal Sciences **196** (2024), 108686.

[129] Lakowicz, J. R.
Principles of fluorescence spectroscopy
Springer, New York (2006).

[130] Bennet, M. A., Richardson, P. R., Arlt, J., McCarthy, A., Buller, G. S., Jones, A. C.
Optically trapped microsensors for microfluidic temperature measurement by fluorescence lifetime imaging microscopy
Lab on a chip **11** (2011), 3821–3828.

[131] Stiti, M., Liu, Y., Chaynes, H., Lemoine, F., Wang, X., Castanet, G.
Fluorescence lifetime measurements applied to the characterization of the droplet temperature in sprays
Experiments in Fluids **62** (2021), 174.

[132] Maqua, C., Castanet, G., Lemoine, F., Doué, N., Lavergne, G.
Temperature measurements of binary droplets using three-color laser-induced fluorescence
Experiments in Fluids **40** (2006), 786–797.

[133] Labergue, A., Deprédurand, V., Delconte, A., Castanet, G., Lemoine, F.
New insight into two-color LIF thermometry applied to temperature measurements of droplets
Experiments in Fluids **49** (2010), 547–556.

[134] Düwel, I., Ge, H.-W., Kronemayer, H., Dibble, R., Gutheil, E., Schulz, C., Wolfrum, J.
Experimental and numerical characterization of a turbulent spray flame
Proceedings of the Combustion Institute **31** (2007), 2247–2255.

[135] Chaze, W., Caballina, O., Castanet, G., Lemoine, F.
Spatially and temporally resolved measurements of the temperature inside droplets impinging on a hot solid surface
Experiments in Fluids **58** (2017), 96.

[136] Mishra, Y. N., Abou Nada, F., Polster, S., Kristensson, E., Berrocal, E.
Thermometry in aqueous solutions and sprays using two-color LIF and structured illumination
Optics express **24** (2016), 4949–4963.

[137] Stiti, M., Kornienko, V., Kristensson, E., Castanet, G., Berrocal, E.
Instantaneous thermometry imaging using two-photon laser-induced fluorescence
Optics letters **49** (2024), 2569–2572.

[138] Svendsen, K., González, I. G., Hansson, M., Svensson, J. B., Ekerfelt, H., Persson, A., Lundh, O.
Optimization of soft X-ray phase-contrast tomography using a laser wakefield accelerator
Optics express **26** (2018), 33930–33941.

[139] Bergman, T. L., Incropera, F. P., DeWitt, D. P., Lavine, A. S.
Principles of heat and mass transfer
Wiley, Hoboken (2013).

Appendix

This chapter includes the three journal publications, summarized in section 3.

P[1]   Ulrich H., Lehnert B., Guénot D., Svendsen K., Lundh O., Wensing M., Berrocal E., Zigan L.
Effects of liquid properties on atomization and spray characteristics studied by planar two-photon fluorescence
Physics of Fluids **34** (2022).
This article is a postprint of the article published in Physics of Fluids special issue 'Development and Validation of Models for Turbulent Reacting Flows'. The original authenticated version is available online at https://doi.org/10.1063/5.0098922.

P[2]   Ulrich H., Sigl S., Möhnle M., Berrocal E., Zigan L.
Droplet thermometry based on an optimized two dye two-color laser-induced fluorescence concept
Frontiers in Physics **11** (2023).
This article is a postprint of the article published in Frontiers in Physics special issue 'Physics of Droplets'. The original authenticated version is available online at https://doi.org/10.3389/fphy.2023.1235847.

P[3]   Ulrich H., Weiß R., Zigan L.
Two-dye two-color laser-induced fluorescence spectroscopy on droplets of green solvent water/ethanol mixtures for thermometry and mixture composition
Experiments in Fluids **65** (2024).
This article is a postprint of the article published in Experiments in Fluids. The original authenticated version is available online at https://doi.org/10.1007/s00348-024-03868-z.

Effects of liquid properties on atomization and spray characteristics studied by planar two-photon fluorescence (EP)

View Online   Export Citation   CrossMark

Hannah Ulrich,[1,2,a)] (iD) Bastian Lehnert,[2,3] Diego Guénot,[4] (iD) Kristoffer Svendsen,[4] (iD) Olle Lundh,[4] (iD)
Michael Wensing,[2,3] (iD) Edouard Berrocal,[2,5] (iD) and Lars Zigan[1,2] (iD)

AFFILIATIONS

[1]Institut für Thermodynamik, Professur für Energiewandlug, Fakultät für Luft- und Raumfahrttechnik, Universität der Bundeswehr
  München (UniBw M), Neubiberg, Germany
[2]Erlangen Graduate School in Advanced Optical Technologies (SAOT), Friedrich-Alexander-Universität Erlangen-Nürnberg (FAU),
  Erlangen, Germany
[3]Professur für Fluidsystemtechnik (FST), Friedrich-Alexander-Universität Erlangen-Nürnberg (FAU), Erlangen, Germany
[4]Division of Atomic Physics, Lund University, Lund, Sweden
[5]Division of Combustion Physics, Lund University, Lund, Sweden

Note: This paper is part of the special topic, Development and Validation of Models for Turbulent Reacting Flows.
[a)]Author to whom correspondence should be addressed: hannah.ulrich@unibw.de

ABSTRACT

In this work, planar two-photon laser-induced fluorescence (2p-LIF) is applied for the first time to analyze the fluid dependent spray structure and atomization behavior of water and ethanol in a quantitative way. A commercial six-hole DISI (Direct-Injection Spark-Ignition) injector was studied at different injection pressures, operated with liquids containing the LIF dye fluorescein. Specifically for DISI-injectors, the fluid-dependent atomization is very complex and not fully understood due to the cavitating, turbulent nozzle flow that dominates the spray formation. Optical access and analysis of the near-nozzle spray are often challenging due to multiple light scattering in dense regions which is reduced by 2p-LIF measurements using a femtosecond laser. This allows high-contrast spray imaging close to the nozzle, resulting in an improved identification of single liquid structures of the spray. Thus, a higher accuracy of sizing is possible. Compared to water, the ethanol spray shape shows increased cone angles in the nozzle near-field of about 6%, which cannot be explained by classical atomization theory based on aerodynamic breakup. The larger cone angle of ethanol was attributed to its larger viscosity, which could decelerate the flow at the wall of the injection hole, affecting the velocity profile of the emerging jet. The atomization shows a main jet breakup distance of 7–10 mm in which the structure sizes decreased drastically, specifically for water. For the size of the liquid structures in the near-nozzle region, which show dimensions of about 80–130 μm, ethanol exhibited about 2% smaller Feret's diameters than water for the tested time steps at 20 MPa. This effect is even more distinct for other injection pressures and positions at a further distance to the injector. For all investigated conditions and measurement positions downstream of the nozzle, ethanol showed on average about 24% smaller structures compared to the water spray. Although this trend is in accordance with the classical atomization theory based on the aerodynamic breakup mechanism, other effects, such as cavitation and nozzle-flow induced breakup, contribute to this behavior.

INTRODUCTION

Atomization of liquids and spray formation is particularly important for fuel injection in IC engines, rocket engines, or gas turbines since the efficiency of the combustion process is determined by the rapid fuel evaporation and mixture with oxidizer.[1,2] Controlling and optimizing atomization, fuel dispersion,[3] and evaporation through a well-designed injection system allows reducing fuel consumption as well as pollutant emissions such as nitric oxides (NO_x) or soot.[4,5] A well-controlled atomization is also important for other injection processes,[1] such as powder generation from spray drying, printing,[6] surface coating,[7] flame spray pyrolysis, or spray cooling.

For optimization of atomizers and spray processes, an enhanced understanding of the complex fluid dynamics inside and outside of the nozzle is required. Furthermore, liquid properties determine the internal nozzle flow, the atomization, and spray structure. For example, in combustion applications such as IC engines, aircraft engines, or gas turbines, the application of modern biofuel and synthetic fractions may vary the nozzle flow and atomization, which again determine evaporation, mixing, and combustion behavior.[5,8]

The injection system should be also capable to atomize different liquids with comparable quality in order to enable, e.g., ignitability in the case of combustion applications. For example, Qavi and Jiang reported a poor ignition performance of highly viscous fuels for some injectors.[9] This can be due to the limited viscosity tolerance of the applied fuel injection systems. For example, the pressure swirl injector is able to produce narrow size distributions, but just for fuels with low viscosity and surface tension.[10] The atomization of this injector type is solely based on aerodynamic breakup, which is also true for air blast injectors. In these "classical" injectors, droplets are generated following the Kelvin–Helmholtz (KH) or Rayleigh–Taylor (RT) induced instabilities on the interface between liquid and gas. These wave-like disturbance on the jet (and/or droplet) will break up into ligaments and lead subsequently to droplet detachment[11,12] as depicted in Fig. 1. In principle, the surface wave amplitude rises with increasing relative velocity between the liquid and the ambient gas flow. Contrary, these oscillations are damped by the viscosity of the fluid so that this fluid property is a limiting factor for fine atomization. This aerodynamic-induced droplet formation process is relatively well understood, and models (e.g., the "wave model"[13]) are widely applied in computational fluid dynamics (CFD) packages. Additionally, most of the published direct numerical simulation (DNS)-like simulations of the jet disintegration are based on this breakup mechanism.[14]

However, the influence of the inner nozzle flow on jet atomization is often not considered.[16] Specifically, turbulent fluctuations in the nozzle flow may lead to initial disturbances on the liquid jet that promote its disintegration. Those turbulence-induced surface waves at the nozzle grow subsequently due to aerodynamic instabilities of the liquid jet.[17] Figure 1 illustrates the spray breakup due to aerodynamic influences and also cavitation inside the nozzle. Transient two-phase flows occur specifically in diesel or gasoline injectors due to cavitation.
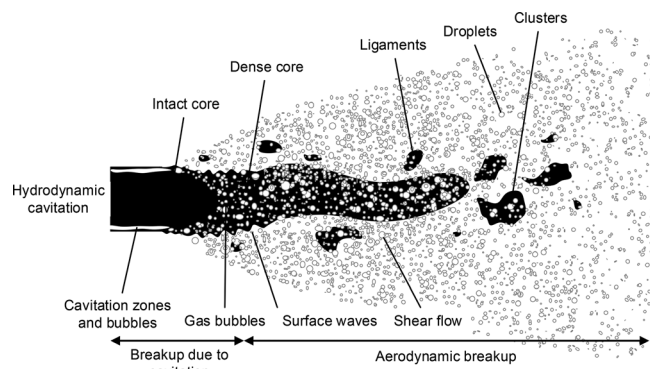

FIG. 1. Spray breakup model with aerodynamic and cavitation induced breakup after.[15]

In the subsequent paragraphs, a short review of cavitation in diesel and gasoline nozzles is presented, as these two-phase flows determine the spray formation at the injector outlet. The breakup in the near-nozzle field is the focus of the present paper. The cavitating flow inside the injector is not accessible with the present optical setup of this paper. However, some fundamentals of cavitation are necessary in order to understand the cavitation-induced breakup and the origin of cyclic variations in the spray under investigation.

Specifically, in high-speed diesel nozzle flows, two-phase regions are generated due to cavitation.[18] "Geometric cavitation" occurs specifically near the sharp corner of a hole inlet where the pressure drops locally below the vapor pressure of the fuel.[19] The collapse of vapor bubbles at the nozzle outlet again leads to strong turbulence supporting ligament formation in the liquid jet. Specifically for geometric cavitation conditions, a large part or the whole nozzle hole surface may be covered with vapor so that the wall is not in contact with liquid fuel. This results in a very slim jet at the nozzle outlet, which is known as "hydraulic flip." This slim jet does not show large surface waves, which also indicates that the simple presence of cavitation does not guarantee jet disintegration.[20]

Furthermore, specifically at high pressure and in high velocity flows occurring under diesel injection conditions, geometric cavitation leads to erosion in the nozzle, and this must be avoided,[21] for example, by conical nozzle holes. Consequently, the atomization process in diesel jets is realized less by cavitation but mainly due to aerodynamic and turbulence-induced breakup. For direct injection spark ignition (DISI, often just called "gasoline direct injection") conditions, cavitation is a very relevant atomization process. The two-phase flow in the nozzle already contains a high amount of gas (vapor and entrained ambient gas, contrary to diesel primary jets) so that the actual jet disintegration is initiated inside the nozzle and the typical step-hole of current injector geometries. This is confirmed by CFD-simulations and x-ray measurements.[22,23] For example, Guenot et al. determined a maximum liquid volume fraction of water at the exit of the DISI nozzle of 55% and a rapid atomization of the liquid jet by using laser-plasma-driven x-ray transmission radiography measurements.[22] Here, a multi-hole nozzle was analyzed with a step-hole geometry. CFD simulations resulted in vapor fractions at the nozzle outlet of a DISI three-hole injector in the range of about 5%–11%[23] depending on the needle lift and the fuel (n-hexane and n-decane were tested in this case). However, in this simulation, only cavitation was considered without any gas entrainment into the nozzle, which is promoted by step-hole nozzles. Both the simulation and the experiments (microscopic planar Mie-scattering was conducted at the nozzle outlet) confirmed the existence of string cavitation (vortex type cavitation) and large cavities in the liquid fuel jet. String cavitation is another type of vapor formation in the nozzle.[24] It occurs in low pressure regions in the liquid bulk, which can be a consequence of large-scale vortices produced in the nozzle sac or nozzle hole. These cavitation structures propagate into the injector hole determining the flow of the liquid jet at the outlet of the nozzle. The formation of cavitation strings is very irregular. These structures may affect the cone and bend angle of the jet and strongly support spray instabilities such as cyclic spray variations,[23,25] i.e., the spray targeting and width varies from injection to injection. This means the atomization and liquid fuel distribution also varies from injection to injection, which is another disadvantage of cavitation. In addition to the variation of the spray angle, cavitation may lead to an

increase in the velocity of liquid jet, which is due to a reduced effective hole diameter. This may also vary from injection to injection and contributes to cyclic spray shape variations.

This complex atomization and spray behavior can hardly be predicted by semi-empirical breakup models that are included in CFD software packages. Most of these atomization models mainly take aerodynamic breakup effects into account and fewer also consider turbulence- or cavitation-induced breakup. However, the instationary nozzle flow may superimpose and even control the aerodynamic breakup, so that the atomization process is not fully understood. In principle, there are many studies focusing on aerodynamic breakup for various liquids; however, in these cases, usually the nozzle flow is relatively simple and cavitation effects play a minor role. For example, recently Qavi and Jiang studied the effects of fuel properties on the near nozzle spray characteristics of a twin-fluid injector.[9] The base jet-A fuel (kerosene) with a low viscosity was compared to two higher viscous fuel blends. A similar atomization completion length of about four times the nozzle diameter (4D) downstream the nozzle was detected for all fuels. The final droplet size is 6% to 10% larger for the higher viscous fuels than for the base fuel. From these observations, the authors concluded that surface tension and liquid density do not have a significant effect on the breakup.

Contrary results were presented by Tareq *et al.* who studied air blast atomization of water compared to kerosene.[26] The surface tension of water is much larger than for kerosene, while the dynamic viscosity is doubled for kerosene. This resulted in larger droplet sizes for water and larger cone angles for kerosene. It was concluded that the surface tension effects are more significant than the viscous effects for this liquid sheet breakup mode being controlled by Kelvin–Helmholtz instabilities.

Reitz and Bracco studied the effects of dynamic viscosity on the jet cone angle for different nozzle geometries and injection conditions.[20] They found a decrease in the jet angle with increasing liquid dynamic viscosity. This trend can mainly be explained by aerodynamic breakup theory and fits roughly to respective phenomenological models. However, it was also mentioned that different nozzle geometries with varied flow profiles and onset of cavitation could lead to deviations from this behavior.

As mentioned above, the nozzle flow cannot be neglected in the case of cavitation and distinct turbulence, which complicates the modeling of atomization processes. In general, there are a few works and correlations of fuel dependent cavitation and turbulent nozzle flow on the spray shape and atomization.[23,27,28] Both cavitation and turbulence increase with lower viscosity[28] determining the liquid flow, specifically the axial and radial velocity field at the outlet. For example, a lower liquid viscosity may accelerate the liquid flow exiting the nozzle also at the nozzle wall. This may lead to larger injection velocities and to a reduced spray cone angle for the lower viscosity fuel as shown for n-hexane, in comparison to higher viscous n-decane for a DISI injector in Ref. 23. Furthermore, this is opposed to the study of Reitz and Bracco mentioned above.[20] For the lower viscosity fuel, fewer large structures (ligaments, clusters) were observed in the near-nozzle region.[23] It was concluded that these fuel-dependent effects cannot be described by the aerodynamic breakup alone. Contrary, the spray shape is mainly determined by the highly unsteady, cavitating nozzle flow and specifically by the developed flow profile at the nozzle outlet, which again depends on the viscosity of the liquid. This liquid

property also determines cyclic variations of the spray shape and targeting. However, the effects of the surface tension on the spray shape and ligament formation could not be clearly identified, and only injection pressures of 5 and 10 MPa were studied.[23]

Consequently, there are still many open questions on dependencies of liquid properties on the spray formation for various injectors and conditions. Thus, the analyzation of such sprays is useful for a further understanding of atomization in manifold energy and process engineering applications. In spray imaging, there are a great variety of approaches to examine the characteristics of the liquid jets. The range of conventional methods extends from macroscopic and microscopic imaging over planar and tomographic measurements to qualitative and quantitative analyzations. Each region of the spray has a different characteristic (e.g., liquid volume fraction, droplet number, etc.), and thus variable visualization techniques have emerged in the last decades.[29] As for the nozzle near-field, the sprays are usually very dense, and hence the illumination and detection of the spray structure suffer from multiple light scattering. The majority of the detected photons have been scattered multiple times by ambient off-axis liquid structures. This effect leads to a masking of the investigated liquid structures in the core spray.[29–31]

In recent years, various measurement techniques such as x-ray radiography, ballistic imaging (BI), or structured laser illumination planar imaging (SLIPI) have been established for the attempt to suppress multiple scattering.[30,32,33] One approach to circumvent the detection of multiply scattered photons is to suppress the light, which is scattered by structures from outside of the focus plane. For example, in BI, the photons refracted by large fluid structures are preserved, while multiply scattered photons are filtered by a temporal gate to avoid misleading effects.[33,34] Another way to correct corruption of the data is filtering the erroneously detected photons in the post processing. This method is applied in SLIPI where a spatially modulated laser sheet is used to visualize the spray.[35,36]

In a previous work, Guénot *et al.*[31] introduced the combination of x-ray and 2p-LIF measurements to get insight into the detailed spray structure. Both techniques avoid the generation of multiple scattering, and thus the intensity of the ambiguous off-axis signals is insignificant. A comparison between the usual one- and the used two-photon fluorescence is depicted in Fig. 2.

The approach of 2p-LIF is based on the probability of a simultaneous absorption event of two photons. This probability is high in the focus plane, where the liquid structures absorb the fs-laser light and emit fluorescing photons. In the turbid spray region outside of the laser light sheet, the scattering effects occur with a wide spatial and temporal distribution. Consequently, the energy of an absorbed photon in the fluorescence dye is insufficient to elevate electrons from their electronic ground state to an excited state. This means that the dye will not show fluorescence in the case of one-photon excitation. Only two-photon excited dye molecules will show fluorescence, which leads to high-contrast spray imaging close to the nozzle, resulting in an improved identification of single liquid structures compared to conventional LIF techniques. The planar detection of the signal from a thin laser sheet allows a precise sizing of liquid structures, which is not possible in dense sprays with line-of-sight techniques such as shadowgraphy,[11,37] BI or x-ray radiography.[22] 2p-LIF has been widely applied in, e.g., biological microscopy[38] or in flame species measurements.[39–41] Berrocal *et al.*[30] introduced this technique to visualize atomizing water
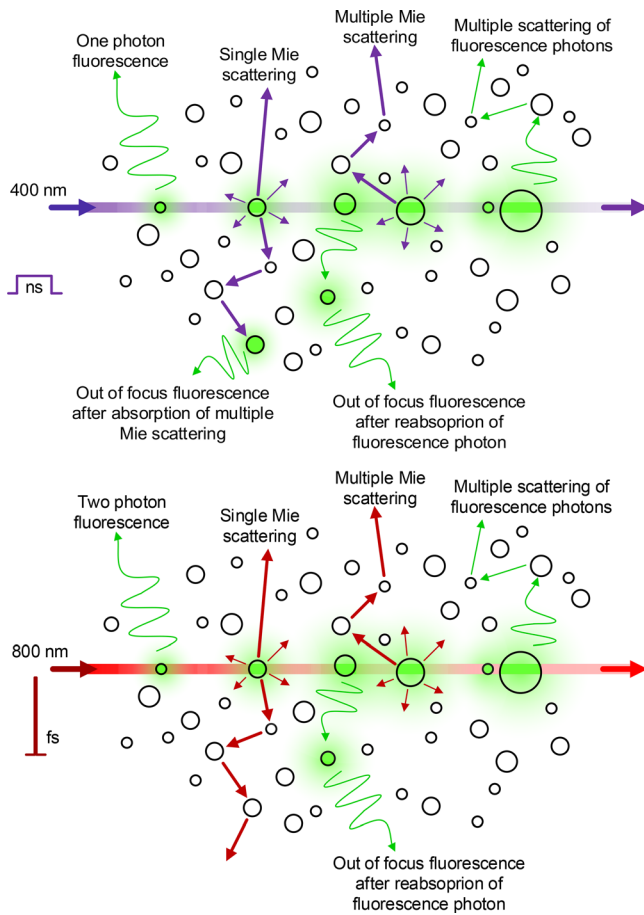
FIG. 2. Comparison of single- (top) and two-photon (bottom) laser induced fluorescence following Ref. 30. Note that different excitation laser wavelengths are applied.

sprays and presented a comparison to the common single-photon LIF approach.

In this work, we continued the investigations by operating the injector with different liquids at different injection pressures with a detection at various points in time during the injection [after the visible start of injection (vSOI)]. As mentioned above, the fluid properties like surface tension and viscosity determine the size, shape, and local distribution of the resulting liquid spray structures, as well as the spray width and cone angle. Furthermore, they control cyclic variations of the spray shape and targeting, which again determines the atomization quality, droplet dispersion as well as the subsequent mixing process.

Two fluids are selected with distinct differences in surface tension and viscosity. Different injection pressures of a DISI injector are studied to realize larger relative velocities that determine atomization especially in terms of aerodynamic breakup. Water and ethanol are selected as they are both common solvents in various spraying processes such as painting, cooling, particle synthesizing, and fuel combustion. Ethanol is a relevant synthetic fuel or biofuel for automotive or aerospace application. Water is also applied in combustion or industrial applications including exhaust gas after treatment (in mixtures with ammonia for selective catalytic reduction of nitrous oxides,

NO_x) or water/oil or water/fuel emulsions.[42] Water/fuel emulsions are promising for IC engine applications specifically at higher loads for improved fuel efficiency. Usually, fuel and water are injected separately with different injectors, but the injection of a mixture with different water content (depending on the engine load, with larger water concentration at higher load) using the same injection system would be advantageous.[43] In the case of emulsions, ethanol is also a promising solvent to stabilize the fuel/water mixture.[44] The microscopic spray shape was analyzed in the near-nozzle region using two photon LIF. These experiments can provide conclusions on the near-nozzle flow and primary spray formation for a detailed comparison of the fluid-dependent breakup process and the resulting liquid structures in dense sprays. Dimensions of liquid structures such as ligaments and clusters are determined based on the Feret's diameter in different positions downstream the nozzle and at various points in time after start of injection. The microscopic spray shape is analyzed in this paper via the cone angle, which is also discussed in terms of cyclic variability.

MATERIAL AND METHODS

The measurements were performed using a titanium-sapphire chirped pulse amplification system at Lund High-Power Facility, being further described in Ref. 45. The light intensity needs to be sufficient to overcome the energy gap of the fluorescent molecules with two photons. Therefore, the femtosecond laser generates pulses with a pulse energy of 10 mJ and a duration of 38 fs. With a center wavelength of 800 nm, two photons match the necessary energy for a two-photon fluorescence of the LIF dye fluorescein. A fraction of 0.1% fluorescein is added to both investigated liquids, water and ethanol. According to Guénot *et al.*, the equivalent fuel properties were determined to be unaffected by adding only this small amount of dye.[31] Additional measurements were conducted and showed no difference in dynamic viscosity and surface tension. Regarding the density, the mixture of ethanol with the dye shows a slight but negligible deviation of the density of pure ethanol. For the measurements, a commercial six-hole DISI injector with one optically clearly separable (as some jets overlap in some perspectives) definable spray cone is studied. It should be noted that a single-hole nozzle would provide better optical access. However, a single-hole injector or the blocking of individual nozzles of a multi-hole injector would lead to a changed and nonrealistic internal nozzle flow (i.e., varied turbulence and cavitation in the sac hole and injection holes) as well as spray behavior. Furthermore, a blocking of single holes could potentially result in a destruction of the injector.

The considered nozzle has a diameter of 100 μm. The injector is operated at the three different injection pressures of 10, 20, and 30 MPa. By increasing the pressure, a larger liquid mass is injected. Four different points in time after the visible SOI are recorded.

The imaging system of the setup is depicted in Fig. 3. A cylindrical lens with a focal length of 150 mm was utilized to generate a light sheet of ~2 cm × 100 μm at the nozzle exit. The detection system consists of a telecentric lens combined with a high resolution 5.5 megapixel sCMOS camera (Andor Zyla 5.5) resulting in a resolution of 6.5 μm/pixel.

For additional comparison, further images are taken with backlight illumination. For this purpose, the laser beam was directed straight to a fluorescing background behind the spray. Hence, the detection system collects a shadowgraphy image of the spray in that case, i.e., an integral spray image is taken. These
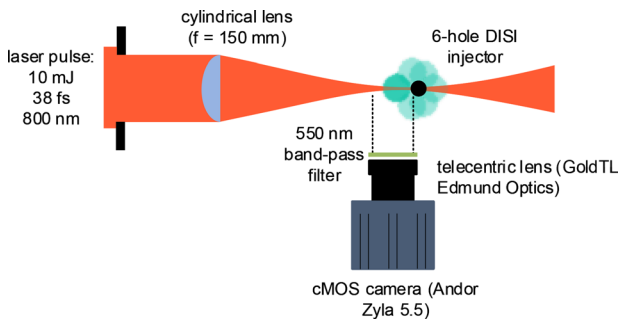
FIG. 3. Optical setup for the 2p-LIF measurements.

images are only used to reassess the information obtained by the 2p-LIF measurements.

The LIF images are post-processed with a routine in the software package ImageJ, which consists of a binarization of the maximal recorded 50 single-shot raw images, see Fig. 4. For this purpose, an intensity threshold of 25/255 is set for the converted eight-bit pictures, according to the method of Zantow et al.[46] This value is determined to separate between in-focus liquid structures (for signal intensities ≥ 25) and "background/noise signal" (for signal intensities < 25). The latter consists of camera noise and possibly fluorescence signal of very small droplets in the plane of the laser sheet. For the threshold determination, several methods were tested, and the above stated value of 25/255 was found to be optimum.

For the determination of the near-field cone angle, a linear interpolation of the radial spray boundary is conducted from the nozzle exit up to a 1 mm distance from the nozzle. The angle of the spray is measured within this region for the single-shot images. A 95% confidence interval is calculated using Student's t-distribution.

Additional post-processing provides information about the dimensions of the liquid structures located in the area up to 4 mm distance downstream the nozzle exit. An analysis of all structures with an overall size >15 arbitrarily connected pixels rejects droplets and small ligaments to reduce an overestimation of the size due to the resolution. All larger structures are evaluated by measuring Feret's diameter,

which is the maximum distance between any two points of the liquid body.

The Feret's diameter is also analyzed downstream in 0.5 mm steps from the nozzle exit. As the liquid structures in the nozzle far-field are smaller, compared to the ones in the 4 mm surrounding of the nozzle, the rejection threshold is lowered to 10 pixels. Thus, the considered structures exceed the size of 3×3 pixels, which is a common accuracy limit for sizing of liquid structures.[47,48]

For the angles and the Feret's diameters, values of all recorded single images are determined and averaged afterwards.

RESULTS AND DISCUSSION

Figure 5 shows enlargements of the liquid structures of a water and an ethanol spray. With the suppression of multiple light scattering, the main advantage of the two-photon approach, it was possible to image the structure of an optically dense liquid jet of a single spray plume near the nozzle. Generally, the recorded images provide deep insights into the atomization behavior including the emerged formations of ligaments, clusters, and droplets. These structures may be hidden or blurred and thus optically distorted when other planar 1p-LIF techniques or Mie-scattering are utilized. However, in these 2p-LIF-images, some fluorescence signal is visible in the right part of the plume, which also appears blurred. In these areas, the spray plume merges with the other jets (which is known as jet-to-jet interaction). The fluorescence signal originates from small droplets emanating from the out of focus spray plumes. These small structures refract the light randomly and not in unison. The spatial and temporal dispersion of secondary scattered fluorescence photons could also lead to a LIF signal in these regions. An attenuation of the fluorescence signal can be related to reabsorption effects of the dense spray partially covering the jet under study.

For clarification of the overlap of the plumes and jet-to-jet interaction, an exemplary shadowgraphy image is shown in Fig. 6 in comparison to an inverted raw 2p-LIF intensity image. By including the shadowgraphy images, the position of the adjacent off-axis spray cones is estimated. In the region of the single spray plume under investigation, the fluorescence image shows a clear signal. As for the interference with the remaining spray jets, the fluorescence intensity signal gets blurry and prevents a clear separation of the single plumes.
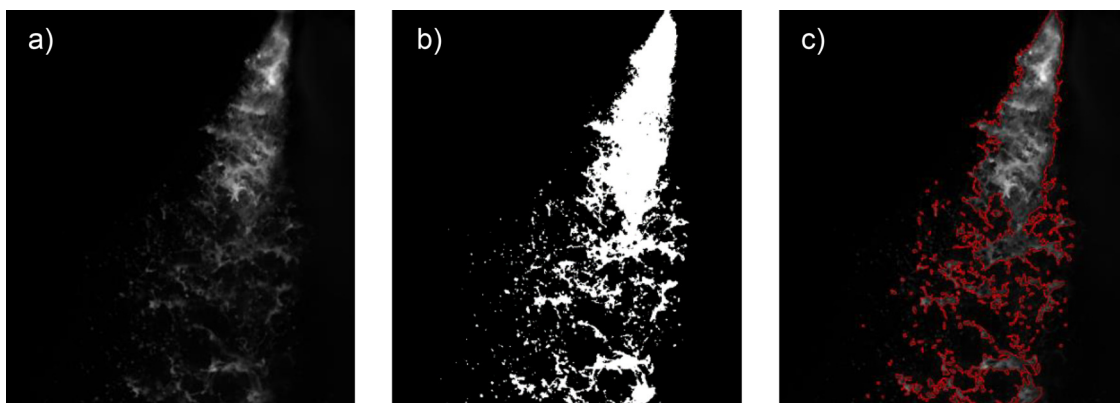

FIG. 4. Post processing of the images. (a) shows the original image, (b) the binarized structures, and (c) the contours superimposed with the original picture.
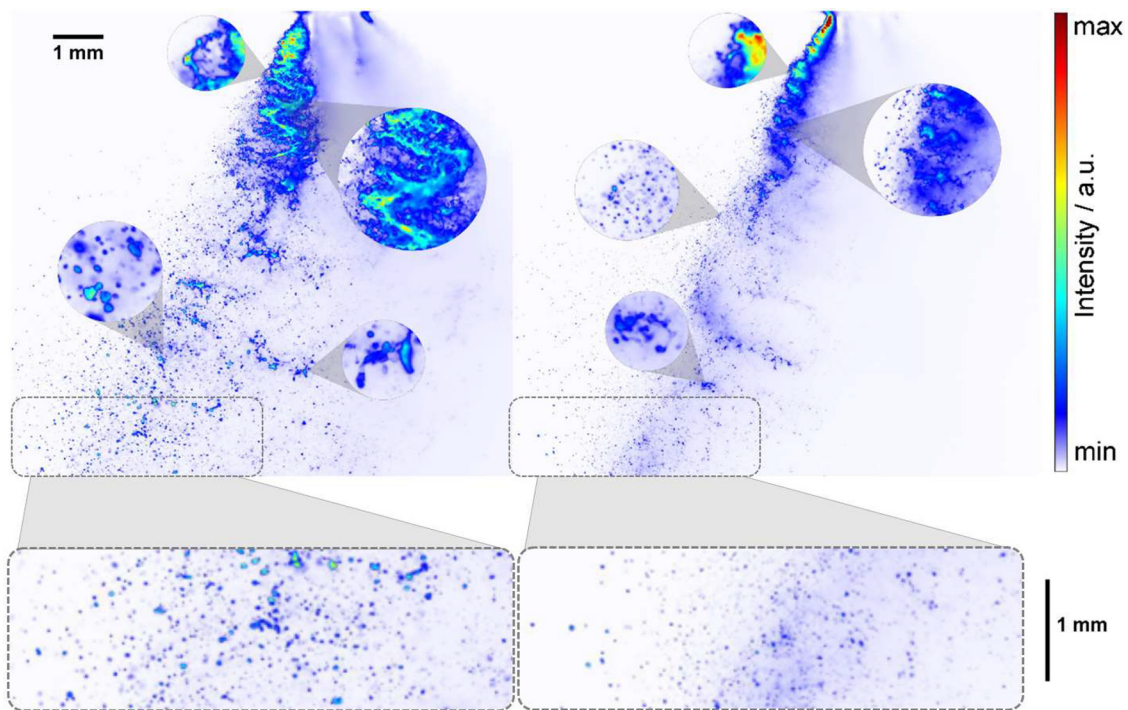
FIG. 5. Liquid fuel structure of a single plume of a water (left) and an ethanol spray (right) including magnifications of ligaments, wavy jet breakup zones, clusters, and droplets in the nozzle near and far-field (marked by separate boxes in the bottom row).

Consequently, in the subsequent analysis, the spray cone angle is related to the left boundary of the spray and the injector body axis (vertical line from nozzle exit). The width of the spray plume cannot be determined reliably.

Figure 7 depicts the sprays at 20 MPa, and this between 20 and 320 μs after visible injection start. Until the first pictures are taken at 20 μs, no distinct atomization takes place, and for both liquids, no ligaments are formed yet. In the latter time steps, the difference in the liquid breakup gets clearly visible, showing larger structures and oscillating/wavy jets in the water spray. After 220 μs, the spray exceeds the light sheet and the spray front cannot be tracked further. Since the spray images are taken for different injections, the development of the spray shape (esp. the spray width) is also superimposed with effects of cyclic variations.

Figure 8 shows the second picture series with single shots of ethanol and water sprays at three different injection pressures, all at 220 μs. With increasing pressure, the spray core breaks up faster, leading to smaller structures and a shorter spray penetration.
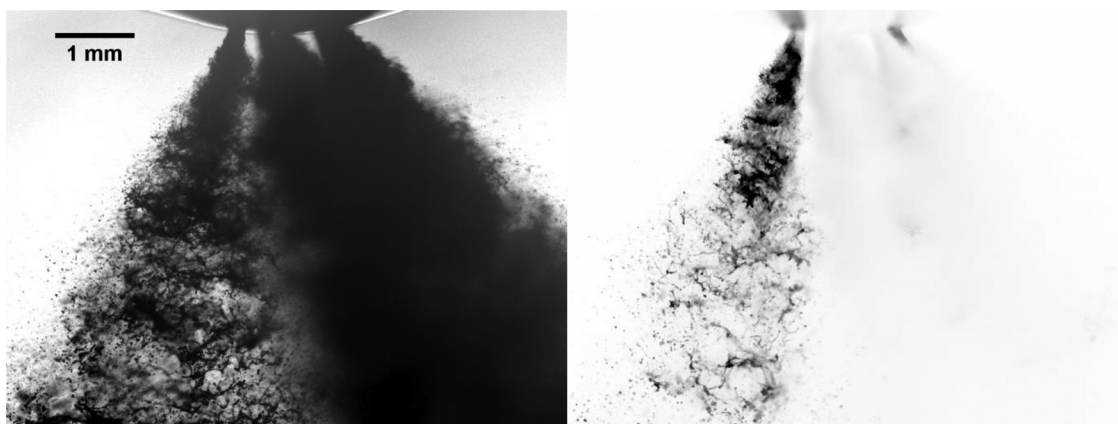

FIG. 6. Shadowgraphy image (left) and an inverted 2p-LIF image (right) of the water spray at 20 MPa and 220 μs after vSOI. Only spray structures at the left side of the single spray plume can be analyzed using 2p-LIF due to overlap of single plumes that may disturb optical access.
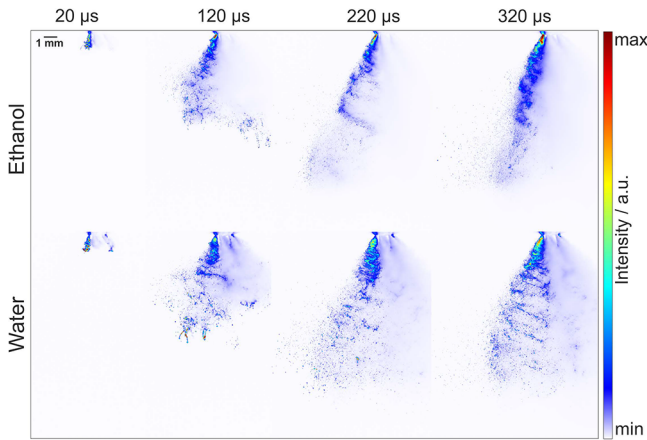
FIG. 7. Single shot LIF images for ethanol and water sprays at different detection points in time after vSOI at an injection pressure of 20 MPa.

Due to an increasing liquid pressure, a larger liquid mass is injected and the opening behavior of the needle changes. This leads to an increase in the ligament size and very large structures in the spray front specifically at 30 MPa. Mainly, the water spray shows an increased number of large structures in the form of blobs and sheets, which is also distinct at 30 MPa. Obviously, the breakup into smaller droplets is more efficient for ethanol. These resulting structure dimensions and droplet sizes would also affect the subsequent processes evaporation and mixture formation. In the next paragraph, the effects of the fluid properties on the spray shape and structure are analyzed in more detail.

Two main properties determining the nozzle flow and atomization are the viscosity and the surface tension. Density and vapor pressure of the liquids are provided as well. A larger vapor pressure will promote cavitation (geometric and string cavitation). The values are shown in Table I.
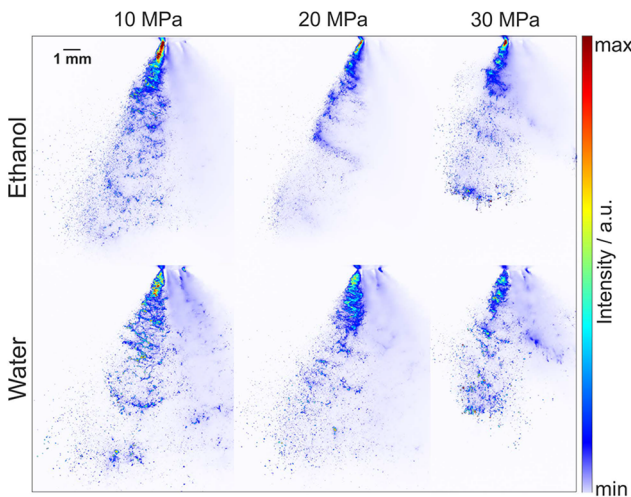

FIG. 8. Single shot LIF images of ethanol (top) and water (bottom) for an injection pressure variation at a point in time of 220 μs after vSOI.

TABLE I. Fluid properties of ethanol and water at 293 K and 0.1 MPa.[49,50]

	Density (kg/m^3)	Dynamic viscosity (mPa s)	Surface tension (mN/m)	Vapor pressure (kPa)
Ethanol	789.42	1.194	22.39	5.88
Water	998.21	1.002	72.88	2.34

Two pressure dependent dimensionless numbers—the Reynolds (Re) and Weber numbers for liquid flows (We$_L$)—were determined and are shown in Table II. The Reynolds number is defined by

$$Re = \frac{\rho \cdot D \cdot u}{\eta}, \quad (1)$$

whereas the Weber number can be mathematically formulated as

$$We_L = \frac{\rho \cdot D \cdot u^2}{\sigma}. \quad (2)$$

The included quantities are liquid density ρ, nozzle diameter D, velocity (at nozzle exit) u, dynamic viscosity η, and surface tension σ. The (average) velocity is calculated after Bernoulli's law as conducted in Ref. 51. It reaches values between 120 m/s for 10 MPa and 250 m/s for 30 MPa, depending on density and pressure difference. These values correlate with velocities of Diesel and DISI injectors at similar pressures, analyzed by x-ray phase contrast measurements of Neubauer.[52]

Due to its large surface tension, a significantly smaller Weber number is obtained for water, which will affect the droplet formation. The enlarged sections in Fig. 5 show a difference in drop sizes in the nozzle far-field (i.e., at the spray front). Experiments of Shin et al. based on Phase Doppler Particle Analyzer (PDPA) and spray tomography confirm that an increase in surface tension leads to larger droplets.[53] Based on the lower Weber number a comparably slow breakup is expected for water, explaining the larger droplets observed in Fig. 5.[54] With both Re und We$_L$, the Ohnesorge number (Oh) can be calculated. Eliminating the velocity, it describes the ratio of frictional to surface forces and is defined as follows:

$$Oh = \frac{\sqrt{We_L}}{Re} = \frac{\eta}{\sqrt{D \cdot \rho \cdot \sigma}}. \quad (3)$$

A higher Ohnesorge number indicates a faster liquid jet breakup into smaller droplets. For ethanol, an Oh number of 0.028 is received, while

TABLE II. Calculated values for Reynolds and Weber numbers at different injection pressures.

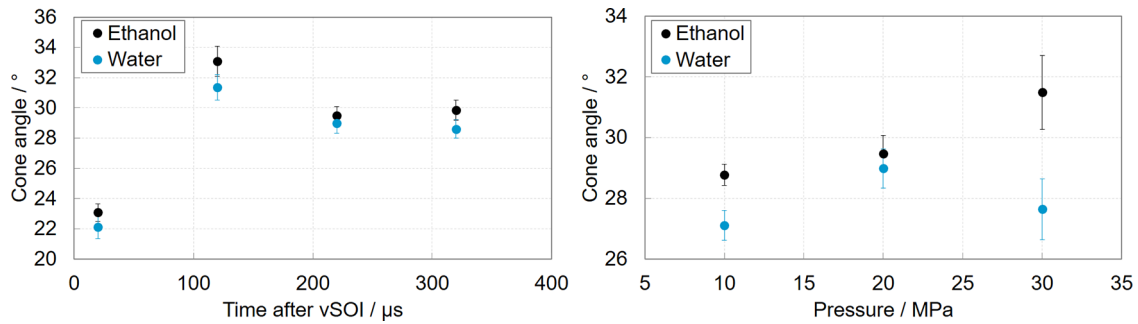|	10 MPa	20 MPa	30 MPa
Re			
Ethanol	9473	13 397	16 407
Water	12 696	17 955	21 990
We$_L$			
Ethanol	72 367	144 733	217 100
Water	22 228	44 457	66 685

FIG. 9. Time dependent spray cone angle at 20 MPa (left) and injection pressure dependent cone angle at 220 μs (right) with 95% confidence interval.

for water the Ohnesorge number is 0.012. According to the Ohnesorge-diagram, this means that the breakup mode is closer to the "2nd wind-induced regime" for water, while it is clearly in the atomization regime for ethanol. Thus, by trend a faster breakup and smaller droplets are expected for ethanol. This coincides qualitatively with the spray images and a quantitative analysis is presented below in terms of the Feret's diameter of liquid structures.

The Reynolds number is also relevant for the nozzle flow, which determines cavitation and the turbulence-induced breakup. Re is more than 30% larger for water than it is for ethanol. As for the fluid behavior, increased turbulence and cavitation inside the nozzle are expected for larger Reynolds numbers. This may lead to a reduced cone angle according to references.[23,28]

The determined spray cone angles are provided in Fig. 9 at various points in time (left) and for various injection pressures (right). As anticipated, the resulting spray angles for water are smaller for all injection pressures and points in time studied due to the lower liquid viscosity.

Regarding the time-dependent behavior, both liquids show a similar trend. The incipient nozzle near-field cone angle is small, while in the subsequent time step, a strong increase is observed, which can be explained by the increasing flow velocity and developing flow profile during needle opening. It can be assumed that the axial injection velocity is roughly doubled between part lift ($\sim$10 μm) and full needle lift, see, e.g., Ref. 23. When the injector is fully opened (i.e., the needle is completely lifted, which occurs at about 220 μs), the nozzle flow is in a more stationary phase leading to a further decline of the cone angle (by about 8%–12%) and reduced confidence intervals with advanced time (compare, e.g., 120 and 220 μs), see Table III. In Ref. 55, it is argued that the larger cone angle during needle opening is due to a more distinct cavitation. The larger relative vapor fraction in the injection hole due to cavitation during partial needle lift was also confirmed by Zigan et al.,[23] who also showed lower cone angles at full needle lift conditions in the stationary phase.

Now, the spray cone angle is studied at 220 μs for the two liquids and injection pressures. This is a relatively early point in time of the spray formation, but the integral macroscopic spray shape (especially spray length and width) is determined in this period. The angle of the ethanol spray at 220 μs is again always larger (on average 7.3%) than the one of water and it shows a steady increase with rising injection pressure. This is probably due to two reasons: First, the higher viscosity (and lower Reynolds number) leads to a more distinct flow deceleration at the nozzle wall and larger velocity gradients at the radial boundary of the emerging fuel jet. For ethanol, the flow is in the transition region and behaves more "laminar-like," which could result in larger spray cone angles.[23,28] Second, and additionally, the aerodynamic breakup is more distinct for ethanol compared to water, which is indicated by the much higher Weber number of ethanol. This leads to a faster atomization, and due to the larger radial velocity component induced by the nozzle flow, the surface waves grow in the jet specifically at the radial boundaries. This effect was less clear in previous investigations,[23,28] in which the surface tension difference between the liquids was not that distinct. Obviously, the aerodynamic breakup is more relevant in the near nozzle region in the present study due to the larger differences in surface tensions, which even complicates the jet breakup. The larger injection pressure leads to an increased velocity difference between spray and air so that these aerodynamic effects become more important. Consequently, the spray is pushed aside of its original propagation direction resulting in a broadened spray plume, which again supports aerodynamic breakup.

Additionally, the higher vapor pressure of ethanol leads to a higher probability of cavitation in the nozzle. Together with the lower Reynolds number and a transitional flow behavior, larger fluctuations in the spray shape can be observed and the angle increases. In general, the same trend was reported for the near-nozzle cone angle of DISI spray for a pressure change from 5 to 10 MPa.[56] There, an increased spray angle was observed for increased pressures as well. For water, a similar tendency is observed for the lower injection pressures, however, at 30 MPa injection pressure, the measurements reveal a lower

TABLE III. Average cone angles and 95% confidence intervals at 20 MPa.

	20 μs	120 μs	220 μs	320 μs
Ethanol	23.07° ± 0.56	33.08° ± 0.99	29.48° ± 0.59	29.85° ± 0.66
Water	22.13° ± 0.79	31.36° ± 0.85	28.98° ± 0.65	28.60° ± 0.62

angle for water than it was evaluated for 20 MPa. Payri *et al.* reported larger spray angles for larger injection pressures (30 and 60 MPa were studied for one liquid), which was explained by increasing cavitation tendency with pressure.[55]

In general, the increased confidence intervals for both liquids at higher pressures indicate a rise of the cyclic variations, which can be explained by larger wrinkling of the liquid surface in the near-nozzle region due to the aerodynamic breakup. The cyclic variations (in terms of 95% confidence interval) at 30 MPa are for ethanol 51.7% and for water 35.8% higher than at 20 MPa. These elevations in the cyclic variation cannot be explained by the nozzle flow since a larger Reynolds number due to larger flow velocity would imply a more stable flow behavior.

Regarding Feret's diameter of the liquid structures in the near-nozzle region up to 4 mm distance from the nozzle exit, no clear trend relating to the liquid properties could be observed for varied pressures at 220 μs. The time-dependent (left) and pressure (right) variation of the mean values including the 95% confidence intervals are presented in Fig. 10. The analyzed liquid structures show average dimensions of about 80–130 μm.

For water, the length of the liquid structures is reduced with an increase in the injection pressure. At high injection pressures, the flow is accelerated and the Reynolds number rises. The intensified turbulence and aerodynamic breakup results in smaller spray structures. Ethanol shows a different breakup behavior with larger structures at 20 MPa. At 30 MPa the turbulent and aerodynamic breakup predominates, which may be supported by cavitation-induced breakup, leading to smaller Feret's diameters.

At the incipient time step, high values for Feret's diameter with large fluctuations are observed. The images show only very little breakup of the jet and the (few) larger liquid structures explain the augmented confidence intervals. Due to further jet breakup because of the increased velocity when the needle is fully opened, the subsequent decline in the diameter was presumed. For the following time steps, the spray front exceeds the analyzed region, leading to a shift to slightly larger structures. In principle, the size of the liquid bodies is very similar for both liquids in the near-nozzle region. In Ref. 56, the differences in structural dimensions depending on the liquid viscosity and surface tension were also small, in general, although a higher number of large structures were observed for a higher viscous fuel with larger surface tension. Most probably, a larger number of images and measurement positions are necessary for clearer dependencies of

Feret's diameter on the liquid properties. This analysis is conducted in the subsequent paragraphs.

To get better statistics for the structure sizes, the nozzle far-field was added to the analysis in another routine. With this method, up to around 2000 structures are evaluated in some of the investigated regions. In Fig. 11, the Feret's diameters for both, ethanol and water, downstream the nozzle exit are shown for all three investigated injection pressures at 220 μs. Due to the high surface tension of water and the resulting lower Weber number, a slower jet breakup is expected for water. Thus, compared to ethanol, larger liquid structures can be observed in the region from 5 up to 10 mm distance to the nozzle in all operating points. At 20 MPa, the difference is most distinct: The structures of water are about 116% larger on average compared to ethanol. Measurements of Kooji *et al.* showed the same tendency of smaller droplets with lower surface tension and thus a higher Weber number.[57] However, no primary spray structures were reported. At 30 MPa, larger structures can be found in the spray front, specifically for ethanol. This may be explained by the needle opening, which is much more forceful at higher pressures and may lead to a "blob"-injection. Please note that the position of the spray front is different for the various injection pressures (as the breakup distance of the spray is shorter at increased pressure).

Generally, the analyzed ligaments and clusters range from 20 μm up to 90 μm. The largest structures are perceived close to the nozzle, where liquid jet breakup scarcely starts. In a region 1 to 3 mm, only very few small droplets are separated from the spray core and can be recognized. After the breakup of the main jet at 3 to 5 mm distance from the nozzle exit, the average Feret's diameter decreases almost continually. In the spray front, most operating points show an increase in the structure size. These large structures are attributable to the behavior during the needle opening, which is still recognizable in the detected spray front region at 220 μs. However, also droplet coalescence and coagulation lead to an increase in the Feret's diameter at the denser spray front.

At all three injection pressures, water has a maximum in the Feret's diameter close to the nozzle. For ethanol, the peak is not as clearly apparent due to the different breakup behavior especially at 20 and 30 MPa. In Fig. 7, the contrast in atomization for both liquids is also visible in the single shot images and fits the analyzed data. Water tends to a complete disintegration into long, wavy ligaments and sheet-like structures, whereas ethanol breaks up into smaller clusters and droplets in the dense spray region. Additionally, due to the low
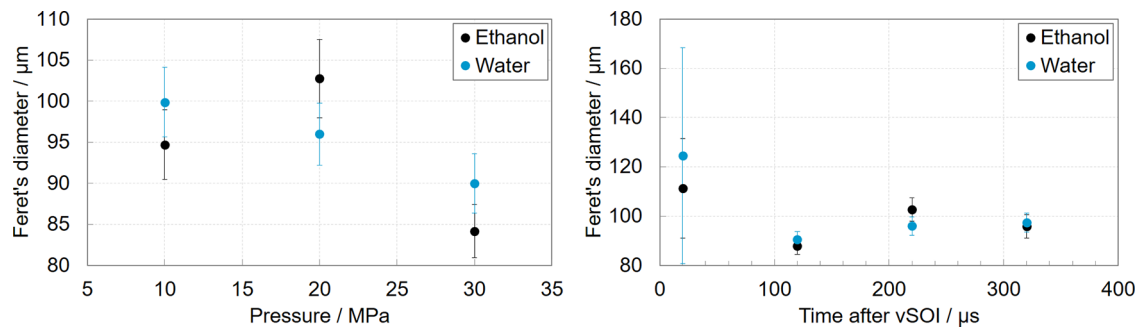

FIG. 10. Injection pressure dependent Feret's diameter at 220 μs (left) and time dependent Feret's diameter at 20 MPa (right) with 95% confidence interval. The measurement positions are up to 4 mm distance from the nozzle exit.
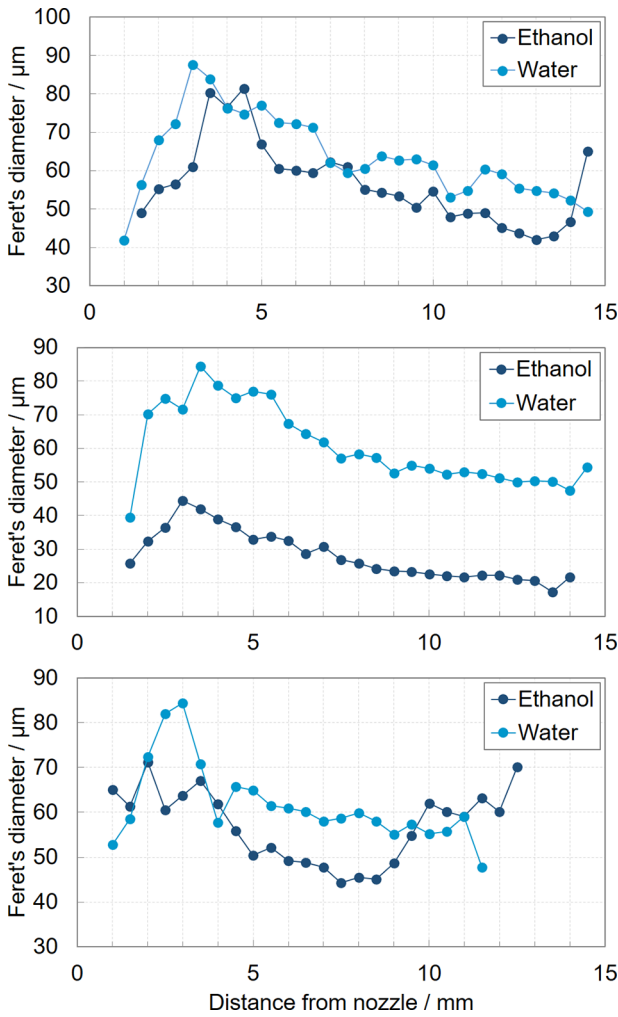
FIG. 11. Comparison of ligament sizes downstream the nozzle for water and ethanol at 10 MPa (top), 20 MPa (middle), and 30 MPa (bottom) and 220 μs after vSOI.

boiling temperature, droplets in the ethanol spray should evaporate faster than in a water spray. However, the evaporation enthalpy is also relatively large and for the large structures studied here, the evaporation should be insignificant. For example, the diameter of a 10 μm ethanol droplet is reduced due to evaporation by about 3.4% after 2 ms following Koegl et al.[58] under similar conditions, and the timescale studied here is maximal 320 μs.

Figure 12 shows these values of the Feret's diameter over nozzle distance at 10, 20, and 30 MPa for water on the left and ethanol on the right side. For water, the ligament sizes between 10 and 20 MPa differ mostly in the nozzle far field, whilst the difference is only of about 10 μm. The diameters are slightly smaller at a higher injection pressure, as assumed due to higher velocities and turbulences in the nozzle and therefore an increased Reynolds and Weber number. At 30 MPa the analysis reveals a faster atomization with a decrease in the ligament sizes close to the nozzle. Small diameters of around 60 μm are detected in the area from 4 mm to around 10 mm.

For ethanol shortly after the nozzle, a decline in diameter can be observed until large structures are detected in the spray front. For ethanol the ligament sizes at 20 MPa injection pressure differ most from the other measurements, revealing much lower values than all other considered operating points. On average ethanol showed about 24% smaller structures compared to the water spray for all investigated positions downstream the nozzle and injection pressures. This behavior could be explained due to different interfering effects. In comparison to water, the ethanol spray remains broader. However, the ethanol spray breaks up faster and into smaller structures, as indicated by the Ohnesorge number in Table I. In principle, this trend can be explained by the classical aerodynamic atomization theory, but additionally, the larger near-nozzle jet cone angle of ethanol supports the jet disintegration. Consequently, the differences of the Feret's diameter are smaller over the distance from the nozzle for ethanol, which is much more pronounced for water. At 20 MPa, in particular, the increased liquid momentum leads to more detected and smaller droplets, but the spay is not affected by the needle opening as much as at 30 MPa.

In general, we could observe relatively large structures also in downstream distances of 14 mm from the nozzle. Typically, they are not spherical, and consequently, they cannot be detected by conventional sizing techniques such as phase Doppler interferometry (PDI).
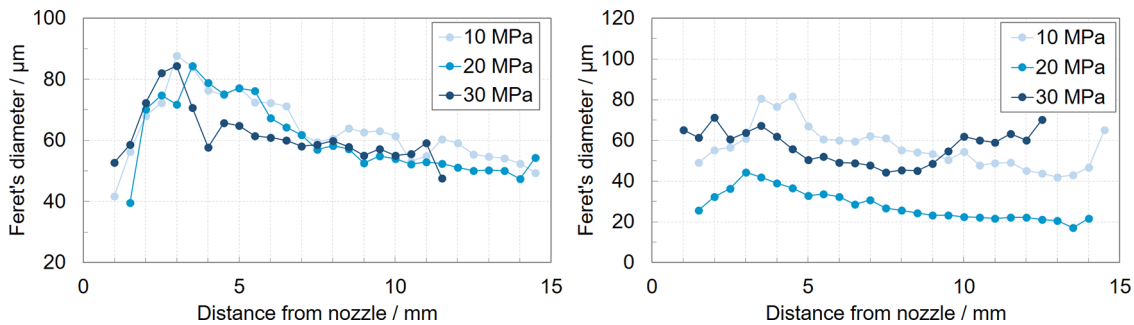

FIG. 12. Depiction of the ligament sizes in radial distance from the nozzle exit for water (left) and ethanol (right). For both liquids, three different injection pressures are considered at 220 μs after vSOI.

The largest structures were found at about 3 mm. After 7 mm (30 MPa) to 10 mm (10 MPa), no significant change of the size of large-scale structures occurs anymore. Droplets of smaller size ($< 20 \mu m$) were not analyzed in the framework of this study as the focus was on primary spray structures. In general, there is almost no information on such spray structures available in the literature since most of these studies focus on droplet sizing using point-wise measurements based on PDI (or PDPA).[53,59]

CONCLUSIONS

The 2p-LIF approach was applied to a common DISI injector to quantitatively analyze the spray shape and primary spray structures depending on the liquid properties. A high-resolution imaging of the dense spray core enabled a comprehensive analysis of the atomization process close to the nozzle exit at different injection pressures. The recorded images were evaluated in terms of the cone angle and liquid structure lengths such as ligaments and clusters in the nozzle near-field. So far, there were almost no quantitative studies of primary spray structures to the best of the authors' knowledge. The basic model presumption from 2013[23] which predicts that higher viscosities will result in increased plume angles, could be verified and extended to much higher injection pressures (up to 30 MPa, i.e., ~factor 3 larger) and Weber numbers (up to about 217 000, i.e., ~factor 5 larger). It could also be proved that the surface tension and vapor pressure affect the cone angle less significantly. This model is in contrast to classical atomization models that just include aerodynamic breakup. Largest cyclic variations of the spray angle were observed during needle opening, i.e., early points in time after start of injection. Higher injection pressures showed larger cone angles and smaller liquid structures of the primary jet for both tested liquids. The atomization shows a main jet breakup distance of 7–10 mm, in which the structure sizes decreased drastically, especially for water. The jet breakup was much faster for ethanol, which showed on average about 24% smaller structures compared to the water spray for the studied injection pressures in the complete spray region. More homogeneous structural sizes and no clear main breakup distance could be observed for ethanol further downstream the nozzle. The injection pressure showed a relatively small effect on the dimensions of the primary structures for water. This effect was larger for ethanol, especially the larger injection pressure of 20 MPa resulted in about 50% smaller structures on average compared to 10 MPa.

In future work, it is necessary to study the effects of the nozzle flow in more detail, which requires optical accessible nozzles. Additionally, a combination of different optical diagnostics is required for better optical access of the spray, which could also allow tomography of several jets (such as x-ray tomography). The model should be tested for modern synthetic or biogenic fuels that can be better designed and varied regarding fuel properties. This could allow a better decoupling of different effects of the determining fuel properties, viscosity, vapor pressure, and surface tension for much deeper insights into nozzle flow and breakup processes.

ACKNOWLEDGMENTS

AUTHOR DECLARATIONS
Conflict of Interest

The authors have no conflicts to disclose.

Author Contributions

Hannah Ulrich: Data curation (equal); Formal analysis (lead); Investigation (equal); Software (lead); Validation (lead); Visualization (lead); Writing – original draft (lead); Writing – review and editing (lead). **Bastian Lehnert:** Data curation (equal); Investigation (equal); Software (supporting); Validation (supporting). **Diego Guénot:** Investigation (equal). **Kristoffer Svendsen:** Investigation (equal). **Olle Lundh:** Conceptualization (equal); Resources (equal); Supervision (equal). **Michael Wensing:** Resources (equal); Supervision (equal). **Edouard Berrocal:** Conceptualization (equal); Funding acquisition (lead); Investigation (supporting); Methodology (equal); Project administration (equal); Resources (equal); Supervision (equal); Visualization (equal); Writing – original draft (supporting). **Lars Zigan:** Conceptualization (equal); Funding acquisition (equal); Methodology (equal); Project administration (lead); Supervision (equal); Writing – original draft (supporting); Writing – review and editing (supporting).

DATA AVAILABILITY

The data that support the findings of this study are available from the corresponding author upon reasonable request.

REFERENCES

[1]N. Ashgriz, *Handbook of Atomization and Sprays: Theory and Applications* (Springer, New York, 2011).

[2]G. O. Erol, J. Hasslberger, M. Klein, and N. Chakraborty, "A direct numerical simulation analysis of spherically expanding turbulent flames in fuel droplet-mists for an overall equivalence ratio of unity," Phys. Fluids **30**, 086104 (2018).

[3]L. Angelilli, P. P. Ciottoli, F. Picano, M. Valorani, and H. G. Im, "Assessment of subgrid dispersion models for large eddy simulations of turbulent jet flows with dilute spray droplets," Phys. Fluids **34**, 073305 (2022).

[4]F. Ferraro, S. Gierth, S. Salenbauch, W. Han, and C. Hasse, "Soot particle size distribution reconstruction in a turbulent sooting flame with the split-based extended quadrature method of moments," Phys. Fluids **34**, 075121 (2022).

[5]M. Koegl, B. Hofbeck, S. Will, and L. Zigan, "Investigation of soot formation and oxidation of ethanol and butanol fuel blends in a DISI engine at different exhaust gas recirculation rates," Appl. Energy **209**, 426 (2018).

[6]Y. Liu and B. Derby, "Experimental study of the parameters for stable drop-on-demand inkjet performance," Phys. Fluids **31**, 032004 (2019).

[7]A. Sankaran, J. Wu, R. Granda, V. Yurkiv, F. Mashayek, and A. L. Yarin, "Drop impact onto polarized dielectric surface for controlled coating," Phys. Fluids **33**, 062101 (2021).

[8]K. Meng, L. Li, X. Zhang, Z. Huang, F. Wang, R. Li, and Q. Lin, "Comparison of combustion and micro-explosion characteristics of droplet group of biodiesel/ethanol and biodiesel/RP-3/ethanol," Phys. Fluids **34**, 061903 (2022).

[9]I. Qavi and L. Jiang, "Optical characterization of near-field sprays for various alternative and conventional jet fuels using a flow-blurring injector," Flow, Turbul. Combust. **108**, 599 (2022).

[10]V. Dorfner, J. Domnick, F. Durst, and R. Kohler, "Viscosity and surface tension effects in pressure swirl atomization," Atomization Sprays **5**, 261 (1995).

[11]T. G. Theofanous and G. J. Li, "On the physics of aerobreakup," Phys. Fluids **20**, 052103 (2008).

[12]W. Zhu, N. Zhao, X. Jia, X. Chen, and H. Zheng, "Effect of airflow pressure on the droplet breakup in the shear breakup regime," Phys. Fluids **33**, 053309 (2021).

[13]R. D. Reitz, "Modeling atomization processes in high-pressure vaporizing sprays," Atomisation Spray Technol. **3**, 309 (1987).

[14]O. Desjardins, G. Blanquart, G. Balarac, and H. Pitsch, "High order conservative finite difference scheme for variable density low Mach number turbulent flows," J. Comput. Phys. **227**, 7125 (2008).

[15]A. Fath, "Charakterisierung Des Strahlaufbruch-Prozesses Bei Der Instationären Druckzerstäubung," Dissertation (FAU Erlangen-Nürnberg/ESYTEC-Verlag, Erlangen, 1997).

[16]X. Jiang, G. A. Siamas, K. Jagus, and T. G. Karayiannis, "Physical modelling and advanced simulations of gas–liquid two-phase jet flows in atomization and sprays," Prog. Energy Combust. Sci. **36**, 131 (2010).

[17]K. Y. Huh and A. D. Gosman, in "Phenomenological model of diesel spray atomisation," in Proceedings of the international Conference on Multiphase Flows, Tsukuba, Japan, 24–27 September 1991, pp. 515–518.

[18]G. Stiesch, *Modeling Engine Spray and Combustion Processes* (Springer, Berlin, 2003).

[19]A. Sou, S. Hosokawa, and A. Tomiyama, "Effects of cavitation in a nozzle on liquid jet atomization," Int. J. Heat Mass Transfer **50**, 3575 (2007).

[20]R. D. Reitz, "Mechanism of atomization of a liquid jet," Phys. Fluids **25**, 1730 (1982).

[21]M. Hosbach, R. Skoda, T. Sander, U. Leuteritz, and M. Pfitzner, "On the temperature influence on cavitation erosion in micro-channels," Exp. Therm. Fluid Sci. **117**, 110140 (2020).

[22]D. Guénot, K. Svendsen, B. Lehnert, H. Ulrich, A. Persson, A. Permogorov, L. Zigan, M. Wensing, O. Lundh, and E. Berrocal, "Distribution of liquid mass in transient sprays measured using laser-plasma-driven x-ray tomography," Phys. Rev. Appl. **17**, 064056 (2022).

[23]L. Zigan, J.-M. Shi, I. Krotow, I. Schmitz, M. Wensing, and A. Leipertz, "Fuel property and fuel temperature effects on internal nozzle flow, atomization and cyclic spray fluctuations of a direct injection spark ignition–injector," Int. J. Engine Res. **14**, 543 (2013).

[24]A. Andriotis, M. Gavaises, and C. Arcoumanis, "Vortex flow and cavitation in diesel injector nozzles," J. Fluid Mech. **610**, 195 (2008).

[25]D. Mamaikin, T. Knorsch, P. Rogler, J. Wang, and M. Wensing, "The effect of transient needle lift on the internal flow and near-nozzle spray characteristics for modern GDI systems investigated by high-speed X-ray imaging," Int. J. Engine Res. **23**, 300 (2022).

[26]M. M. Tareq, R. A. Dafsari, S. Jung, and J. Lee, "Effect of the physical properties of liquid and ALR on the spray characteristics of a pre-filming airblast nozzle," Int. J. Multiphase Flow **126**, 103240 (2020).

[27]L. Lešnik, B. Kegl, G. Bombek, M. Hočevar, and I. Biluš, "The influence of in-nozzle cavitation on flow characteristics and spray break-up," Fuel **222**, 550 (2018).

[28]R. Torelli, S. Som, Y. Pei, Y. Zhang, and M. Traver, "Influence of fuel properties on internal nozzle flow development in a multi-hole diesel injector," Fuel **204**, 171 (2017).

[29]T. D. Fansler and S. E. Parrish, "Spray measurement technology: A review," Meas. Sci. Technol. **26**, 012002 (2015).

[30]E. Berrocal, C. Conrad, J. Püls, C. L. Arnold, M. Wensing, M. Linne, and M. Miranda, "Two-photon fluorescence laser sheet imaging for high contrast visualization of atomizing sprays," OSA Continuum **2**, 983 (2019).

[31]D. Guénot, K. Svendsen, J. Björklund Svensson, H. Ekerfelt, A. Persson, O. Lundh, and E. Berrocal, "Simultaneous laser-driven x-ray and two-photon fluorescence imaging of atomizing sprays," Optica **7**, 131 (2020).

[32]A. Coghe and G. E. Cossali, "Quantitative optical techniques for dense sprays investigation: A survey," Opt. Lasers Eng. **50**, 46 (2012).

[33]M. Linne, "Imaging in the optically dense regions of a spray: A review of developing techniques," Prog. Energy Combust. Sci. **39**, 403 (2013).

[34]M. Rahm, M. Paciaroni, Z. Wang, D. Sedarsky, and M. Linne, "Evaluation of optical arrangements for ballistic imaging in sprays," Opt. Express **23**, 22444 (2015).

[35]E. Berrocal, E. Kristensson, P. Hottenbach, M. Aldén, and G. Grünefeld, "Quantitative imaging of a non-combusting diesel spray using structured laser illumination planar imaging," Appl. Phys. B **109**, 683 (2012).

[36]T. Breuninger, K. Greger, and E. H. K. Stelzer, "Lateral modulation boosts image quality in single plane illumination fluorescence microscopy," Opt. Lett. **32**, 1938 (2007).

[37]E. Berrocal, E. Kristensson, and L. Zigan, "Light sheet fluorescence microscopic imaging for high-resolution visualization of spray dynamics," Int. J. Spray Combust. Dyn. **10**, 86 (2018).

[38]C. Xu, W. Zipfel, J. B. Shear, R. M. Williams, and W. W. Webb, "Multiphoton fluorescence excitation: new spectral windows for biological nonlinear microscopy" Proc. Natl. Acad. Sci. U. S. A. **93**, 10763 (1996).

[39]J. H. Frank, X. Chen, B. D. Patterson, and T. B. Settersten, "Comparison of nanosecond and picosecond excitation for two-photon laser-induced fluorescence imaging of atomic oxygen in flames," Appl. Opt. **43**, 2588 (2004).

[40]W. D. Kulatilaka, B. D. Patterson, J. H. Frank, and T. B. Settersten, "Comparison of nanosecond and picosecond excitation for interference-free two-photon laser-induced fluorescence detection of atomic hydrogen in flames," Appl. Opt. **47**, 4672 (2008).

[41]D. R. Richardson, S. Roy, and J. R. Gord, "Femtosecond, two-photon, planar laser-induced fluorescence of carbon monoxide in flames," Opt. Lett. **42**, 875 (2017).

[42]C. K. Law, C. H. Lee, and N. Srinivasan, "Combustion characteristics of water-in-oil emulsion droplets," Combust. Flame **37**, 125 (1980).

[43]B. Franzke, T. Voßhall, P. Adomeit, and A. Müller, "Water injection for meeting future RDE requirements for turbocharged gasoline engines," MTZ Worldwide **80**, 30 (2019).

[44]M. Koegl, C. Mull, Y. N. Mishra, S. Will, and L. Zigan, "Characterization of fuel/water mixtures and emulsions with ethanol using laser-induced fluorescence," Appl. Opt. **59**, 1136 (2020).

[45]K. Svendsen, I. G. González, M. Hansson, J. B. Svensson, H. Ekerfelt, A. Persson, and O. Lundh, "Optimization of soft X-ray phase-contrast tomography using a laser wakefield accelerator," Opt. Express **26**, 33930 (2018).

[46]M. Zantow, R. Dendere, and T. S. Douglas, in *Annual International Conference of the IEEE Engineering in Medicine and Biology Society* (IEEE, 2013), p. 1776.

[47]A. Asgarian, Z. Yang, Z. Tang, M. Bussmann, and K. Chattopadhyay, "An image feature consolidation technique (IFCT) to capture multi-range droplet size distributions in atomizing liquid sheets," Exp. Fluids **61**, 1–22 (2020).

[48]L. P. Chin, P. G. LaRose, R. S. Tankin, T. Jackson, J. Stutrud, and G. Switzer, "Droplet distributions from the breakup of a cylindrical liquid jet," Phys. Fluids A **3**, 1897 (1991).

[49]J. A. Dean and N. A. Lange, *Lange's Handbook of Chemistry* (McGraw-Hill, New York, 1999).

[50]E. W. Lemmon, M. L. Huber, and M. O. McLinden, "REFPROP 9.1, Reference Fluid Thermodynamic and Transport Properties Database" (NIST, 2013).

[51]S. Bornschlegel, C. Conrad, A. Durst, J. Wang, and M. Wensing, "Multi-hole gasoline direct injection: In-nozzle flow and primary breakup investigated in transparent nozzlesand with X-ray," Int. J. Engine Res. **19**, 67 (2018).

[52]A. Neubauer, "Messtechnische Erfassung primärer Strahlstrukturen von Benzin- und Dieselsprays," Dissertation (FAU Erlangen-Nürnberg, Erlangen, 2020).

[53]J. Shin, D. Kim, J. Seo, and S. Park, "Effects of the physical properties of fuel on spray characteristics from a gas turbine nozzle," Energy **205**, 118090 (2020).

[54]L. Zigan, I. Schmitz, A. Flügel, M. Wensing, and A. Leipertz, "Structure of evaporating single- and multicomponent fuel sprays for 2nd generation gasoline direct injection," Fuel **90**, 348 (2011).

[55]F. Payri, V. Bermúdez, R. Payri, and F. J. Salvador, "The influence of cavitation on the internal flow and the spray characteristics in diesel injection nozzles," Fuel **83**, 419 (2004).

[56]L. Zigan, I. Schmitz, M. Wensing, and A. Leipertz, in 23rd Annual Conference on Liquid Atomization and Spray Systems, 2010.

[57]S. Kooij, R. Sijs, M. M. Denn, E. Villermaux, and D. Bonn, "What determines the drop size in sprays?," Phys. Rev. X **8**, 031019 (2018).

[58]M. Koegl, Y. N. Mishra, K. Baderschneider, C. Conrad, B. Lehnert, S. Will, and L. Zigan, "Planar droplet sizing for studying the influence of ethanol admixture on the spray structure of gasoline sprays," Exp. Fluids **61**, 209 (2020).

[59]Z. Zhang and S. Ziada, "PDA measurements of droplet size and mass flux in the three-dimensional atomisation region of water jet in air cross-flow," Exp. Fluids **28**, 29 (2000).

frontiers | Frontiers in Physics

Droplet thermometry based on an optimized two dye two-color laser-induced fluorescence concept

Hannah Ulrich[1,2]*, Sophie Sigl[3], Michael Möhnle[3], Edouard Berrocal[2,4] and Lars Zigan[1,2]

[1]Fakultät für Luft- und Raumfahrttechnik, Institut für Thermodynamik, Universität der Bundeswehr München (UniBw M), Neubiberg, Germany, [2]Erlangen Graduate School in Advanced Optical Technologies (SAOT), Friedrich-Alexander-Universität Erlangen-Nürnberg (FAU), Erlangen, Germany, [3]Lehrstuhl für Technische Thermodynamik (LTT), Friedrich-Alexander-Universität Erlangen-Nürnberg (FAU), Erlangen, Germany, [4]Department of Physics, Faculty of Engineering, Lund University, Lund, Sweden

In this work two-color laser-induced fluorescence (2c-LIF) is applied to calibrate and measure the temperature in a micrometric monodisperse ethanol droplet chain. A dye mixture of fluorescein disodium (FL) and sulforhodamine 101 (SRh) is used, in order to form a sensitive signal ratio of one temperature dependent and one independent fluorophore. Spectral and planar fluorescence detection via a fiber-coupled spectrometer and a camera system, consisting of two sCMOS cameras, is set up around the droplet chain. Additionally, absorption measurements of the dye mixture in ethanol are conducted using a photo-spectrometer to analyze the temperature sensitivity of the dyes as well as potential re-absorption and fluorescence cross-talk effects. The spectral setup allowed an investigation of the wavelength range in which morphology dependent resonances (MDR) occur at the phase boundary of the droplet. Thus, the optical filters, determining the color channels in the camera system, are chosen to avoid detection of the lasing signal and providing maximal temperature sensitivity at the same time. The calibrated signal ratios are applied in temperature measurements of evaporating heated droplets in the droplet chain, showing the cooling with larger distance from the nozzle.

1 Introduction

Liquid phase and especially droplet thermometry are essential for the development of various industrial and technical spraying applications like spray drying, spray cooling or liquid fuel injection in internal combustion (IC) engines, rockets or burners [1, 2]. In the last decades several approaches were introduced to measure the temperature in the liquid phase of sprays or droplets [3–6], one of which is 2c-LIF thermometry [7, 8]. The concept is based on the Boltzmann distribution of a fluorescent dye molecule. In the absorbing as well as excited state, the respective population shows a specific temperature dependency. This effect is used to form a temperature dependent signal ratio of two wavelength areas, which are recorded by two detectors and respective filters (referred to as "color channels"). Based on their research on concentration studies via LIF, Lemoine et al. [9, 10] applied the 2c-LIF technique to measure the temperature in a turbulent water jet. Therefore, a fiber coupled

detection system with two photo multiplier tubes (PMTs) was set up around a water jet doped with rhodamine B (RhB) as fluorescent dye. The same detection system was used by Perrin et al. [11] in a droplet stream injected into a heated environment. The applicability of the dye pyrromethene 597-C8 (Pyr) as fluorescent dye is tested in various fuels. However, for this dye lasing effects (or morphology-dependent resonances, MDR), which occur at the phase boundary inside the droplets due to their spherical shape, are very distinct. One approach to circumvent the detection of this adverse signal is the admixture of an additional light absorber to the dye/solvent mixture, for example, Oil Blue N (OBN). Based on these measurements, Palmer et al. [12, 13] continued the research of the two-dye mixture in an n-dodecane droplet stream. The concept of enhanced energy transfer (EET) onto an absorber dye was approved and investigated in a spray. Using a pulsed laser and an electron-multiplying charge-coupled device (EMCCD), the detection of spatially resolved droplets could be conducted. In a range from 300 K to 340 K the ratio change with temperature shows linear behaviour and a temperature sensitivity of 0.29%/K could be obtained [14]. However, the fluorescence of Pyr is also drastically reduced by the absorber and other dye concepts and methods to reduce MDRs need to be analysed. Natrajan et al. [15] proposed a dye mixture of temperature-sensitive RhB and temperature-insensitive sulforhodamine 101 (SRh) and calibrated the signal ratio with two CCD cameras detecting the signal of a heated microfluidic device. The RhB–SRh dye combination in ethanol and water showed temperature sensitivities of 1.5 %/K and 2.7 %/K, respectively. To get and share further insight into the variety of fluorescent dyes for thermometry, several authors published overviews of various fluorescent dyes in different solvents [16–18]. Accordingly, Prenting et al. [16] suggest the use of a single dye coumarin 152 for measurements in an ethanol SpraySyn flame. Except for two coumarin derivates (152 and 153) none of the other dyes (such as RhB, Rh101, Pyr, DCM, etc.) exhibited a higher ratio change than 1.0%/K in cuvette measurements. 2c-LIF was successfully applied to measure averaged temperature field images in the SpraySyn flame. Other auspicious dyes in polar and non-polar liquids for thermometry are, for example, Eosin-Y with a sensitivity of 1.6%/K in water (2.0%/K in glycol) and Nile red (for non-polar heat transfer oils such as Marlotherm LH with a sensitivity of 4.2%/K), both measured in a tempered cuvette [19]. However, both dyes showed MDRs in the LIF signal in droplet sizing experiments based on the LIF/Mie ratio [20–22].

The dye mixture of fluorescein disodium (FL) and sulforhodamine 101 (SRh) is promising for polar liquids. It was first proposed by Chaze et al. [23] and successfully applied for temperature measurements in impinging 2.5 mm-sized water droplets on a heated surface. The detection of the FL color band is only recommended above 540 nm, avoiding the detection of the spectral region in which self-absorption of FL occurs. This way a temperature sensitivity of 2.7%/K could be achieved. Mishra et al. [17] attained a sensitivity of 2.4%/K calculated from the single dye spectra detected in a cuvette with ethanol as a solvent. However, this 2-dye concept was not utilized in micrometric ethanol droplets before, which is the aim of the present paper. Ethanol is an important solvent for many pharmaceutical or process engineering systems and it is also an important fuel component. Its atomization and evaporation behaviour and its liquid

temperature under various injection conditions must be studied, e.g., by using optical techniques. For this purpose, the dye concentration of this two-dye 2c-PLIF concept must be adjusted. Reabsorption as well as signal crosstalk is studied in a spectral characterization of absorption and fluorescence of the dye couple. Still, the challenge of MDR needs to be addressed. After identification of spectral positions of MDRs, filter regions for two-colour LIF can be identified in order to achieve a maximal temperature sensitivity and reducing effects of re-absorption and dye concentration on the signal ratio. Afterwards, a planar LIF setup is utilized for calibration of the signal ratio in a wide temperature range of the micrometric droplets. Finally, the droplet temperature is measured using 2c-PLIF in evaporating ethanol droplets downstream the nozzle of a droplet generator.

2 Materials and methods

The following section covers fundamentals on LIF and explains the benefit of the two-color approach. Furthermore, the experimental setup and the implementation are described.

2.1 Theory of 2c-LIF

The 2c-LIF technique is based on the simultaneous detection and ratio formation of two differently temperature dependent fluorescence signals in a spectrum. Therewith, the contribution of several influencing factors on the signal can be eliminated for the temperature determination. Fundamentals are only briefly addressed in this work, as several works report a detailed derivation of the intensity equations relevant for 2c-LIF, see, e.g., Lemoine et al. [10] and Lavieille et al. [10, 24]. Accordingly, the fluorescence signal intensity I_fl/W/m^2 after the absorption of laser photons can be expressed with

$$I_\mathrm{fl}(\lambda) = K_\mathrm{opt}(\lambda)K_\mathrm{spec}(\lambda)I_0 V C e^{\beta(\lambda)/T}$$

while β/K and K_spec/mol^{-1} are constants describing the physical and fluorescent properties of the respective dye in a two-dye concept. K_spec relates to the molar absorption coefficient ε and the fluorescence quantum yield (FQY) [11]. In this formulation of the LIF working equation, the temperature dependence of the quantities $\beta(\lambda)$ and $K_\mathrm{spec}(\lambda)$ is considered in the e-function. The FQY for example, is affected by temperature dependent photo-physical processes such as quenching. In general, the FQY of the dyes used in this work are very high: for FL it is 0.97 (ethanol) and for SRh it is 0.90 (in ethanol as well) [25]. The molar absorption coefficients are 92,300 L/(cm·mol) (at 499 nm) for FL in ethanol and 110,000 L/(cm·mol) (at 577 nm) for SRh in methanol [25]. However, the absorption coefficients are lower at the intended excitation line of 532 nm, which is described in Section 3.3.

The exponential part of the equation results from the Arrhenius approach, including the influence of the absorption cross section and the quenching rate on the temperature dependence. β is the wavelength dependent temperature sensitivity factor, which expresses the signal change per unit kelvin [10]. The equation contains another constant $K_\mathrm{opt}(\lambda)$/-, which is the efficiency of the

TABLE 1 Fluid properties of ethanol and the mixtures with fluorescein disodium and additional admixture of sulforhodamine 101.

	Density/kg/m³	Surface tension/mN/m	Dynamic viscosity/mPas
Ethanol	790	22.3	1.156
Ethanol + FL	790	22.3	1.194
Ethanol + FL + SRh	790	22.3	1.194

detection system. I_0 is the incident laser fluence, $C/\text{mol}\cdot\text{m}^{-3}$ the concentration of the dye molecules, T/K the temperature and V/m^3 the sample volume. The equation is only valid in the linear range at low laser fluence $I_0/\text{W}\cdot\text{m}^{-2}$ (below a saturation threshold I_{sat}). This regime is intended in order to avoid a non-linear behavior of the signal intensity due to saturation effects or photobleaching of the dye.

The 2c-LIF approach uses a ratio R_{fl} of two signal intensities, which is derived from two selected wavelength bands in the fluorescence spectrum of the dye. Therefore, the dependence on the laser intensity, the sample volume and the molecular dye concentration can be eliminated from the ratio equation:

$$R_{fl} = \frac{I_{fl,1}}{I_{fl,2}} = \frac{K_{\text{opt},1}K_{\text{spec},1}}{K_{\text{opt},2}K_{\text{spec},2}}e^{\frac{\beta_1-\beta_2}{T}}$$

To further cancel out the system dependencies K, the ratio is normalized to a reference operating point at a known temperature.
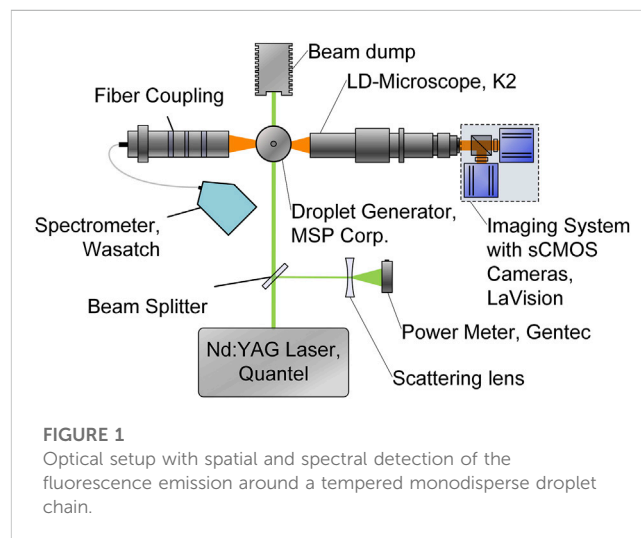
2.2 Experimental setup

A V-750 UV/VIS-spectrophotometer (Jasco) is used for investigations of the absorption behavior of the dissolved dye mixtures. The calculation of the absorbance from the measured transmittance T values can be expressed *via* Lambert Beer's law:

$$A = 2 - log_{10}\,(\%T)$$

A closable Hellma quartz cuvette (10 mm optical path) containing the sample is tempered in the cuvette holder and a transmission measurement is conducted. When measuring in the cuvette, the optical path length is relatively large compared to the droplet diameter in the emission measurements. This means that a large dye concentration is required for the droplet fluorescence measurements in order to achieve a sufficiently high signal to noise ratio (SNR). Therefore, solutions with deviating dye concentrations are prepared for absorption (cuvette) and emission (droplet) investigations as specified below. As solvent, absolute ethanol (EMSURE, purity >99.9%) is used and dosed with 10 mg/L FL (CAS: 518-47-8) and 1 mg/L SRh (CAS: 60311-02-6), investigating the absorption behaviour. Additionally, in order to clarify the influence of the dye admixture on the physical properties of the solvents, measurements of density, surface tension and dynamic viscosity were conducted, see.
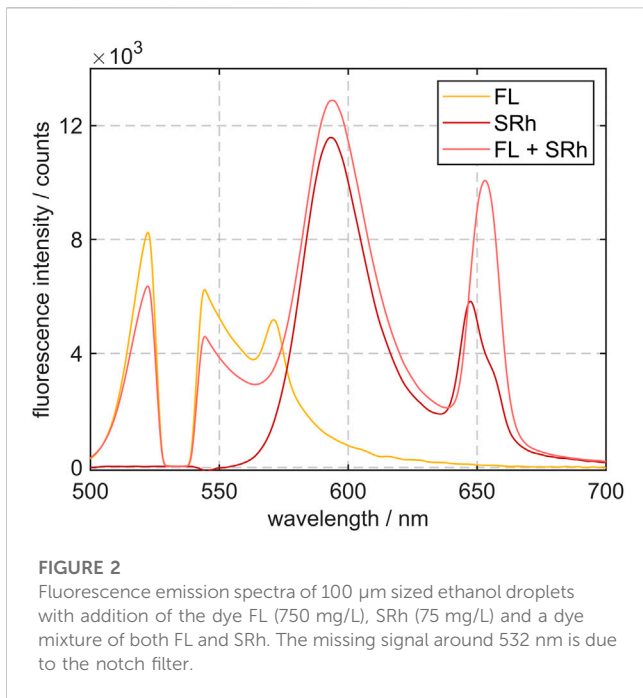
Table 1 These properties are essential for the droplet formation in sprays and changes with dye addition would make the spray investigations redundant. Three different mixtures (pure ethanol, ethanol dosed with FL and ethanol dosed with FL and SRh) are tested and only a slight increase in viscosity (i.e., a difference of 0.038 mPas) could be detected when the dyes are added. All

FIGURE 1
Optical setup with spatial and spectral detection of the fluorescence emission around a tempered monodisperse droplet chain.

measurements were conducted at 293 K. Density and dynamic viscosity determination is performed with a Stabinger viscometer (SVM 3001, Anton Paar) after ASTM D 7042:2021 and the detection of the surface tension after DIN EN 14370:2004.

Figure 1 shows the experimental fluorescence emission measurement setup. A pulsed Nd:YAG laser (Q-SMART, Quantel) is operated at 532 nm with a fluence of 2.7 mJ/cm², ensuring measurements within the linear LIF signal intensity regime. The expanded, collimated laser beam passes the monodisperse droplet chain, generated by a tempered droplet generator (FMAG 1520, TSI). The FMAG is dosed with the dye-solvent mixture by a syringe pump and additional tempered focussing air, forming 100 μm sized droplets (for most of the studies, smallest droplet sizes are around 20 μm depending on the investigated liquid). The droplet size is determined by previously calibrating the resolution with a multi-frequency grid distortion target (Thorlabs, R1L3S3P) in the focal plane. Two recirculating chillers (for the liquid and air flow) regulate the mixture to temperatures between 283 K and 343 K, while the maximal temperature range is limited by the boiling point of the solvents. Deviating to the absorption measurements, a dye concentration of 750 mg/L FL and 75 mg/L SRh is applied in the droplet chain. These higher dye concentrations are necessary for sufficiently high LIF signals of the micrometric droplets. Preliminary measurements were performed to find an optimum in the mixture ratio of both dyes regarding reabsorption between the molecules and a similar high emission signal.

At 90° detection angle a long-distance microscope (Infinity K2 DistaMax) is mounted to an imaging system which includes two sCMOS cameras (Imager, LaVision), resulting in a resolution of 3.25 pixel/μm. This system includes a dichroic mirror to split the

FIGURE 2
Fluorescence emission spectra of 100 μm sized ethanol droplets with addition of the dye FL (750 mg/L), SRh (75 mg/L) and a dye mixture of both FL and SRh. The missing signal around 532 nm is due to the notch filter.

FIGURE 3
Fluorescence emission spectra (including MDR) of ethanol droplets with addition of the dye FL (750 mg/L **(A)**) and SRh (75 mg/L **(B)**) at droplet sizes ranging from 60 μm to 120 μm.

signal into two wavelength ranges. Both parts of the signal pass through a specific band-pass filter (554/23 BrightLine HC and 615/24 BrightLine HC), only allowing a detection of the shaded color bands as indicated in Figure 4 (the filter selection is discussed below in detail). For the imaging measurements, 2,000 pictures were recorded at a frame rate of 10 Hz and repeated on three different days. Every image contains two or three droplets of the droplet chain, leading to a total of several thousand droplets per operating point. On the opposite side of the droplet generator, a fiber-coupled spectrometer (WP-VIS-A-S-50, Wasatch Photonics) is mounted. Preceding the optical fiber, the optical system consists of two achromatic doublets and a notch filter, ensuring the screening out of the excitation wavelength. Each measurement is integrated for 50 ms and 100 single spectra are averaged. This procedure is conducted ten times on three different days, leading to a total of 3,000 spectra.

In the imaging setup, the signal is split by a dichroic mirror and further detected by two cameras. In the post-processing of the calibration data, one image is mapped onto the other via a transformation matrix and a warping algorithm. Using a binarization, the edges and thus the droplets in the pictures are detected and further evaluated. Single droplets are selected as "useful" or are otherwise not considered, according to their size and deformation. Only droplets close to 100 μm with no perceptible deformation are considered for calibration measurements (although thermometry is also possible in non-spherical structures, see below). The measurement location is about 5 mm below the nozzle exit at which spherical droplets are formed (the downstream distance depends on the temperature, determining, e.g., the surface tension and liquid viscosity and thus the droplet stability). For calibration measurements the droplet temperature is assumed to be the same as the adjusted temperature of the droplet generator and corrected afterwards, see Section 3.3.

With these specifications, a minimum of 12,500 droplets is taken into account for further evaluation. The integrated LIF-signal of the
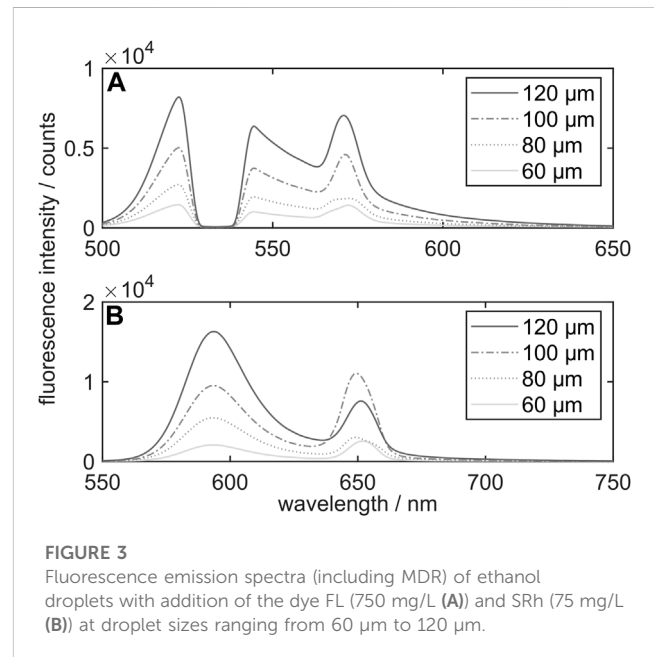
droplet is strongest in its center. This is because of the maximum depth in *z*-direction of the droplet and since the whole droplet is illuminated by the laser beam (beam diameter of 8 mm). A circular region of interest (ROI) is determined for evaluation, excluding the droplet rim. In this outer area the lowest SNR is achieved, which leads to the highest temperature variations as also shown by Palmer et al. [14]. In this ROI, the signal is spatially averaged for both channels and a signal ratio is calculated for the single images. Afterwards the single signal ratios are averaged for determination of the temperature dependent calibration curve.

3 Results and discussion

The next section shows all results ranging from MDR studies and the filter selection to calibration data. Finally, an evaporation study downstream the droplet generator is conducted to apply the measurement technique.

3.1 Preliminary studies on MDR effects and their circumvention

When measuring in spherical droplets, lasing effects may occur due to internal total reflections on the droplet/air phase boundary. These amplified emission signals are also known as whispering gallery modes (WGM) or MDR. Different refractive indices between the liquid in the droplet and the ambient air lead to a high total internal reflection (TIR) angle, which can be determined to be 47.2° for ethanol/air after Snell's law. The combination of the TIR angle and the spherical shape lead to the droplet acting as an optical cavity with resonating light circulating along the internal rim.

The resonance wavelengths and the respective emission linewidths are affected by the morphology of the scattering media. This includes the droplet size and its shape, as well as the
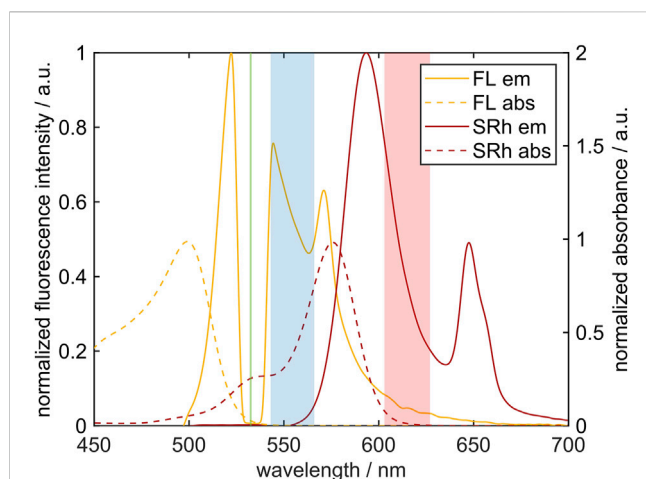
FIGURE 4
Absorption spectra (dashed line) measured in a cuvette and fluorescence emission spectra (solid line) measured in the droplet chain of both single dyes FL and SRh in ethanol. The color channels of the selected optical filters are depicted as shaded rectangles. The Nd:YAG laser line for excitation of both dyes is marked in green at 532 nm. Please note that the *y*-axis of the absorption spectra is extended to 2 for better visualization.

refractive index of the solvent [26]. In a previous work based on the dye nile red in ethanol/isooctane mixtures, the lasing peak was a function of the ethanol concentration. The peak position was red-shifted with larger ethanol amount and pure ethanol showed the lowest MDR peak [20]. Larger droplet sizes exhibited more distinct MDRs in the LIF signal in accordance with the theory [21]. Consequently, MDR can be useful, e.g., for the determination of droplet properties such as the diameter [27, 28]. For 2c-LIF thermometry, MDR pose a major signal influence and disturb the signal ratio approach if detected in one of the color channels. One proposal to circumvent the detection of MDR effects is the addition of an absorber molecule, which does not emit fluorescence itself (e.g., OBN as an absorber for Pyr lasing, as mentioned in the introduction) [11]. Another possibility is to use 'controlled color switching' (of the MDR) to another wavelength outside of the color channels [27]. Both options are based on an effective energy transfer between the dye molecules.

The subsequent investigation serves for analysis of MDR effects for the individual dyes and the dye combination in ethanol. The fluorescence spectra of the single dyes FL and SRh, as well as a mixture in ethanol droplets at ambient temperature are shown in Figure 2. The FL spectrum shows a gap from the 532 nm notch filter applied and a MDR peak at 571 nm. SRh indicates an emission maximum at 593 nm with a lasing maximum at 648 nm. A reduction of the signal at the FL peak with simultaneous increase of the SRh peak is observed in the mixture. This can be explained by reabsorption of the FL emission by SRh molecules.

Due to the high molecular weight of both dyes, the mixture ratio of the dyes is assured in case of evaporation of ethanol. Both dyes remain in the droplet leading to a dye enrichment and a fluorescence signal increase. However, this will hardly affect the signal ratio, when the filters are chosen accordingly and as long as no concentration quenching of the LIF signal occurs. In addition to the signal
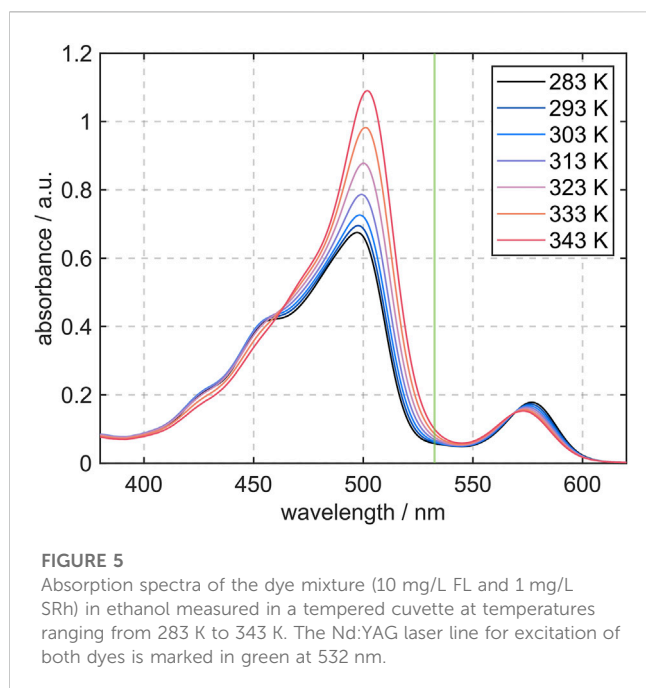
reabsorption, the MDR peak in the FL spectrum is absorbed by SRh in the mixture. Instead the MDR signal of the dye mixture shows a peak at 652 nm, which means at higher wavelengths than the MDR peak of the solely studied dye SRh. Consequently, the optical filters are chosen outside of this wavelength area, as specified above.

Supplementary measurements have been performed in the possible droplet diameter range of the droplet generator to ensure that for a diameter variation no additional MDR modes are detected. Tang et al. [29] stated that the number of lasing modes could be increased in the case of larger droplets in comparison to smaller droplets. For the present solutions with the single dyes FL and SRh, spectra in droplets from 60 μm up to 120 μm have been recorded and are shown in Figure 3. In general, no clear droplet-size dependence of the average MDR peak position could be observed. However, the MDR peak rises relatively to the main fluorescence peak of SRh for smaller droplets. A deviation from this pattern can be observed for 100 μm sized ethanol droplets dosed with SRh, showing a higher MDR peak than the 120 μm sized droplets. This deviation could be explained by a correlation of the spectral position of the MDR and the droplet size, resulting in intensity variations of the lasing signal. Koegl et al. [21] presented similar findings of certain droplet sizes showing larger MDR in the LIF signal images.

3.2 Filter selection

The 2c-LIF approach is based on the ratio of two intensity signals, each originating from a respective color channel in the fluorescence spectrum. These color channels can cover two differently sensitive segments of one single dyes' emission spectrum. Therefore, using only one dye, it may be difficult to reach a high temperature dependence of the signal ratio. Furthermore, the 'blue' part of the spectrum may be affected by re-absorption effects and a varying dye concentration intensifies this problem. Palmer et al. [14] successfully performed micrometric droplets measurements in a heated surrounding with only Pyr as fluorophore. To avoid MDR effects, OBN was added, which contributes to the spectrum without fluorescence emission but by absorption of the emitted photons of Pyr. A temperature sensitivity of 0.29%/K could be reached in this application. In order to raise the sensitivity, a two-dye approach using two different dyes with contrary temperature dependent emission behaviors may be promising. In general, two-dye 2c-LIF concepts for increased sensitivity were proposed by Sakakibara et al. [30] and were recommended in several works [15, 30, 31]. Thus, each color channel covers one emission spectrum of the two opposed temperature dependent fluorescence signals.

Figure 4 shows both, the absorption and fluorescence emission spectra of the single dyes used in this work. Absorption measurements were carried out in a cuvette, while the emission spectra were detected in droplets and thus, show MDR peaks. Shaded color bands describe the two intensity color channels representing the selected optical filters. The "blue" channel (at lower wavelengths) equals the transmission curve of the Semrock 554/23 BrightLine HC filter and covers wavelengths from 543 nm to 566 nm. In this wavelength segment the detected emission signal originates mostly from FL molecules. Absorption by SRh is relatively

FIGURE 5
Absorption spectra of the dye mixture (10 mg/L FL and 1 mg/L SRh) in ethanol measured in a tempered cuvette at temperatures ranging from 283 K to 343 K. The Nd:YAG laser line for excitation of both dyes is marked in green at 532 nm.

FIGURE 6
Fluorescence emission spectra of the dye mixture (750 mg/L FL and 75 mg/L SRh) measured in 100 μm sized ethanol droplets at temperatures ranging from 293 K to 343 K. The color channels of the selected filters (based on temperature sensitivity) are marked in blue and red. The signal increase in the region around 650 nm corresponds to the MDR signal.

strong in this color channel and reduces the fluorescence signal, which however is the fundamental for color switching (red-shifting) of the MDR peak. The 'red' channel corresponds to the transmission of the Semrock 615/24 BrightLine HC filter between 603 nm and 627 nm. Reabsorption of SRh-fluorescence plays only a minor role in this wavelength region and the emission is dominated by SRh. Ultimately, both filters were chosen so that fluorescence crosstalk and self-absorption can be neglected in these wavelength areas.
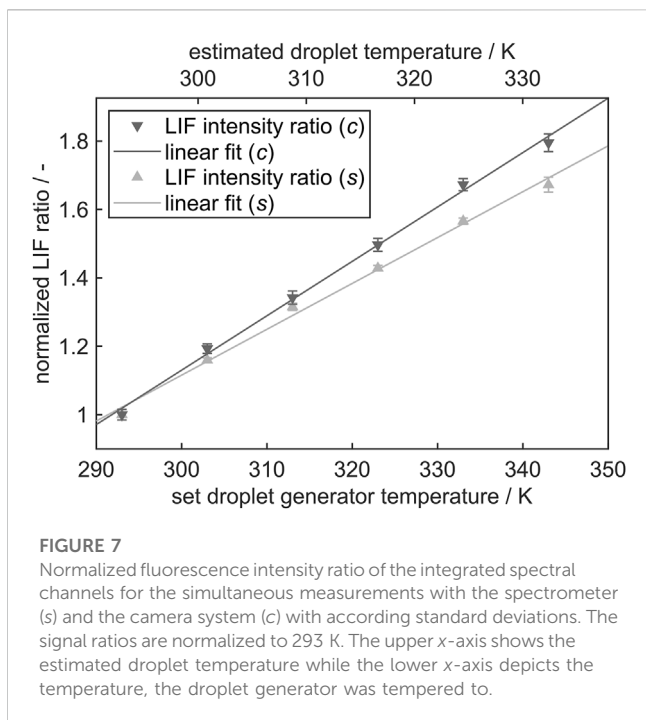
3.3 Calibration data

The results of the absorption measurements from 283 K to 343 K and the excitation wavelength of the laser at 532 nm are depicted in Figure 5. Two major peaks at λ ≈ 500 nm and 550 nm can be observed. The first one at shorter wavelengths is due to the absorption of FL and this maximum is significantly higher than the second peak, which is attributed to absorption of SRh. This difference in absorption is partly due to the mixture composition of 10:1 (FL:SRh). At higher temperatures, the FL absorption peak increases whereas the SRh peak only shows a slight blue shift. The very small and additionally negative temperature dependence and the superimposition with the increased FL band lead to this shift. A similar trend with a higher temperature increase for FL is consequently expected for the fluorescence of both dyes.

The graphs in Figure 6 show the fluorescence emission spectra of the utilized dye mixture at different temperatures, indicating the MDR peak at wavelengths of λ > 640 nm. Moreover, the combination of the temperature sensitive FL and the temperature insensitive SRh leads to a high sensibility of the fluorescence intensity ratio. For this ratio, two color bands with an optimum high ("blue") and low ("red") temperature sensitivity were elaborated and accordingly, the filters for further measurements
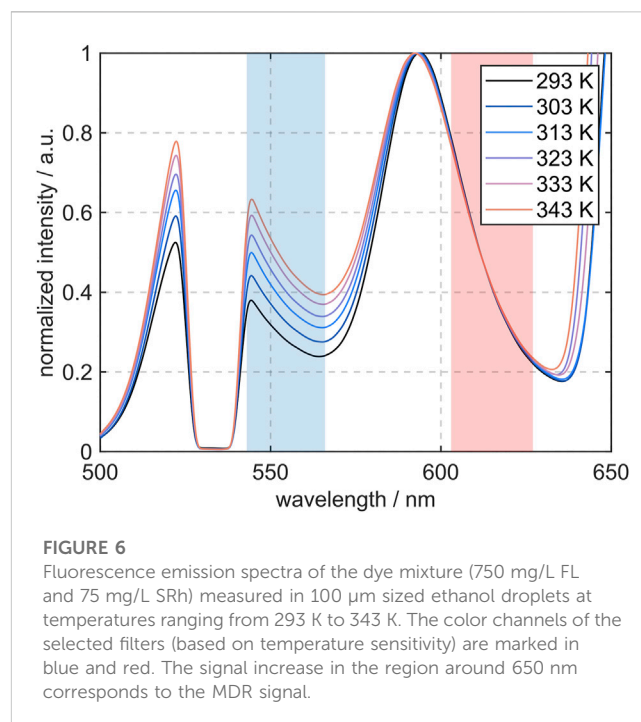
with an imaging system were selected as described before. These filter regions are hereafter referred to as channel 1 ("blue") and channel 2 ("red"). The integrated signals under the graph in the shaded regions are applied for the subsequently built signal ratio. The range around 532 nm is blocked by the notch filter and would otherwise show the maximum of the FL spectrum. Compared to the absorption spectra, the emission peaks attributable to the single dyes show a signal intensity in the same order of magnitude, despite the different dye concentration in the mixture. With a concentration of $1.99 \cdot 10^{-3}$ mol/L for FL, the number of moles in the volume is approximately 16 times as high as it is for SRh with a concentration of $1.24 \cdot 10^{-4}$ mol/L. This is due to the absorption cross section of FL, which is very low at the 532 nm and therefore only a low share of photons is absorbed. With a higher temperature, the absorption range of FL increases and shows a slight red-shift, increasing the absorbance of laser photons. Accordingly, the temperature dependence of the FL spectrum is visible in the fluorescence emission. The FL peak (in the blue channel) increases with more than factor 1.5 for a temperature rise of 70 K, while normalized to the SRh maximum (which accordingly does not change in this depiction). This behavior of SRh emission was predictable from the absorption spectrum in Figure 5, as no strong dependence on the temperature could be observed.

Figure 7 shows the normalized LIF ratios at different temperatures and the resulting linear fit for the measurements with the spectrometer (s) and with the cameras in the imaging system (c). The slope of the imaging system calibration curve is steeper than the one of the spectrometer. For a direct comparison, the inclusion of the quantum efficiencies and detection angles of the optical components and the incorporation of the signals at the droplet rim in the image processing are missing or rather leading to a deviation of the slopes. By detecting with the imaging system, the filters limit the evaluated channels, whereas these limits are straight

FIGURE 7
Normalized fluorescence intensity ratio of the integrated spectral channels for the simultaneous measurements with the spectrometer (s) and the camera system (c) with according standard deviations. The signal ratios are normalized to 293 K. The upper x-axis shows the estimated droplet temperature while the lower x-axis depicts the temperature, the droplet generator was tempered to.

FIGURE 8
Single images of 100 μm sized droplets at temperatures from 293 K to 343 K viewed through "blue" channel (FL, left) and the "red" channel (SRh, right column). The droplets show no MDR signal at the phase boundary.

theoretical cut-offs in the evaluation of the spectrometer measurements.

It should be noted that two x-axes are included in the diagram. One presents the set temperature of the droplet generator, the other one is the estimated temperature in the measurement location. The estimated temperature curve is based on a two-point calibration at 293 K (ambient temperature) and the maximal studied temperature of 343 K. The temperature difference between the adjusted liquid temperature in the droplet generator (343 K, which is also assumed to be constant within the first 2 mm downstream) and the liquid temperature at the measurement position for calibration (5 mm downstream) is 10.7 K. This difference is determined iteratively by conducting 2c-PLIF measurements downstream. The spatial differences in signal ratios and thus temperatures were extrapolated linearly in order to find the most plausible temperature evolution, see Figure 9. Further details are provided in the subsequent section.

By adjusting the temperature to the estimated droplet temperature at the measurement position as described above, the calibration curve for the imaging system shows a slope of 2.02%/K, the curve for the spectrometer setup a slope of 1.71%/K, describing the resulting temperature sensitivity. In comparison, Chaze et al. [31] and Mishra et al. [5] achieved higher values for the sensitivity of the same dye combination, stating values of 2.5%/K to 3.0%/K (in water) and 2.4%/K (in ethanol). However, different setups (mm-sized droplets and cuvettes, different band-pass filters), dye concentrations or liquids (water) were used and no standard deviations are shown for an estimation of the reproducibility. As MDR effects were not considered, much broader color channels were chosen in the previous publications, probably leading to higher differences in the signal ratio and thus a steeper slope. It was mentioned that the temperature insensitive SRh band showed certain fluctuations, which could be due to the reported ring structures in a later work of Chaze et al. [23]. As shown in the
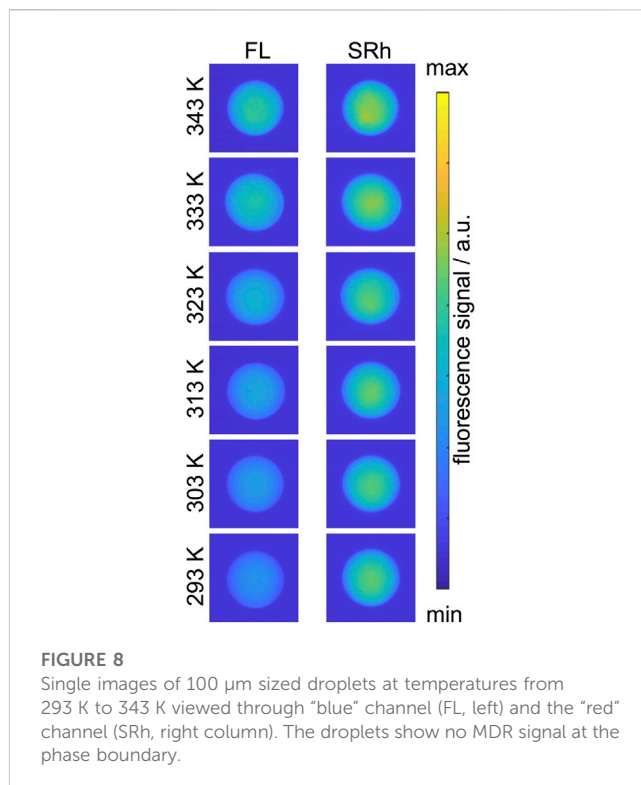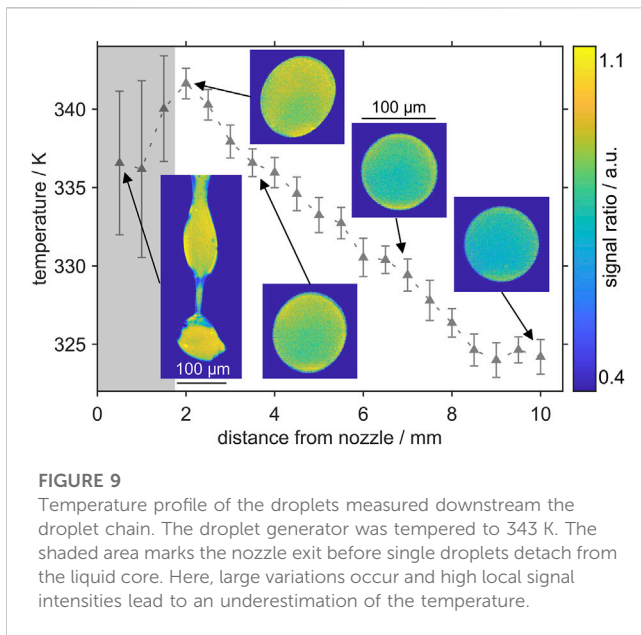
present work, MDR effects can be avoided by selection of according optical filters. Using a dichroic mirror instead of a beam splitter, the signal loss was counteracted.

Respective single shot images of both channels ("FL" at lower and "SRh" at higher wavelengths) are shown in Figure 8. The temperature dependent signal variation in the "blue" channel (FL) is clearly visible between the coldest and the hottest operating point. No apparent temperature dependence can be observed in the 'red channel' (SRh) images. MDR effects, normally visible as very bright ring structures around the droplet, are not detected.

3.4 Evaporation study downstream the droplet chain

The evaporation of heated ethanol droplets alongside the droplet chain is investigated at distance intervals of 0.5 mm, starting at the nozzle exit. The initial temperature was adjusted to 343 K. At each measurement point 300 images are recorded and the signal ratio and thus the average temperature are evaluated. The temperature course over the distance from the nozzle with exemplary single shot intensity ratio images are shown in Figure 9.

At 2 mm distance from the nozzle, actual droplets have detached from the liquid core and show transient oscillation. The image at 3.5 mm distance shows still a slightly deformed droplet before a stable spherical droplet is formed further downstream. In general, a decrease of the temperature with distance from the nozzle can be observed. A temperature of 341.6 K is determined at 2 mm. The cooling of the liquid is considered to be marginal in the first 2 mm of the droplet chain due to the surrounding hot shielding gas, which

FIGURE 9
Temperature profile of the droplets measured downstream the droplet chain. The droplet generator was tempered to 343 K. The shaded area marks the nozzle exit before single droplets detach from the liquid core. Here, large variations occur and high local signal intensities lead to an underestimation of the temperature.

was also heated to 343 K. Other groups using droplet generators for calibration assumed no evaporation until the formation of spherical droplets [32]. Consequently, between 0 mm and 2 mm the measured temperatures are underpredicted and show a larger uncertainty in terms of shot-to-shot standard deviations. In this first section of the droplet chain, Rayleigh breakup of the liquid core is observed and no droplets have formed yet. In this area, the temperature detection shows largest shot to shot deviations of up to +/-5.6 K (8.2%). Further discussion on the underprediction is provided below.

At the distances further downstream the nozzle decreasing temperatures are detected until a minimum temperature is reached. The slope between 2 mm and 9 mm is almost constant. In this study the temperature does not vary anymore between 9 mm and 10 mm. Within the studied spatial domain of 7 mm length (2 mm–9 mm distance to the nozzle), a temperature reduction of about 17.7 K was observed, which will be discussed in the subsequent paragraphs. In general, the droplet evaporation and cooling/heating are transient problems. The heated droplet is cooled down due to the heat transfer with the ambient air and the large evaporation enthalpy of the ethanol droplets. The relative velocity is reduced by drag, which varies due to slight droplet deformations. Under the present conditions, the internal temperature of a droplet can be assumed as uniform, which is confirmed by the experiments showing no distinct temperature stratification in the droplet. The measured temperature deviations at the droplet boundary, which are visible in some single-shot images of Figure 9 (e.g., at 2 mm), are not physical and occur due to larger measurement uncertainties (local SNR). The SNR is very low close to the droplet surface and the droplets do not show a uniform signal ratio over the droplet diameter. These inhomogeneities could also be explained by internal optical effects, like reflection and subsequent refraction on the phase boundary. Depending on the ray angle of the fluorescence emission, a "false" image may appear in the camera detector, as described further by Dulin et al. [33] for transparent pipes. In general, the uniform temperature condition is true for a rapid

mixing inside the droplet (i.e., a fast internal heat conduction) compared to the slow heat transfer between the droplet and the ambience. The instationary cooling behavior is expressed by the non-dimensional Biot number Bi

$$Bi = \frac{\alpha\, L}{\lambda_L}$$

which is the ratio of the heat transfer coefficient α between the droplet and the ambience and the liquid heat conductivity λ_L of the droplet. The characteristic length scale L of a sphere equals one-third of droplet radius [34]. At the present conditions, $Bi = 0.103$ is obtained, which implies that internal heat conduction is very fast so that almost no temperature gradient can be observed in the droplet. The Biot number was calculated for an average droplet velocity $u_D = 1.24$ m/s and an initial liquid heat conductivity of ethanol $\lambda_L = 156$ mW/(m·K) at 343 K [35]. Under comparable conditions but other liquids (fuels), similar Biot numbers were reported in the literature [36, 37]. Furthermore, for small Biot numbers in the range of 0.1–0.25, effects of droplet distortions of up to 35% were studied by Dai et al. [36]. However, the droplet deformation due to drag showed no significantly improved internal heat transfer [36].

The temperature reduction of about 17.7 K within 7 mm is partly due to the cooling of the hot droplet in the cold ambient air. This cooling by the heat transfer with the ambience accounts for a temperature decrease of about 7.3 K within 7 mm (or within about 6 ms) estimated by using the lumped capacitance model being valid for small Biot numbers (Bi < 0.1) [34]. Additionally, a temperature reduction due to evaporation of at least 10 K is reasonable for ethanol droplets. In a numerical simulation, a droplet temperature reduction of about 17 K for isolated ethanol droplets was observed for initial droplet diameters of 5 µm–40 µm within the first 1.2 ms [38] (the initial droplet temperature was 293 K). This corresponds to a droplet size reduction of 3.4% for an initially 10 µm large droplet. In the present measurements, no droplet size variations were evaluable, since the droplets showed large initial deformations. However, a simplified evaporation model for the steady phase following Sazhin et al. [39] confirmed a small droplet size reduction to about 98.9 µm at the present conditions.

In general, it could be shown that the optimized two-dye 2c-PLIF technique is able to provide droplet temperatures of evaporating droplets in a heated droplet chain on a single shot basis. Depending on the temperature the typical SNR were in the range of 21–105 (average of 47) for the blue channel and between 379 and 662 (average of 446) for the red channel. Temperature variations of 1.4 K could be resolved, for example, between 4.0 mm and 4.5 mm. The average temperatures are 336.0 K and 334.6 K, respectively. The standard deviations were typically around +/-1.0 K.

The larger uncertainty in the jet breakup region may have various reasons. In this near-nozzle region, some "hot" and "cool" spots are observed in the liquid jet, which are not physical. Probably, this is due to fluorescence light reflections at the bare surface of the droplet generator or at the liquid jet itself originating from other regions in the jet, which are projected on the droplet under investigation. These background reflections or scattering effects cannot be compensated easily and other measures such as 2-photon LIF [40] could be required for this purpose. These reflections are partly reabsorbed in the jet or droplets and lead to falsified signal ratios and temperatures as well. This fluorescence scattering and reabsorption is also an issue for

droplets close to the liquid core. There, in some images a much brighter illuminated droplet surface is clearly visible originating from fluorescence of neighboring droplets. This also contributes to higher and unphysical droplet temperatures in the near-field of the droplet generator.

4 Conclusion

This work presents the optimization of a two-dye 2c-LIF thermometry approach and its first-time application for measurements in a monodisperse ethanol droplet chain. With the use of two contrarily temperature dependent fluorescence dyes (FL and SRh) calibration measurements were conducted in a tempered cuvette (absorption) and a droplet generator (emission). Two detection systems - a fiber-coupled VIS spectrometer and a camera system with two sCMOS cameras - enabled detailed measurements of interfering MDR signals. With the two-dye approach 'controlled color switching' of the MDR signal to a high wavelength was possible without addition of another absorber dye, which is common practice for other LIF dyes. At around 652 nm the average MDR peak is located outside of the main fluorescence emission bands of the dye mixture spectrum. Thus, two optical filters for the camera system could be selected in wavelength regions without lasing signal. The filter bands are different from the suggested ones in the literature for water. With this improved approach, a calibration curve with a promising temperature sensitivity of the signal ratio (2.02%/K for detection with the camera system) was attained in micrometric droplets of 100 μm without detection of MDR signals. Additionally, first-time investigations of the droplet cooling and evaporation were successfully performed downstream the droplet chain in form of temperature measurements with the two-dye 2c-LIF imaging approach. A cooling of around 20 K could be measured for a distance of 10 mm. Images detected close to the nozzle show the Rayleigh breakup of the liquid core. In this region of primary breakup, the results show strong deviations, probably resulting from optical effects inside the non-spherical structures and droplets. At distances between 2 mm and 9 mm more spherical droplets are formed. There, a linear decay of the temperature is observed, which amounts to about 17.7 K. This is a realistic value for cooling by evaporation and heat transfer with the cold ambient air. An estimation of the cooling due to convective heat transfer is attained after the lumped capacitance model and accounts for a decrease by 7.3 K.

In conclusion, successful exemplary thermometry measurements in the droplet chain could be performed, but also showed the necessity of further fundamental investigations on this approach. Droplet size dependent studies on MDR with the present two-dye LIF concept should be part of future work since the MDR signals themselves were not the focus of the present work. Furthermore, simulations and experimental studies of possible lens effects, leading to distortions in the signal ratios in the droplets, could help to understand and minimize variations in the results. Additionally, extensive simulations of the droplet formation by the droplet generator and evaporation should be conducted for better understanding of the underlying heat and mass transfer mechanisms.

Data availability statement

The raw data supporting the conclusion of this article will be made available by the authors, without undue reservation.

Author contributions

HU, LZ, and EB developed the diagnostic concept. HU designed the experiment and performed it together with SS and MM. HU processed the data. HU and LZ interpreted the data and wrote the manuscript. EB corrected the paper. LZ is the project leader and responsible for funding acquisition and supervision. All authors contributed to the article and approved the submitted version.

Acknowledgments

Conflict of interest

The authors declare that the research was conducted in the absence of any commercial or financial relationships that could be construed as a potential conflict of interest.

Publisher's note

All claims expressed in this article are solely those of the authors and do not necessarily represent those of their affiliated organizations, or those of the publisher, the editors and the reviewers. Any product that may be evaluated in this article, or claim that may be made by its manufacturer, is not guaranteed or endorsed by the publisher.

References

1. Ashgriz N. *Handbook of atomization and sprays: Theory and applications*. New York, NY: Springer (2011).

2. Lefebvre AH, McDonell VG. *Atomization and sprays*. Boca Raton, London, New York: CRC Press Taylor and Francis Group (2017).

3. Wang M, Stiti M, Chaynes H, Becker S, Berrocal E, Lemoine F, et al. Two-photon fluorescence lifetime imaging applied to the mixing of two non-isothermal sprays: Temperature and mixing fraction measurements. *Experiments in Fluids* (2022) 63:172. doi:10.1007/s00348-022-03515-5

4. Berrocal E, Paciaroni M, Chen Mazumdar Y, Andersson M, Falgout Z, Linne M. Optical spray imaging diagnostics. In: *Optical diagnostics for reacting and non-reacting flows: Theory and practice publisher*. Reston VA: American Institute of Aeronautics and Ast (2023).

5. Mishra YN, Abou Nada F, Polster S, Kristensson E, Berrocal E. Thermometry in aqueous solutions and sprays using two-color LIF and structured illumination. *Opt express* (2016) 24(5):4949–63. doi:10.1364/OE.24.004949

6. Wu Y, Heyne JS, Zhang Z. Simultaneous measurements of refractive index, surface tension, and evaporation rate of Jet A fuel. *Appl Opt* (2019) 58(16):4326–31. doi:10.1364/AO.58.004326

7. Lemoine F, Castanet G. Temperature and chemical composition of droplets by optical measurement techniques: A state-of-the-art review. *Experiments in Fluids* (2013) 54:1572. doi:10.1007/s00348-013-1572-9

8. Fansler TD, Parrish SE. Spray measurement technology: A review. *Meas Sci Tech* (2015) 26:012002. doi:10.1088/0957-0233/26/1/012002

9. Lemoine F, Wolff M, Lebouche M. Simultaneous concentration and velocity measurements using combined laser-induced fluorescence and laser Doppler velocimetry: Application to turbulent transport. *Experiments in Fluids* (1996) 20(5): 319–27. doi:10.1007/BF00191013

10. Lemoine F, Antoine Y, Wolff M, Lebouche M. Simultaneous temperature and 2D velocity measurements in a turbulent heated jet using combined laser-induced fluorescence and LDA. *Experiments in Fluids* (1999) 26(4):315–23. doi:10.1007/s003480050294

11. Perrin L, Castanet G, Lemoine F. Characterization of the evaporation of interacting droplets using combined optical techniques. *Experiments in Fluids* (2015) 56(2):29–16. doi:10.1007/s00348-015-1900-3

12. Palmer J, Reddemann MA, Kirsch V, Kneer R. Temperature measurements of micro-droplets using pulsed 2-color laser-induced fluorescence with MDR-enhanced energy transfer. *Experiments in Fluids* (2016) 57:177. doi:10.1007/s00348-016-2253-2

13. Palmer J, Reddemann M, Kirsch V, Kneer R. Development steps of 2-color laser-induced fluorescence with MDR-enhanced energy transfer for instantaneous planar temperature measurement of micro-droplets and sprays. In: 28 thEuropean Conference on Liquid Atomization and Spray Systems; September. 6-8 2017; Valencia, Spain (2017).

14. Palmer J, Schumacher L, Reddemann MA, Kirsch V, Kneer R. Applicability of pulsed 2cLIF-EET for micro-droplet internal thermometry under evaporation conditions. *Experiments in Fluids* (2020) 61:99. doi:10.1007/s00348-020-2935-7

15. Natrajan VK, Christensen KT. Two-color laser-induced fluorescent thermometry for microfluidic systems. *Meas Sci Tech* (2009) 20(1):015401. doi:10.1088/0957-0233/20/1/015401

16. Prenting MM, Bin Dzulfida MI, Dreier T, Schulz C. Characterization of tracers for two-color laser-induced fluorescence liquid-phase temperature imaging in sprays. *Experiments in Fluids* (2020) 61:1–15. doi:10.1007/s00348-020-2909-9

17. Mishra YN, Yoganantham A, Koegl M, Zigan L. Investigation of five organic dyes in ethanol and butanol for two-color laser-induced fluorescence ratio thermometry. *Optics* (2020) 1:1–17. doi:10.3390/opt1010001

18. Prenting MM, Shilikhin M, Dreier T, Schulz C, Endres T. Characterization of tracers for two-color laser-induced fluorescence thermometry of liquid-phase temperature in ethanol, 2–ethylhexanoic-acid/ethanol mixtures, 1-butanol, and o-xylene. *Appl Opt* (2021) 60(15):C98–C113. doi:10.1364/AO.419684

19. Koegl M, Delwig M, Zigan L. Characterization of fluorescence tracers for thermometry and film thickness measurements in liquid coolants relevant for thermal management of electric and electronic components. *Sensors* (2022) 22:8892. doi:10.3390/s22228892

20. Koegl M, Dai H, Baderschneider K, Ulrich H, Zigan L. Polarization-dependent LIF/Mie ratio for sizing of micrometric ethanol droplets doped with Nile red. *Appl Opt* (2022) 61(14):4204–14. doi:10.1364/AO.457685

21. Koegl M, Dai H, Qomi MP, Bauer F, Eppinger B, Zigan L. Morphology-dependent resonances in laser-induced fluorescence images of micrometric gasoline/ethanol droplets utilizing the dye nile red. *Appl Opt* (2021) 60(17):5000–11. doi:10.1364/AO.423059

22. Koegl M, Hofbeck B, Baderschneider K, Mishra YN, Huber FJT, Berrocal E, et al. Analysis of LIF and Mie signals from single micrometric droplets for instantaneous droplet sizing in sprays. *Opt express* (2018) 26(24):31750–66. doi:10.1364/OE.26.031750

23. Chaze W, Caballina O, Castanet G, Lemoine F. Spatially and temporally resolved measurements of the temperature inside droplets impinging on a hot solid surface. *Experiments in Fluids* (2017) 58:1–16. doi:10.1007/s00348-017-2375-1

24. Lavieille P, Lemoine F, Lavergne G, Lebouché M. Evaporating and combusting droplet temperature measurements using two-color laser-induced fluorescence. *Experiments in Fluids* (2001) 31:45–55. doi:10.1007/s003480000257

25. Taniguchi M, Lindsey JS. Database of absorption and fluorescence spectra of 300 common compounds for use in PhotochemCAD. *Photochem Photobiol* (2018) 94(2):290–327. doi:10.1111/php.12860

26. Pastel R, Struthers A. Measuring evaporation rates of laser-trapped droplets by use of fluorescent morphology-dependent resonances. *Appl Opt* (2001) 40(15):2510–4. doi:10.1364/ao.40.002510

27. Zheng L, Zhi M, Chan Y, Khan SA. Multi-color lasing in chemically open droplet cavities. *Scientific Rep* (2018) 8(1):14088. doi:10.1038/s41598-018-32596-8

28. Chen G, Mohiuddin Mazumder M, Chang RK, Christian Swindal J, Acker WP. Laser diagnostics for droplet characterization: Application of morphology dependent resonances. *Prog Energ Combustion Sci* (1996) 22(2):163–88. doi:10.1016/0360-1285(96)00003-2

29. Tang SKY, Derda R, Quan Q, Lončar M, Whitesides GM. Continuously tunable microdroplet-laser in a microfluidic channel. *Opt express* (2011) 19(3):2204–15. doi:10.1364/OE.19.002204

30. Sakakibara J, Adrian RJ. Whole field measurement of temperature in water using two-color laser induced fluorescence. *Experiments in Fluids* (1999) 26:7–15. doi:10.1007/s003480050260

31. Chaze W, Caballina O, Castanet G, Lemoine F. The saturation of the fluorescence and its consequences for laser-induced fluorescence thermometry in liquid flows. *Experiments in Fluids* (2016) 57:1–18. doi:10.1007/s00348-016-2142-8

32. Maqua C, Depredurand V, Castanet G, Wolff M, Lemoine F. Composition measurement of bicomponent droplets using laser-induced fluorescence of acetone. *Experiments in Fluids* (2007) 43(6):979–92. doi:10.1007/s00348-007-0368-1

33. Dulin V, Cherdantsev A, Volkov R, Markovich D. Application of planar laser-induced fluorescence for interfacial transfer phenomena. *Energies* (2023) 16:1877. doi:10.3390/en16041877

34. Bergman TL, Incropera FP, DeWitt DP, Lavine AS. *Principles of heat and mass transfer*. Hoboken, NJ: Wiley (2013).

35. Lemmon EW, Huber ML, McLinden MO. *REFPROP 9.1 "reference fluid thermodynamic and transport properties database* (2013).

36. Dai M, Perot JB, Schmidt DP. Heat transfer within deforming droplets. In: ASME 2002 Internal Combustion Engine Division Fall Technical Conference; September 8–11, 2002. Louisiana, USA: New Orleans (2002).

37. Keller P, Bader A, Hasse C. The influence of intra-droplet heat and mass transfer limitations in evaporation of binary hydrocarbon mixtures. *Int J Heat Mass Transfer* (2013) 67:1191–207. doi:10.1016/j.ijheatmasstransfer.2013.08.104

38. Koegl M, Mishra YN, Baderschneider K, Conrad C, Lehnert B, Will S, et al. Planar droplet sizing for studying the influence of ethanol admixture on the spray structure of gasoline sprays. *Experiments in Fluids* (2020) 61:209. doi:10.1007/s00348-020-03040-3

39. Sazhin SS, Krutitskii PA, Gusev IG, Heikal MR. Transient heating of an evaporating droplet. *Int J Heat Mass Transfer* (2010) 53:2826–36. doi:10.1016/j.ijheatmasstransfer.2010.02.015

40. Ulrich H, Lehnert B, Guénot D, Svendsen K, Lundh O, Wensing M, et al. Effects of liquid properties on atomization and spray characteristics studied by planar two-photon fluorescence. *Phys Fluids* (2022) 34:083305. doi:10.1063/5.0098922

Glossary

List of abbreviations

2c-LIF	Two-color laser-induced fluorescence
Bi	Biot number
DCM	Dichloromethane
EET	Enhanced energy transfer
EMCCD	Electron-multiplying charge-coupled device
FL	Fluorescein disodium
FQY	Fluorescence quantum yield
IC	Internal combustion
MDR	Morphology dependent resonances
Nd:YAG	Neodymium-doped yttrium aluminum garnet
OBN	Oil Blue N
PLIF	Planar laser-induced fluorescence
PMT	Photo multiplier tube
Pyr	Pyrromethene 597-C8
RhB	Rhodamine B
ROI	Region of interest
sCMOS	Scientific complementary metal–oxide–semiconductor
SNR	Signal-to-noise ratio
SRh	Sulforhodamine 101
TIR	Total internal reflection
UV	Ultraviolet
VIS	Visible
WGM	Whispering gallery modes

List of symbols

A	Absorbance
C	Concentration
I	Intensity
K	Constant
L	Length
R	Ratio
T	Transmittance
u	Velocity
V	Volume

Greek symbols

α	Heat transfer coefficient
β	Temperature dependent sensitivity factor
ε	Molar absorption coefficient
λ	Heat conductivity
λ	Wavelength dependence

Subscripts

0	Incident
1	Temperature 1
2	Temperature 2
D	Droplet
fl	Fluorescence
L	Liquid
opt	Optical
sat	Saturation
spec	Spectral

RESEARCH ARTICLE

Two-dye two-color laser-induced fluorescence spectroscopy on droplets of green solvent water/ethanol mixtures for thermometry and mixture composition

Hannah Ulrich[1,2] · Richard Weiß[1] · Lars Zigan[1,2]

Abstract

This work shows new insights on the application of two-color laser-induced-fluorescence (2c-LIF) thermometry in a droplet chain. A two-dye mixture is used in ethanol, water and ethanol/water mixtures in order to reach a high-temperature sensitivity and avoid the detection of lasing effects in the droplets. Various droplet sizes are recorded in regard to the limitation of the detection system for very small micrometric droplets. The breakup of a droplet chain is measured to assess the spectral detection system in applications with liquid structures of different sizes. Additionally, a proposal to expand the 2c-LIF application for studying ethanol/water droplets regarding mixture composition with a third color channel is presented. Forming two intensity ratios, the spectra can be used to obtain information on the mixture composition of the solvent. Measurements in different ethanol/water mixtures containing 0–100 vol% water are evaluated to show this possibility.

1 Introduction

Determining "responsible consumption and production" as one of the United Nations' goals for sustainable development, a specific focus was set on chemicals and waste. This goal is mainly addressed to the industry, having a significant potential for climate-friendly changes. In order to reach a higher sustainability in technical applications, the utilization of green solvents is decisive. Water and ethanol substitute more complex solvents, showing advantages like ecological manufacturing, reusability or biodegradation, as well as reduced health and safety risks (Capello et al. 2007; Chemat et al. 2019). Both liquids and their mixtures are found in various industrial areas, being used in spray or film cooling (Bhatt et al. 2017; Najim et al. 2020), as coolants in electrosprays for high power density devices (Taheri et al. 2024), or in regular adsorption coolers (Dzigbor and Chimphango 2019; Lache et al. 2023). Many other fields of applications

for the solvent mixtures can be named, ranging from a use as biofuel additives or ethanol fuel blends (Qi et al. 2010) or as solvents for extraction in pharmaceutical, medical or food industries (Amyrgialaki et al. 2014; Monroy et al. 2016; Mylonaki et al. 2008; Plaskova and Mlcek 2023; Zhang et al. 2007). Regarding the development and optimization of these solvent-based industrial processes, important variables are the liquid phase temperature and also the mixture fraction. Therefore, the focus of this work is the limitations and opportunities of two-dye 2c-LIF measurements in droplets, as the basic thermometry concept was presented in our recent work (Ulrich et al. 2023). Investigations are extended to measurements in ethanol, water and their mixtures, especially for very small droplets and atomizing jets.

2c-LIF allows the temperature determination in liquid flows or two-phase flows, e.g. dense and dilute sprays (Düwel et al. 2007; Mishra et al. 2016; Prenting et al. 2020) or liquid films (Collignon et al. 2021, 2022; Koegl et al. 2024). By admixing a temperature-sensitive fluorescent dye to the liquid, an emission signal ratio can be detected and used to infer the temperature. The ratio is formed from the signals of two wavelength areas of the emission spectrum of the dye. Ideally one of these color bands maps a temperature-sensitive, and the other band an oppositely sensitive or temperature-insensitive spectral excerpt. The selection of these spectral bands by respective filters may lead to a higher-temperature sensitivity of the signal ratio. In case

✉ Hannah Ulrich
  hannah.ulrich@unibw.de

1 Institut für Thermodynamik, Professur für Energiewandlung, Fakultät für Luft- und Raumfahrttechnik, Universität der Bundeswehr München (UniBw M), Neubiberg, Germany

2 Erlangen Graduate School in Advanced Optical Technologies (SAOT), Friedrich-Alexander-Universität Erlangen-Nürnberg (FAU), Erlangen, Germany

of evaporation, a related change in dye concentration in the liquid probe can result in self- or reabsorption of the fluorescence signal by other dye molecules. Approaching the 2c-LIF technique with two different dyes (two-dye two-color LIF) allows for a wider selection of color channels to form a maximum temperature-sensitive signal ratio. Additionally, the influence of solvent evaporation on the signal reabsorption and resulting signal ratio can be reduced. Therefore, the selection of the dyes and the accompanying filter set is conducted in consideration of the overlap of absorption and emission spectra.

Several authors characterized different fluorescent dyes for the use of liquid phase thermometry in cuvettes (Mishra et al. 2020; Prenting et al. 2020). To the authors best knowledge, Chaze et al. (2016) were first to propose the dye mixture of fluorescein (FL) and sulforhodamine 101 (SRh) in water for 2c-LIF thermometry. Temperature fields of a heated water jet are measured by injecting into stationary water doped with the dye mixture. In a further study, temperatures of millimetre-sized water droplets impinging on a hot surface were investigated (Chaze et al. 2017). The use of this dye mixture was adopted by Collignon et al. (2021) to study the temperature distribution in wavy liquid films. Earlier works presented thermometry in single droplets, studying rhodamine dyes with a PMT (photomultiplier tube) detection system (Castanet et al. 2003; Lavieille et al. 2001; Maqua et al. 2006). Evaporation measurements of millimetre-sized droplets doped with rhodamine were conducted with imaging systems for two-color LIF thermometry (Strizhak et al. 2018; Volkov and Strizhak 2020). Droplet images were shown with a minimum droplet size of around 0.5 mm (Volkov and Strizhak 2020). In our previous work, the dye combination of FL and SRh was used for temperature calibration and evaporation studies in 100 μm sized ethanol droplets in a monodisperse droplet chain (Ulrich et al. 2023). An imaging and a spectral detection system were used to record the fluorescence emission. Investigations of the detection limitation in regard to small μm-size droplets are a focus of the present work. Although there are liquid temperature measurements based on 2c-LIF in sprays available in the literature as mentioned above, there are few papers available on thermometry in individual μm-sized droplets (e.g. Palmer et al. 2016 in droplets with diameter of 67 μm). Because of the polydisperse nature of sprays, it is not clear, whether the smallest droplets can be detected at all. This is because the LIF signal roughly depends on the volume of the droplet and thus larger droplets in sprays dominate the signal intensity distribution, while signals of small droplets in dense sprays may be lost (Storch et al. 2016b). Additionally, there are challenges for laser diagnostics in droplets because of lens effects (Ulrich et al. 2023). This leads to "dead zones" in the LIF signal, appearing due to light refraction and convergence (Volkov and Strizhak 2020). These optical effects

may also be present in the non-spherical structures during breakup and need further investigation (Ulrich et al. 2023). Other effects are bright signals due to dye lasing or so-called morphology-dependent resonances (MDR, or sometimes named "whispering gallery modes", WGM) occurring at the phase boundary of the droplet. These optical effects are present in sprays as well, but may not be detected due to the limited resolution of the optical setup. However, these effects may bias the fluorescence signals and derived quantities such as temperature, droplet size (e.g. in planar droplet sizing based on LIF/Mie ratio) or concentration.

As mixture composition is another relevant variable in the solvent industry, the application of 2c-LIF with the proposed dyes is considered for composition measurements in water/ethanol mixtures. The dependency of the fluorescence signal and its spectral shift in various solvents is known for many dyes, e.g. for Rhodamine 6G (Zehentbauer et al. 2014) or Coumarin 152, Rhodamine B and Pyrromethene 597 (Prenting et al. 2020). However, such fluorophores were rarely applied for composition measurements in, e.g. binary liquid mixtures. Storch et al. (2016a) applied triethylamine (TEA) in different liquid ethanol/isooctane fuel blends and observed a shift of the fluorescence spectrum towards larger wavelength with increase in ethanol content. However, the signal for large ethanol concentrations (85% and 100%) was extremely low. Koegl et al. (2022) proposed the dye Nile Red for composition determinations of isooctane/ethanol mixtures (for ethanol volume fractions between 0% and 100%) with a 2c-LIF concept. A similar approach was applied for fuel mixtures of n-decane and butanol (Koegl et al. 2020b). Maqua et al. (2006) added another color channel to apply 3c-LIF with the dye Rhodamine B for thermometry in binary ethanol/acetone droplets with varying compositions (Maqua et al. 2006). A red-shift of the emission spectrum of Eosin-Y fluorescence was observed for the solvent ethanol compared to water (Koegl et al. 2020c). Although LIF was proposed for studying water/fuel emulsions for addition of ethanol (Koegl et al. 2020a), there is no LIF technique available for composition measurements of liquid binary ethanol/water mixtures until now. Other diagnostics based on light scattering (Raman, rainbow refractometry, etc.) for studying droplet compositions are reviewed by Lemoine and Castanet (Lemoine and Castanet 2013).

In the present work, the two-dye two-color LIF imaging system with two sCMOS cameras is utilized for the determination of droplet sizes, as well as for a visualization of jet breakup and optical processes inside liquid structures and droplets. For a better insight into optical effects, like MDR and the avoidance of their detection, simultaneous spectral measurements are conducted with a VIS spectrometer. Furthermore, these measurements provide a simple and quick solution to compare spectra and to recognize effects like spectral shifts depending on temperature and

composition. Due to fibre couplings and their flexible and compact sizing, the application and post-processing of spectral measurements for LIF is more feasible and favourable than imaging systems, especially in case of limited optical access. Therefore, the main focus in this paper lies on the spectrally detected fluorescence emission. Additionally, the data to verify the size limitation is recorded in several ethanol/water mixtures. This demonstrates the usability of the selected dye combination in different solvents. Important factors are the solubility of the dyes, the excitation at 532 nm and the temperature-dependent behaviour of the dye/solvent mixture.

2 Materials and methods

This section contains an abridgement of LIF fundamentals and the experimental setup. 2c-LIF techniques are based on the photo-physics of organic dyes, diluted in the respective solvent. Due to the absorption of photons of the laser wavelength (here 532 nm), the dye molecules are excited to an elevated energetic state. Fluorescence describes the process of spontaneous light emission of the excited molecule, to lose this excess energy and reach its' energetic ground state again. Transitional processes reduce the emitted energy, which leads to a reduction and an according Stokes shift (red-shift) of the fluorescence signal, compared to the absorbed wavelength (Schulz and Sick 2005). The emitted spectrum may also be sensitive to parameters, e.g. temperature. In this case, a temperature change leads to a different energetical distribution of the dye molecules over vibrational or rotational energy levels. The Boltzmann distribution describes this population dispersion and can lead to a temperature-sensitive shift of the spectrum (Bräuer 2015). A detailed discourse regarding the theory of 2c-LIF and the applied two-dye concept can be found in the authors previous work (Ulrich et al. 2023).

Using a signal ratio R_{fl} of two fluorescence intensities I_{fl}, the 2c-LIF approach eliminates the influence of several variables. Both fluorescence intensities I_{fl} represent a signal, simultaneously detected in a respective wavelength band.

Each wavelength band depicts a section of the two-dye fluorescence emission spectrum. In the linear range of the laser fluence, the emission signal ratio is expressed as

$$R_{fl} = \frac{I_{fl,1}}{I_{fl,2}} = \frac{K_{opt,1}(\lambda)K_{spec,1}(\lambda)I_0 VCe^{\beta_1(\lambda)/T}}{K_{opt,2}(\lambda)K_{spec,2}(\lambda)I_0 VCe^{\beta_2(\lambda)/T}} = \frac{K_{opt,1}K_{spec,1}}{K_{opt,2}K_{spec,2}}e^{\frac{\beta_1-\beta_2}{T}}$$

while β/ K, K_{spec}/ mol^{-1} and K_{opt} (λ)/— are wavelength-dependent constants (Lemoine et al. 1999). β and K_{spec} characterize physical and fluorescent properties of the predominating dye (Perrin et al. 2015). The detection systems' efficiency is described by K_{opt}. Building a ratio, the influence of the laser fluence I_0, the liquid volume V/ m^3 and the dye concentration C/ mol·m^{-3} is eliminated. Furthermore, the dependencies on the constants K_{spec} and K_{opt} are eliminated, normalizing the ratio to a reference measurement.

The 2c-LIF approach is based on the admixture of a fluorescent dye to the investigated fluid. In our work, water and ethanol (EtOH) are studied, as well as their mixtures in several compositions (EtOH0 to EtOH100). These are referred to by their volume fraction of ethanol. A mixture of two dyes, FL (CAS: 518-47-8) and SRh (CAS: 60311-02-6), with a mass ratio of 10:1 (750 mg$_{FL}$/l and 75 mg$_{SRh}$/l) is diluted in all respective solvents. Therefore, a higher-temperature sensitivity can be achieved as with the use of only one dye. Furthermore, fluorescence reabsorption by the respective dye molecules itself can be avoided, taking the absorption spectra into account. With the proposed mixture and filter combination in the detection system, the recording of MDR, leading to very high LIF signals on the droplet rim, can be circumvented.

To measure the addressed two-dye fluorescence emission spectrum, an experimental setup is equipped with a fibre-coupled spectrometer to deliver spectral information, as depicted in Fig. 1 (left). A monodisperse droplet chain with droplet sizes from 30 to 120 μm is generated by a piezoelectrically controlled droplet generator (FMAG 1520, TSI). The tempered droplet generator is assembled with a compressed air supply and a syringe pump (AL1000-220, Aladdin), containing a mixture of solvent and fluorescent dyes. Producing droplets of various sizes, the liquid flow

Fig. 1 Left: Optical setup with spectral detection of the fluorescence emission around a heated droplet generator. Right: Example single-shot LIF images of FL and SRh emissions with respective BP filters (top row) and without BP filters (bottom row). Measurements are for ethanol at 293 K
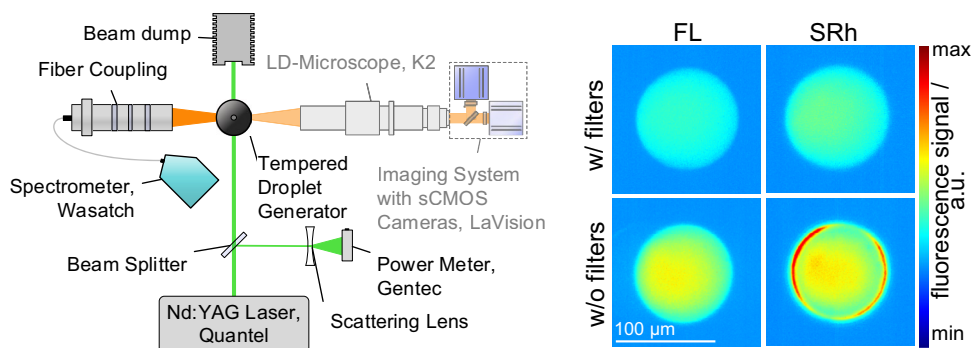
rate is varied between 2 ml/h and 70 ml/h and the applied frequency of the ultrasound actuator between 20 and 50 kHz. The tempered and dry focussing air for droplet formation, which also shields the droplets at the nozzle exit against ambient air, comes from a compressor system with at least 253 K pressure dewpoint corresponding to a water vapour pressure of a maximum of 0.5204 Pa. Later on, droplets mix with ambient air, while temperature and humidity are constantly measured with a thermo-hygrometer in the laboratory. To illuminate the fluorescent mixture at 532 nm, a pulsed Nd:YAG laser (Q-SMART 850, Quantel) is being operated with a frequency of 10 Hz and a fluence of 2.4 mJ/cm^2. The laser beam has a diameter of 8 mm and is led through the droplet chain into a beam dump.

Orthogonally to the laser beam, an imaging system is mounted for size calibration. This system contains a long-distance microscope (Infinity DistaMax, K2), followed by a dichroic mirror (T588lpxr, Chroma), to separate the signal at 588 nm. The separated wavelength bands are each detected by sCMOS camera (Imager, LaVision) after passing specifically selected bandpass filters (554/23 BrightLine HC and 615/24 BrightLine HC). Images of recorded droplet fluorescence with (top) and without (bottom) these bandpass filters can be seen in the right image in Fig. 1. The picture shows droplets as seen by the two different cameras, after the signal has passed the dichroic mirror. As expected, the signal without the filters is higher, than with the filters mounted in front of each camera. Without the filter mounted to the camera, detecting the SRh signal, strong LIF signals due to MDR occur on the droplet surface.

The investigation of the spectral location of the MDR is performed with another detection system mounted at 90° to the laser beam. A spectrometer (WP-VIS-A-S-50, Wasatch Photonics) is fibre-coupled to an optical system, consisting of a notch filter and two achromatic doublets. Thus, spectral information is obtained, clarifying the wavelength position of the disturbing MDR signal. The spectrometer setup has the advantage of a small dimension, a moveable mounting and a lower cost than the camera system. The recorded data of the spectrometer requires only little memory space and allows for simplified post-processing. Therefore, even technical systems with, e.g. limited optical accessibility can be investigated with this setup. A comparison of the signals detected with the imaging and the spectrometer setup showed very similar results for the signal ratios and resulting temperature calibration curve (Ulrich et al. 2023). In this work, LIF images are only provided for droplet visualization and a better understanding of breakup processes of the jet and occurring lasing effect. All spectra are obtained by five recordings of 100 averaged single spectra per measurement location (as specified below), each with an integration time of 50 ms. Background measurements are subtracted from the spectra and a baseline fit is conducted. The single intensity signals, forming the signal ratio, are the integrated emission signals in the respective color channel region of the fluorescence spectra.

Additional absorption measurements are conducted with an UV/VIS-spectrophotometer (V-750, Jasco). A tempered cuvette holder allows the recording of temperature-dependent absorption spectra. Due to a larger path length in the cuvette, a more diluted mixture (50 mg$_{FL}$/l and 5 mg$_{SRh}$/l) is prepared. This data is recorded to extend the understanding of the interaction of the dyes in different solvents. All temperature-dependent measurements are limited to a maximum temperature of 343 K, due to the boiling point of ethanol.

3 Results and discussion

The following section shows absorption and emission spectra of the dye mixture in different solvents. Absorption spectra are discussed with respect to the temperature dependence. Investigations of the fluorescence emission spectra are conducted to determine the lower signal limit of the detection systems regarding droplet sizes. Furthermore, the impact of structure size, also considering MDR signals, on the signal ratio and the subsequent temperature sensitivity is examined. Additional studies based on the spectral LIF detection system are conducted for various liquid mixtures and temperatures. Furthermore, the setup is applied to measure the temperature evolution downstream an atomizing jet, produced in the droplet generator. Spray-like liquid structures are produced, testing the suitability for detection of various droplet sizes, moving inside and outside the focus. Finally, the established 2c-LIF approach is analysed regarding an application to measure solvent compositions. For this purpose, an improved 3c-LIF method is proposed.

3.1 Absorption spectroscopy

Figure 2 shows the temperature-dependent evolution of the photon absorption in pure water—EtOH0, a mixture of 40 vol% ethanol and 60 vol% water—EtOH40 and pure ethanol—EtOH100, as well as the laser line at 532 nm. With the absorption spectrophotometer, six different ethanol–water mixtures (20 vol% steps) were measured in 10 K intervals from 283 K (marked with "c"-cold) to 343 K ("h"-hot). All measured spectra allow a clear differentiation between one absorption spectrum due to FL at wavelengths from 410 to 540 nm and another due to SRh, around 555 to 610 nm. In cold conditions, FL absorbs more light, the higher the water fraction. Additionally, a blue-shift of the peak can be observed, which is a possible explanation for a lower emission signal in fluorescence measurements. At 343 K, the mixtures show a counter wise behaviour for EtOH0 with the lowest absorption and
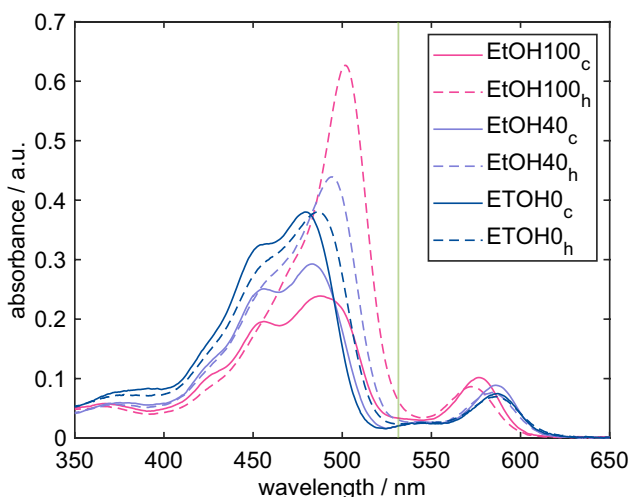
Fig. 2 Absorption spectra of different solvents at temperatures between 283 K ("c"-cold) and 343 K ("h"-hot). The laser line at 532 nm is depicted in green

EtOH100 with the highest. Nevertheless, the absorption rises with temperature in all solvent mixtures. Contrary to the temperature dependence of the FL peak, absorption of SRh in pure ethanol (EtOH100) is lower, the higher the temperature. Also opposing to FL is the shift of the SRh absorption peak towards longer wavelengths with rising water fraction. Due to shifting from the laser line at 532 nm, this trend may be responsible for lower emission signals of the second color channel in watery solvents.

3.2 Fluorescence spectroscopy: droplet size dependency

In the authors previous work, only 100 μm-sized droplets were considered. To show the applicability of the two-dye two-color approach to the complete size range of the droplet generator, measurements were conducted with droplets sized from 30 μm to 120 μm. This data was recorded in spherical droplets—depending on the droplet size and according settings this was at a distance of 2 mm to 4 mm below the nozzle exit. Figure 3 shows fluorescence emission spectra measured in 40 μm and 100 μm sized EtOH100 droplets, both at 293 K and 343 K. The signal reduces with the size of the droplets. For a better comparison, the spectra are normalized to their maximum. In all measurements, the VIS emission spectrum starts at around 490 nm to about 740 nm. A mounted notch filter blocks light around 532 nm to avoid over-exposure due to Mie scattering. The respective blocked wavelength band lies directly in the emission peak of FL. The greenish shaded area visualizes the temperature-dependent color channel. The shaded red color band covers an excerpt of the comparably temperature-insensitive SRh emission, with a peak maximum at 594 nm. A third peak around 649 nm can be observed in the spectra. This peak is due to lasing effects (or MDR) at the droplet rim.

The normalized spectra of the different droplet sizes reveal only little divergence in the emission peak of FL, with a slight red-shift of the big droplets' spectra visible in the anti-stokes spectrum probably due to reabsorption. The wavelength region of the SRh peaks shows a match of the normalized spectra of both droplet sizes. The resulting calibration curves are depicted in the right graph in Fig. 3. Previous studies showed a linear behaviour of the
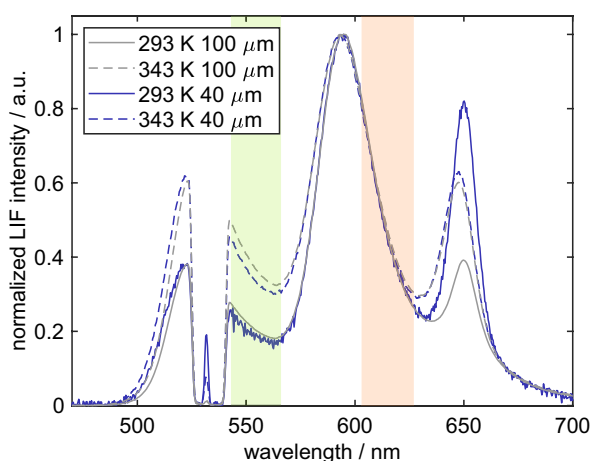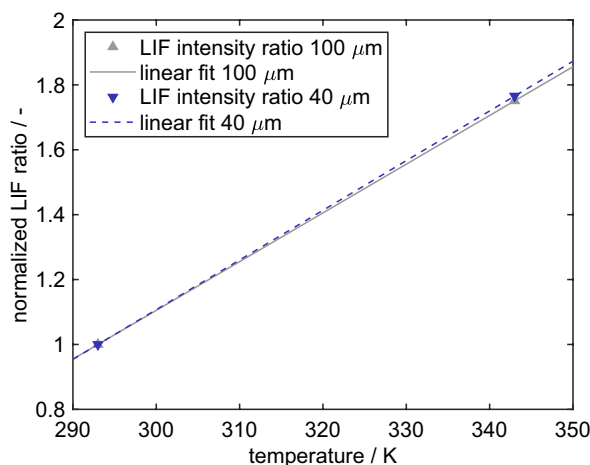

Fig. 3 Left: Normalized fluorescence emission spectra of the dye mixture detected in 40 μm (purple) and 100 μm (grey) sized ethanol droplets. Solid curves are for 293 K, dashed curves for 343 K. The shaded areas visualize the color channels, each representing the pass-

ing band of the respective BP filters in the imaging setup. Right: Normalized calibration curve of the LIF ratios received from respective spectra in the left image

temperature-dependent signal ratio, determined at seven temperatures between 283 and 343 K (Ulrich et al. 2023). The linear behaviour in this temperature range was found for ethanol, water and butanol droplets with a size of 100 µm (Ulrich and Zigan 2023), but the temperature sensitivity is slightly different for the three solvents. Thus, in order to show the influence of droplet size on the temperature sensitivity, calibration curves are fitted to only two calculated ratios, at 293 K and 343 K. In this experiment, measurements in both droplet sizes reveal a temperature sensitivity of the LIF signal ratio of 1.5%/K. To proof that MDR would not affect the temperature sensitivity of the chosen signal ratio, the position of the MDR peaks is detected in the measurements with droplet size variation. This study shows that the whole range of produced structure sizes can be processed further without the risk of influence on the intensity ratio by MDR.

3.3 Thermometry in an atomizing jet

To assess the suitability of the spectral detection system of the setup for, e.g. spray applications, temperature measurements downstream the droplet generator are conducted. Adjusting the droplet generator settings to a large volume flow, spray-like behaviour of the liquid flow is enforced. Reynolds, Weber and Ohnesorge numbers are estimated in the following section based on jet and droplet information rather than nozzle specifications, as the exact nozzle geometry and flow information is not available. These dimensionless numbers are crucial to describe the primary droplet breakup. The liquid Reynolds number Re_L represents the ratio of inertial forces to viscous forces and is defined by $Re_L = \rho \cdot \upsilon \cdot l / \eta$. For the calculation, the liquid-specific properties density ρ and dynamic viscosity η, as well as the velocity υ and the specific length l are relevant. The liquid Weber number We_L serves as a stability criterion for jets and droplets and describes the ratio of inertial force to surface tension. Therefore, it additionally includes the surface tension σ as a relevant parameter: $We_L = \rho \cdot l \cdot \upsilon^2 / \sigma$. Representing a ratio of viscous forces to inertial and surface forces, the Ohnesorge number Oh is a combination of the Weber and Reynolds number and can be calculated by $Oh = \eta \cdot (l \cdot \rho \cdot \sigma)^{-0.5} = We_L^{0.5} / Re_L$. The length scale l corresponds to the jet or droplet diameter, respectively, determined by the LIF images. In the spray, different structure sizes are created, which are both in and out of focus so that the size cannot always be determined reliably with the imaging setup. With the spectral measurement approach, the challenges of differently sized liquid structures and depth of focus should be resolved. The jet is transient and the generated liquid structures are not reproducible regarding their form and shape. Five spectra (each 100 averaged, 50 ms integrated) are recorded at six different distances to the nozzle

exit. Three different injection settings were studied, showing a difference in set temperature at the nozzle and a difference in the liquid volume flow rate. Exemplary measurements are conducted in ethanol. To give an insight to the structure of the created spray, excerpts in form of single images, detected in the SRh color channel, are shown in Fig. 4. For each setting, recordings at the nozzle exit (0 mm), at a distance of 6 mm and 15 mm to the nozzle, are presented. For the first setting (left column), the volume flow rate was set to 15 ml/h and the initial temperature to 293 K. Both other measurements are investigated at an initial temperature of 343 K, one with a liquid flow rate of 15 ml/h (column 2) and the other one of 5 ml/h (column 3). All LIF images are displayed with the same color scale. For a better visibility of droplets at all temperatures, images detected in the temperature-insensitive LIF channel (SRh emission) are shown. This means that the temperature only hardly, but rather the droplet size, affects the signal. Using the initially described dimensionless numbers Re_L and Oh, the jet breakup regime can be estimated according to Ohnesorge (Ohnesorge 1936).The results are depicted in Table 1. With increase in liquid temperature at constant liquid flow, both Reynolds and Weber number rise, since viscosity and surface tension are reduced. A decrease in liquid volume flow leads to lower Reynolds- and Weber
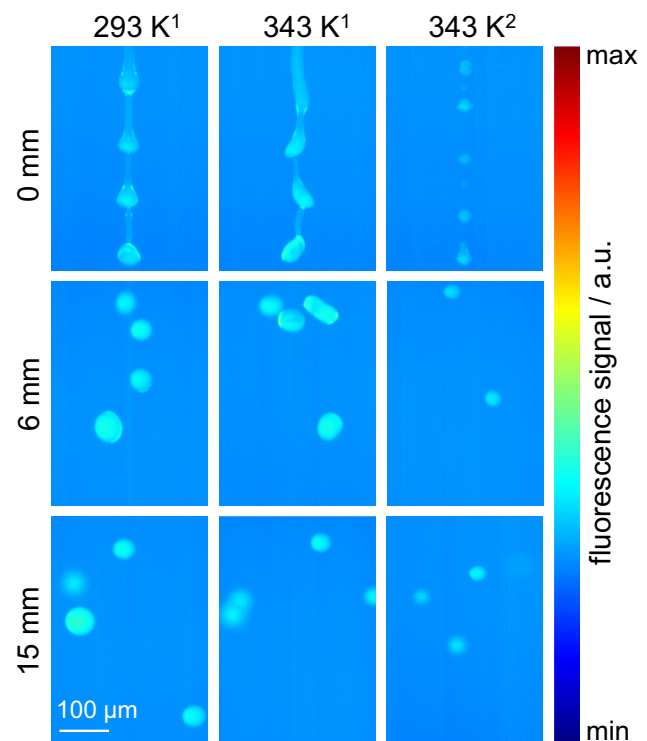

Fig. 4 Single images of the breaking up jet or droplet chain at three different distances downstream the nozzle exit. Temperatures of the droplet generator are set to 293 K and 343 K. LIF images depict the temperature-insensitive SRh color channel. Liquid volume flow rate: [1]15 ml/h, [2]5 ml/h

Table 1 Dimensionless numbers Re_L, We_L and Oh of the three investigated ethanol jets. Respective fluid properties are extracted from (Dean and Lange 1999; FLUIDAT® on the Net 2024)

	293 K[1]	343 K[1]	343 K[2]
Re_L	251.25	435.26	85.63
We_L	73.03	83.28	2.98
Oh	0.36	0.65	0.62
Jet breakup regime	2nd wind-induced	1st wind-induced	1st wind-induced

numbers at constant liquid temperature. All three studied cases are in the "wind-induced" regime.

In the first column, relatively large droplets are periodically released with a droplet diameter of around 39 μm and are subsequently dispersed due to the turbulent gas flow induced by the droplet stream. At increased temperature (central column), a liquid jet is visible at the nozzle outlet, which breaks up into longitudinally stretched droplets with an average diameter of about 35 μm at 6 mm distance to the nozzle exit. The reduced droplet sizes can be explained by the larger Weber numbers. Smaller surface tension may lead to more instable and deformed droplets at similar flow velocities, which tend to a decrease in breakup time. Further downstream the droplets are more dispersed and may show droplet collision and coalescence as well. In the third row at decreased liquid volume flow, smaller droplets with a diameter of about 23 μm are periodically generated forming a droplet chain and some very small (average of 11.3 μm) "satellite" droplets in between are visible. It should be noted that the smaller droplets compared to the previous cases are due to the lower liquid mass flow while the flow focussing air flow is kept constant, which is responsible for setting the initial droplet size inside the droplet generator. An increase in the droplet distance and droplet dispersion is visible further downstream (about 30 μm average diameter at 6 mm distance to the nozzle). At 15 mm, all images show "sharp" in-focus droplets and some blurred droplets are out of focus.

Spectra are being recorded at all three settings, post-processed and signal ratios are formed. Temperatures are obtained, using the calibration curve of the droplet chain measurements. The temperature progression downstream the nozzle exit is depicted in Fig. 5, recorded at all three settings. Two y-axes are shown to provide a better temperature resolution. The left, blue axis corresponds to the blue curve, showing the heat-up of the liquid jet at 293 K injected to ambient air at 296.2 K. Exiting the droplet generator, an initial temperature of 292.3 K is recorded. A temperature rise to 296.1 K at 10 mm after the nozzle exit is plausible, considering the higher ambient temperature. Furthermore, a cooling down to 294.8 K is observed between 10 and 20 mm distance to the nozzle exit, which can be explained
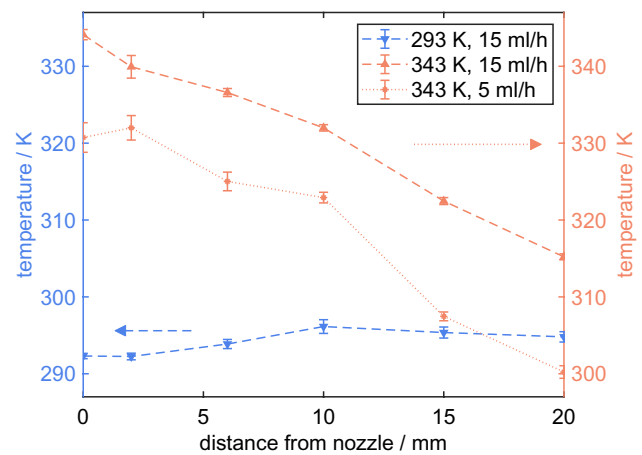

Fig. 5 Temperature progression measured downstream the nozzle exit. Two y-axes offer a better resolution of the temperature course. Blue (left axis): Liquid and air flow are tempered to 293 K. Red (right axis): Liquid and air flow are tempered to 343 K. Different liquid mass flows are measured

by evaporation cooling. These small temperature differences are in the same range as the shot-to-shot variations (maximum of 0.9 K at 10 mm distance) and could thus also result from measurement uncertainties.

The right, red y-axis relates to the two measurements with a set temperature of 343 K in the droplet generator. For both hot jets, being injected into ambient air, a cooling down of around 30 K is measured for the considered 20 mm distance. The first measurement is recorded with the same liquid volume flow (15 ml/h) as in the "cold" measurement. A liquid temperature of 344.1 K is measured at the exit of the droplet generator. A steady decrease of 28.9 K is measured within 20 mm due to convective cooling of the hot droplets by the cold ambient air and evaporation cooling. To further assess the origin of the temperature change, the lumped capacitance model was used to estimate the effect of heat transfer with the ambience. The dimensionless Biot number Bi expresses the instationary cooling or heating behaviour by relating the heat transfer coefficient h between liquid and surrounding to the thermal conductivity λ_L of the liquid: $Bi = h \cdot l / \lambda_L$ (Bergman et al. 2013). For small Biot numbers, a relatively homogeneous droplet temperature can be assumed, which is true for the present cases as well. Here, the Biot numbers are around 0.1 (0.09 to 0.13). A more detailed description of the procedure can be found in the appendix of the paper. For the hot case with 15 ml/h volume flow, approximately 4.6 K of the 29 K temperature reduction within 20 mm (corresponding to 2.2 ms) measurement distance are due to convective heat transfer with the ambiance.

Smaller droplets and liquid structures are generated with a liquid volume flow of 5 ml/h. The setting of the focussing air is similar, which leads to higher evaporation rate at a lower liquid flow. The images in Fig. 4 show single droplets

exiting the nozzle, whereas a liquid jet is visible at the other settings. The droplets have a temperature of 330.7 K at the nozzle exit. Measurements at 2 mm distance to the exit reveal an initial increase of 1.2 K. This temperature rise could be explained by measurement uncertainties due to fluorescence light reflections close to the droplet generator surface. This theory was discussed in more detail in our previous work (Ulrich et al. 2023). Further downstream the spray, a decrease of 30.5 K is recorded for a distance of 18 mm. Considering the smaller droplet size compared to the other "hot" setting with 15 ml/h volume flow, the lower resulting temperatures and the slightly higher-temperature difference over the recorded 20 mm are reasonable. On the one hand, this can be explained by more efficient convective cooling. The larger droplets on the other hand have a larger thermal energy and the cooling is slower. Calculations of the cooling due to heat transfer of 17.7 K confirm the increased temperature reduction of the small droplets.

Furthermore, the temperature reduction induced by evaporation cooling is expected in the order of minimum 10 K. A numerical simulation of isolated ethanol droplets predicted a temperature reduction of about 17 K. The initial droplet and ambient temperature were 293 K and the droplet sizes were in the range of 5 μm to 40 μm, but the flow velocity was much higher (20 m/s) (Koegl et al. 2020a, b, c, d). It should be noted that this simulation is a worst-case scenario and cannot be directly compared to the spray-like conditions in the present study.

Overall, only very little deviations (maximum of 1.9 K measured at the nozzle exit) are obtained within the spray measurements. These deviations arise from the five measured spectra, each consisting of 100 single spectra. Divergences due to different structure sizes and liquid structures out of focus are expected, but could not be observed so far.

3.4 Possibility of 2c-LIF and 3c-LIF for determination of the mixture composition

Apart from thermometry, the 2c-LIF approach can be used to investigate the mixture composition in fluids. Therefore, the dye emission has to spectrally shift, depending on the solvent. To verify the use of the proposed dye combination for determining the solvent mixture ratio, six different ethanol/water mixtures are investigated in the droplet chain. The emission spectra of these solvents, doped with FL and SRh, are shown in Fig. 6 on the left. In these measurements, 30 μm sized droplets were formed with the droplet generator and detected at around 2 mm below the nozzle exit. Due to the droplet shielding by the tempered focussing air, it is assumed that no distinct droplet temperature change nor vaporization takes place in the estimated 0.6 ms up until reaching the measurement position. For a better visibility of the spectral shift, all spectra are normalized to the maximum of the SRh peak. EtOH0 (water) droplets reveal the lowest signal and larger noise of all tested solvents. This can be explained by the lower absorbance of water at 532 nm compared to ethanol (see Fig. 2). The lower fluorescence signal for water compared to ethanol was also observed for other dyes such as Eosin-Y (Koegl et al. 2020c). The FL spectrum, partially covered by the notch filter, reveals a blue-shift, the higher the water content. The SRh spectrum shifts contrary so that a red-shift is visible for higher water shares. This corresponds to the absorption spectra as shown in Fig. 2. Typically, the behaviour in absorption and fluorescence emission is similar. In general, a contradictory signal intensity behaviour in the two color channels is favourable for the use of an intensity ratio. In a first attempt, the same BP filters were taken in the liquid mixture investigation as in the
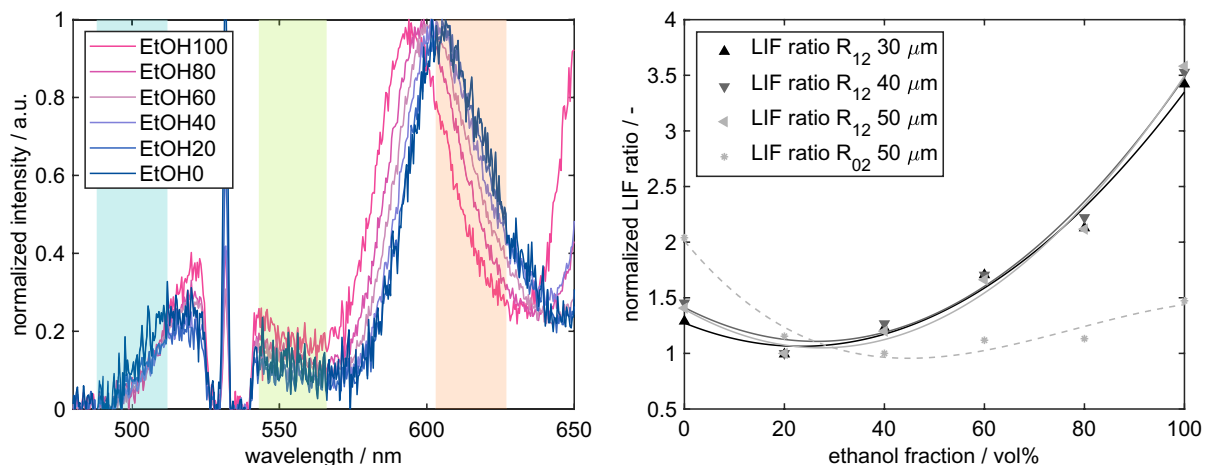

Fig. 6 Left: Fluorescence emission spectra of EtOH0 to EtOH100 in 30 μm sized droplets at 293 K. Shaded areas visualize the color channels (centre wavelengths at 500 nm (channel 0), 554 nm (channel 1) and 615 nm (channel 2)). Right: Calculated spectral LIF ratios of signal intensities of two color channels, each with the corresponding polynomial fit

Table 2 Characteristic properties of liquid ethanol at temperatures of 293 K and 343 K extracted from (FLUIDAT® on the Net 2024)

Ethanol properties		293 K	343 K
Kinematic viscosity ν	m²/s	$1.42 \cdot 10^{-6}$	$6.52 \cdot 10^{-7}$
Density ρ	kg/m³	804.9	747.3
Specific heat capacity c_p	J/kg·K	2409	2632
Thermal conductivity λ	W/m·K	$1.69 \cdot 10^{-1}$	$1.57 \cdot 10^{-1}$
Thermal diffusivity a	m²/s	$8.73 \cdot 10^{-8}$	$7.99 \cdot 10^{-8}$
Surface tension σ	mN/m	22.39	18.23

Table 3 Characteristic fluid properties of air at temperatures of 293 K and 343 K extracted from (FLUIDAT® on the Net 2024)

Air properties		293 K	343 K
Kinematic viscosity ν	m²/s	$1.53 \cdot 10^{-5}$	$2.01 \cdot 10^{-5}$
Density ρ	kg/m³	1.19	1.02
Specific heat capacity c_p	J/kg·K	1009	1006
Thermal conductivity λ	W/m·K	$2.60 \cdot 10^{-2}$	$2.95 \cdot 10^{-2}$
Thermal diffusivity a	m²/s	$2.17 \cdot 10^{-5}$	$2.89 \cdot 10^{-5}$

thermometry study in order to reduce effects of reabsorption and MDR.

The intensity ratio and a polynomial fit are depicted in the right graph for measurements of different ethanol–water mixtures in three differently sized droplets. The comparison of droplet sizes shows only a little divergence of the measurements in 30 μm droplets and mostly in EtOH0. This can be explained by the low signal detected in measurements with water. Diluted in this solvent, both fluorescent dyes absorb less photons, which decreases the probability of an emission event in the molecules. Additionally, the detection of 30 μm water structures represents the limit of both—the spectral and imaging—detection system (results are not shown here). This can be seen by very low signal intensities and thus, higher signal-to-noise ratios (SNR). The comparison of different droplet sizes shows, however, that despite the low signals similar results are achieved for all liquid mixtures studied.

As for the composition dependence, a higher LIF intensity ratio can be observed for increasing ethanol content. This correlation is valid for mixtures with ethanol fractions over 20 vol% and can be used for respective water–ethanol blends. To apply this measurement approach to mixtures with ethanol portions below 20 vol%, the ratio is not sufficient and another measurable variable has to be used, e.g. the location of a spectral maximum. In this case, the dependence of the SRh maximum is similar to the course of the second color channel and offers only little sensitivity at low ethanol fractions. Another possibility is the use of a third wavelength region for three-color LIF. Therefore, another third color channel at a lower wavelength is selected (according to bandpass filter 500/24 BrightLine HC) and an additional LIF ratio is formed. With this additional information, a definite allocation of the ethanol portion can be performed by solving the two-equation system. This concept is further explained by Maqua et al. (2006) for PMT measurements in ethanol/acetone mixtures. An evaluation showed that the ratio R_{02} of the second and an additional color channel (0) in the spectrum of FL has a strong dependence on the ethanol content in mixtures with high water fraction (EtOH0 to EtOH40), as depicted by the dashed curve in Fig. 6 (right). It should be noted that the ratios R_{02} and R_{12} are both dependent on temperature and composition, so that a simultaneous planar measurement of these two quantities needs an iterative solution and further calibration data. For example, in (Ulrich and Zigan 2023) it was shown that the slopes of the temperature calibration curves R_{12} in pure ethanol and water are slightly different. However, it appears feasible to perform simultaneous spectral measurements of thermometry and composition. For this purpose, the concentration measurements can be conducted via the analyzation of the shift of the SRh spectrum in the "red" color channel, which hardly depends on temperature. A spectral fit algorithm is capable to provide information on the mixture composition, but further calibration at smaller temperature and concentration intervals is required.

4 Conclusion and outlook

This work concentrates on the first-time application of a two-dye 2c-LIF approach for thermometry in a droplet chain and atomizing jets with droplets sizes below 50 μm. The dyes, such as FL and SRh, are dissolved in various ethanol/water mixtures and detected with a spectrometer setup. For size calibration and insights into the behaviour of the droplets, an additional imaging setup records the fluorescence emission of the droplets. The focus of the detection lies on the spectral setup, as it has many advantages regarding size, cost and post-processing especially for technical systems with small optical access. Additionally, the occurrence of interference effects such as MDR can be monitored and the respective wavelength regions can be directly determined. Two intensity regions of the spectra are selected to form a temperature-sensitive ratio. These color channels are adopted from the respective bandpass filters with centre wavelengths at 554 nm and 615 nm, which were used for the camera system. Measurements of differently sized droplets between 30 μm and 120 μm demonstrate comparable temperature sensitivities of the intensity ratio. In the studied wavelength range and operating conditions, no influence of droplet size on the spectra and also lasing effects in the droplets (MDR) could be identified. This allows for subsequent atomizing jet measurements using the adjusted droplet generator. Thus,

Table 4 Equations for a step-by-step calculation of the droplet temperature due to contribution of convective heat transfer. For more detailed fundamentals of the model description and the calculations, see (Bergman et al. 2013; Ranz and Marshall 1952)

	293 K[1]	343 K[1]	343 K[2]
Biot number $Bi = h \cdot l/\lambda_L$	0.12	0.13	0.09
Heat transfer coefficient $h = Nu_L \cdot \lambda_G/d_D$	3249.35	4021.92	4823.48
Nusselt number (laminar) $Nu_L = 2 + 0.664 \cdot Re_G^{1/2} \cdot Pr^{1/3}$ for $0 \le Re_G < 200$, $0 \le Pr \le 250$	4.86	4.21	2.98
Reynolds number (gas) Re_G	23.43	14.10	2.77
Prandtl number Pr	0.70	0.70	0.70
Fourier number $Fo = a_L \cdot t/r_D^2$			
Droplet temperature $T = \exp(-Bi \cdot Fo) \cdot \Delta T + T_\infty$			

various droplet sizes were produced, which are located in- and outside of the detection focus of the imaging system. Successful temperature recordings downstream the jet were taken for three settings at two different temperatures and two different liquid volume flows. Within the measured distance of 20 mm, a cooling of about 29 K was obtained for the jet with an initial temperature set to 343 K and average droplet size of 35 μm (at 6 mm distance to the nozzle exit). A slightly larger temperature decrease of 30.5 K was measured for the jet with a lower liquid flow rate and thus smaller droplets with an initial average size of about 18 μm (at the nozzle exit). In the third setting, droplets were tempered to 293 K and a temperature increase of 3.8 K (to 296.2 K ambient air) was recorded.

Apart from the thermometry application, the use of the dye couple for 2c-LIF composition studies in ethanol/water mixtures was considered. For this purpose, a composition-dependent calibration curve was generated with the same color channels as used for thermometry. This allows the identification of ethanol fractions in mixtures with an ethanol content higher than 20 vol%. To enable the determination of smaller ethanol fractions, a third color channel, according to a bandpass filter for imaging, was proposed. Forming a second intensity ratio, the two calibration curves show a promising method for detecting composition dependence, each in a different range of ethanol fraction.

Future work should explore broader excerpts of typical industrial sprays, focussing less on microscopic droplet details and more on macroscopic spray formations and behaviour. Subsequent measurements are necessary to refine the ethanol fraction dependence of the 3c-LIF method. Furthermore, the combination with the thermometry approach would give huge benefits for solvent mixture investigations and should therefore be studied further. Simultaneous planar measurements of these two quantities require an iterative approach and additional calibration data. However, conducting simultaneous spectral measurements of thermometry and composition seems achievable. Concentration measurements can be realized by analysing the shift in the SRh spectrum within the "red" color channel, which is hardly affected by temperature. A spectral fitting algorithm can offer insights into mixture composition, although further calibration is needed at smaller temperature and concentration intervals. Investigations of the application on other solvent mixtures, such as propanol, butanol and water with varied pH value, would be beneficial.

Appendix

Fundamentals of the lumped capacitance model, used to estimate the temperature change in the droplet due to convective heat transfer with the surrounding, are provided

subsequently. Properties with the subscript "L" refer to the liquid, which in this case is ethanol. All relevant liquid properties necessary for the calculations can be found in Table 2.

As the ambient gas is air (subscript "G" for gas), the following Table 3 provides its main fluid properties at both investigated temperatures.

A step-by-step solution of the equations used to calculate the Biot numbers Bi as described in Sect. 3.3 can be obtained in the following overview (Table 4). In detail, Bi is estimated by a heat transfer coefficient h, which includes the Nusselt number Nu. In case of a laminar flow around a sphere (droplet, subscript "D"), Nu can be correlated empirically, which is valid for a specific range of gas-phase Reynolds numbers Re_G and Prandtl numbers Pr (Ranz and Marshall 1952). The values for both characteristic numbers are also listed in the table.

To further assess the temperature reduction by heat conduction and convection, the Fourier number Fo is evaluated, including the droplet radius r_D and a respective residence time t, which is estimated from the initial liquid volume flow. Finally, by means of Bi and Fo, the current average droplet temperature T can be estimated.

Data availability Data can be shared upon request.

Declarations

Conflict of interest The authors declare no competing interests.

References

Amyrgialaki E, Makris DP, Mauromoustakos A, Kefalas P (2014) Optimisation of the extraction of pomegranate (Punica granatum) husk phenolics using water/ethanol solvent systems and response surface methodology. Ind Crops Prod 59:216–222. https://doi.org/10.1016/j.indcrop.2014.05.011

Bergman TL, Incropera FP, DeWitt DP, Lavine AS (2013) Principles of heat and mass transfer. Wiley

Bhatt NH, Lily RR, Varshney P, Pati AR, Chouhan D, Kumar A, Munshi B, Mohapatra SS (2017) Enhancement of heat transfer rate of high mass flux spray cooling by ethanol-water and ethanol-tween20-water solution at very high initial surface temperature. Int J Heat Mass Transf 110:330–347. https://doi.org/10.1016/j.ijheatmasstransfer.2017.02.094

Bräuer A (2015) In situ spectroscopic techniques at high pressure, vol 7. Elsevier, Amsterdam

Capello C, Fischer U, Hungerbühler K (2007) What is a green solvent? A comprehensive framework for the environmental assessment of solvents. Green Chem 9(9):927. https://doi.org/10.1039/b617536h

Castanet G, Lavieille P, Lebouch M, Lemoine F (2003) Measurement of the temperature distribution within monodisperse combusting droplets in linear streams using two-color laser-induced fluorescence. Exp Fluids 35(6):563–571. https://doi.org/10.1007/s00348-003-0702-1

Chaze W, Caballina O, Castanet G, Lemoine F (2016) The saturation of the fluorescence and its consequences for laser-induced fluorescence thermometry in liquid flows. Exp Fluids 57(4):1–18. https://doi.org/10.1007/s00348-016-2142-8

Chaze W, Caballina O, Castanet G, Lemoine F (2017) Spatially and temporally resolved measurements of the temperature inside droplets impinging on a hot solid surface. Exp Fluids 58(8):1–16. https://doi.org/10.1007/s00348-017-2375-1

Chemat F, Abert Vian M, Ravi HK, Khadhraoui B, Hilali S, Perino S, Tixier A-SF (2019) Review of alternative solvents for green extraction of food and natural products: panorama, principles, applications and prospects. Molecules. https://doi.org/10.3390/molecules24163007

Collignon R, Caballina O, Lemoine F, Castanet G (2021) Temperature distribution in the cross section of wavy and falling thin liquid films. Exp Fluids. https://doi.org/10.1007/s00348-021-03175-x

Collignon R, Caballina O, Lemoine F, Castanet G (2022) Simultaneous temperature and thickness measurements of falling liquid films by laser-induced fluorescence. Exp Fluids. https://doi.org/10.1007/s00348-022-03420-x

Dean JA, Lange NA (1999) Lange's handbook of chemistry, vol 15. McGraw-Hill, New York

Düwel I, Ge H-W, Kronemayer H, Dibble R, Gutheil E, Schulz C, Wolfrum J (2007) Experimental and numerical characterization of a turbulent spray flame. Proc Combust Inst 31(2):2247–2255. https://doi.org/10.1016/j.proci.2006.07.111

Dzigbor A, Chimphango A (2019) Evaluating the potential of using ethanol/water mixture as a refrigerant in adsorption cooling system by using activated carbon–sodium chloride composite adsorbent. Int J Refrig 97:132–142. https://doi.org/10.1016/j.ijrefrig.2018.09.025

FLUIDAT® on the Net (2024) FLUIDAT® (V1.86). Bronkhorst High-Tech B.V

Koegl M, Mishra YN, Baderschneider K, Conrad C, Lehnert B, Will S, Zigan L (2020a) Planar droplet sizing for studying the influence of ethanol admixture on the spray structure of gasoline sprays. Exp Fluids. https://doi.org/10.1007/s00348-020-03040-3

Koegl M, Mull C, Mishra YN, Will S, Zigan L (2020b) Characterization of fuel/water mixtures and emulsions with ethanol using

laser-induced fluorescence. Appl Opt 59(4):1136–1144. https://doi.org/10.1364/AO.380392

Koegl M, Pahlevani M, Zigan L (2020c) A novel approach for measurement of composition and temperature of n-decane/butanol blends using two-color laser-induced fluorescence of nile Red. Sensors 20(19):5721. https://doi.org/10.3390/s20195721

Koegl M, Weiß C, Zigan L (2020d) Fluorescence spectroscopy for studying evaporating droplets using the dye eosin-Y. Sensors (basel Switzerland). https://doi.org/10.3390/s20215985

Koegl M, Dai H, Baderschneider K, Ulrich H, Zigan L (2022) Polarization-dependent LIF/Mie ratio for sizing of micrometric ethanol droplets doped with Nile red. Appl Opt 61(14):4204–4214. https://doi.org/10.1364/AO.457685

Koegl M, Milto N, Zigan L (2024) Simultaneous film temperature and film thickness measurements for jet impingement applications using two-color laser-induced fluorescence. Exp Fluids. https://doi.org/10.1007/s00348-024-03782-4

Lache M, Kappelhoff C, Seiler J, Bardow A (2023) Water and ethanol as refrigerant mixture enabling adsorption cooling below 0 °C. Energy Technol. https://doi.org/10.1002/ente.202201158

Lavieille P, Lemoine F, Lavergne G, Lebouché M (2001) Evaporating and combusting droplet temperature measurements using two-color laser-induced fluorescence. Exp Fluids 31(1):45–55. https://doi.org/10.1007/s003480000257

Lemoine F, Castanet G (2013) Temperature and chemical composition of droplets by optical measurement techniques: a state-of-the-art review. Exp Fluids 54(7):1–34. https://doi.org/10.1007/s00348-013-1572-9

Lemoine F, Antoine Y, Wolff M, Lebouche M (1999) Simultaneous temperature and 2D velocity measurements in a turbulent heated jet using combined laser-induced fluorescence and LDA. Exp Fluids 26(4):315–323. https://doi.org/10.1007/s003480050294

Maqua C, Castanet G, Lemoine F, Doué N, Lavergne G (2006) Temperature measurements of binary droplets using three-color laser-induced fluorescence. Exp Fluids 40(5):786–797. https://doi.org/10.1007/s00348-006-0116-y

Mishra YN, Abou Nada F, Polster S, Kristensson E, Berrocal E (2016) Thermometry in aqueous solutions and sprays using two-color LIF and structured illumination. Opt Express 24(5):4949–4963. https://doi.org/10.1364/OE.24.004949

Mishra YN, Yoganantham A, Koegl M, Zigan L (2020) Investigation of five organic dyes in ethanol and butanol for two-color laser-induced fluorescence ratio thermometry. Optics 1(1):1–17. https://doi.org/10.3390/opt1010001

Monroy YM, Rodrigues RA, Sartoratto A, Cabral FA (2016) Influence of ethanol, water, and their mixtures as co-solvents of the supercritical carbon dioxide in the extraction of phenolics from purple corn cob (Zea mays L.). J Supercrit Fluids 118:11–18. https://doi.org/10.1016/j.supflu.2016.07.019

Mylonaki S, Kiassos E, Makris DP, Kefalas P (2008) Optimisation of the extraction of olive (Olea europaea) leaf phenolics using water/ethanol-based solvent systems and response surface methodology. Anal Bioanal Chem 392(5):977–985. https://doi.org/10.1007/s00216-008-2353-9

Najim M, Feddaoui M, Nait Alla A, Charef A (2020) Channel wall cooling by evaporative falling water-ethanol and water-methanol films. Heat Transfer Eng 41(18):1596–1608. https://doi.org/10.1080/01457632.2019.1661688

Ohnesorge WV (1936) Die bildung von tropfen an düsen und die auflösung flüssiger strahlen. ZAMM–J Appl Math Mech 16(6):355–358. https://doi.org/10.1002/zamm.19360160611

Palmer J, Reddemann MA, Kirsch V, Kneer R (2016) Temperature measurements of micro-droplets using pulsed 2-color laser-induced fluorescence with MDR-enhanced energy transfer. Exp Fluids 57(12):1–14. https://doi.org/10.1007/s00348-016-2253-2

Perrin L, Castanet G, Lemoine F (2015) Characterization of the evaporation of interacting droplets using combined optical techniques. Exp Fluids 56(2):1–16. https://doi.org/10.1007/s00348-015-1900-3

Plaskova A, Mlcek J (2023) New insights of the application of water or ethanol-water plant extract rich in active compounds in food. Front Nutrition. https://doi.org/10.3389/fnut.2023.1118761

Prenting MM, Bin Dzulfida MI, Dreier T, Schulz C (2020) Characterization of tracers for two-color laser-induced fluorescence liquid-phase temperature imaging in sprays. Exp Fluids 61(3):1–15. https://doi.org/10.1007/s00348-020-2909-9

Qi DH, Chen H, Matthews RD, Bian Y (2010) Combustion and emission characteristics of ethanol–biodiesel–water micro-emulsions used in a direct injection compression ignition engine. Fuel 89(5):958–964. https://doi.org/10.1016/j.fuel.2009.06.029

Ranz WE, Marshall WR (1952) Evaporation from Drops. Chem Eng Prog 48(3):141–146

Schulz C, Sick V (2005) Tracer-LIF diagnostics: quantitative measurement of fuel concentration, temperature and fuel/air ratio in practical combustion systems. Prog Energy Combust Sci 31(1):75–121. https://doi.org/10.1016/j.pecs.2004.08.002

Storch M, Lind S, Will S, Zigan L (2016a) Influence of ethanol admixture on the determination of equivalence ratios in DISI engines by laser-induced fluorescence. Appl Opt 55(30):8532–8540. https://doi.org/10.1364/AO.55.008532

Storch M, Mishra YN, Koegl M, Kristensson E, Will S, Zigan L, Berrocal E (2016b) Two-phase SLIPI for instantaneous LIF and Mie imaging of transient fuel sprays. Opt Lett 41(23):5422–5425. https://doi.org/10.1364/OL.41.005422

Strizhak PA, Volkov RS, Castanet G, Lemoine F, Rybdylova O, Sazhin SS (2018) Heating and evaporation of suspended water droplets: experimental studies and modelling. Int J Heat Mass Transf 127:92–106. https://doi.org/10.1016/j.ijheatmasstransfer.2018.06.103

Taheri V, Ebrahimi Rahnama H, Morad MR (2024) High flow rate electrospray cooling performance of water–ethanol mixtures. Appl Thermal Eng. https://doi.org/10.1016/j.applthermaleng.2023.122200

Ulrich H, Sigl S, Möhnle M, Berrocal E, Zigan L (2023) Droplet thermometry based on an optimized two dye two-color laser-induced fluorescence concept. Front Physics. https://doi.org/10.3389/fphy.2023.1235847

Ulrich H, Zigan L (2023) Characterization of a Dye Mixture for Two-Color Laser-Induced-Fluorescence Thermometry in Ethanol, Butanol and Water Droplets and Sprays. (11th European Combustion Meeting)

Volkov RS, Strizhak PA (2020) Using Planar Laser Induced Fluorescence to determine temperature fields of drops, films, and aerosols. Measurement, 153. https://doi.org/10.1016/j.measurement.2019.107439

Zehentbauer FM, Moretto C, Stephen R, Thevar T, Gilchrist JR, Pokrajac D, Richard KL, Kiefer J (2014) Fluorescence spectroscopy of Rhodamine 6G: concentration and solvent effects. Spectrochim Acta Part a, Mol Biomol Spectrosc 121:147–151. https://doi.org/10.1016/j.saa.2013.10.062

Zhang Z-S, Li D, Wang L-J, Ozkan N, Chen XD, Mao Z-H, Yang H-Z (2007) Optimization of ethanol–water extraction of lignans from flaxseed. Sep Purif Technol 57(1):17–24. https://doi.org/10.1016/j.seppur.2007.03.006

Student Projects

Student projects and theses supervised within the framework of the dissertation:

M. Möhnle: *Aufbau und Erprobung eines Fluoreszenzspektrometers zur Untersuchung der Tropfenverdampfung* (2021), Project Thesis, Friedrich-Alexander-Universität Erlangen-Nürnberg

S. Keim: *Absorptionsmessungen und Recherche zu Farbstoffen für die Fluoreszenz-Spektroskopie am verdampfenden Tropfen* (2021), Hauptseminar, Friedrich-Alexander-Universität Erlangen-Nürnberg

N. Lankl: *Absorptions- und Emissionsmessungen für die Thermometrie an verdampfenden Tropfen* (2022), Master Thesis, University of the Bundeswehr Munich

R. Weiß: *Spektrale Absorptions- und Fluoreszenzmessungen an Tropfen* (2024), Bachelor Thesis, University of the Bundeswehr Munich

Extended List of Publications

Additional publications and conference contributions, which are not included in this thesis, are listed below:

Peer-Reviewed Journal Contributions

Retzer U., Ulrich H., Will S., Zigan L.
Burst-mode 1-methylnaphthalene laser-induced fluorescence: extended calibration and measurement of temperature and fuel partial density in a rapid compression machine
Applied Physics B: Lasers and Optics **128** (2022), 144.

Guénot D., Svendsen K., Lehnert B., Ulrich H., Persson A., Permogorov A., Zigan L., Wensing M., Lundh O., Berrocal E.
Distribution of liquid mass in transient sprays measured using laser-plasma-driven X-Ray tomography
Physical Review Applied **17** (2022), 064056.

Koegl M., Dai H., Baderschneider K., Ulrich H., Zigan L.
Polarization-dependent LIF/Mie ratio for sizing of micrometric ethanol droplets doped with Nile red
Applied Optics **61** (2022), 4204-4214.

Fendt P., Retzer U., Ulrich H., Will S., Zigan L.
Stability analysis of the fluorescent tracer 1-methylnaphthalene for ic engine applications by supercontinuum laser absorption spectroscopy
Sensors **20** (2020), 2871.

Retzer U., Ulrich H., Bauer F.J., Will S., Zigan L.
UV absorption cross sections of vaporized 1-methylnaphthalene at elevated temperatures
Applied Physics B: Lasers and Optics **126** (2020), 50.

Conference Contributions

Ulrich H., Weiß R., Zigan L.

Anwendung laserinduzierter Zweifarben-Fluoreszenzspektroskopie auf „Green Solvent" Tropfen aus Wasser und Ethanol

31. Fachtagung "Experimentelle Strömungsmechanik", Berlin (2024).

Ulrich H., Zigan L.

Application of Two Dye Two-Color Laser-Induced Fluorescence Spectroscopy on Droplets of Green Solvent Mixtures Containing Water and Ethanol

21th International Symposium on Applications of Laser and Imaging Techniques to Fluid Mechanics, Lisbon (2024).

Ulrich H., Zigan L.

Thermometrie an mikrometrischen Ethanoltropfen basierend auf la-serinduzierter Fluoreszenz unter Nutzung einer Farbstoffmischung

30. Fachtagung "Experimentelle Strömungsmechanik", München (2023).

Ulrich H., Zigan L.

Characterization of a Dye Mixture for Two-Color Laser-Induced-Fluorescence Thermometry in Ethanol, Butanol and Water Droplets and Sprays

11th European Combustion Meeting, Rouen (2023).

Ulrich, H., Sigl, S., Moehnle, M., Berrocal, E., Zigan, L.

Two-Color Laser-Induced Fluorescence Thermometry in Micrometric Ethanol Droplets Using a Fluorescein and Sulforhodamine 101 Dye Mixture

20th International Symposium on Applications of Laser and Imaging Techniques to Fluid Mechanics, Lisbon (2022).

Ulrich H., Lehnert B., Guénot D., Svendsen K., Lundh O., Will S., Wensing M., Berrocal E., Zigan L.

Analysis of liquid spray structures using two-photon fluorescence laser sheet imaging

15th Triennial International Conference on Liquid Atomization and Spray Systems, Edinburgh (online conference) (2021).